Analysis of Social EEG - A Neuroscience Study

Nicolai Mersebak

Kongens Lyngby 2013
DTU Compute-M.Sc.-2013-70

Supervisor: Lars Kai Hansen
Co-supervisor: Carsten Stahlhut and Ivana Konvalinka

Technical University of Denmark
Department of Applied Mathematics and Computer Science
Building 303B, DK-2800 Kongens Lyngby, Denmark
Phone +45 45253031, Fax +45 45882673
compute@compute.dtu.dk
www.compute.dtu.dk DTU Compute-M.Sc.-2013-70

Abstract

The thesis describes a neuroscience study investigating how the presence of another person will effect people's perception of emotional scenes. Will one become more attentive towards the emotional scenes and will they be perceived as more or less extreme? These questions are answered from a 2×3 within-subjects experimental design with the social context (Alone and Together) and the emotional picture content (Positive, Negative and Neutral) as the two factors.

Consistent with similar studies, the emotional picture content is found to modulate how the information is perceived. From an ERP analysis, the LPP distinguishes the affective pictures compared to the neutral pictures. It is suggested to be an enhanced attraction of attentional neural resources for processing the emotional content. Source reconstruction showed increased activity for positive pictures in the left frontal midline gyrus compared to neutral ones. The left frontal midline is suggested to be in a network with the limbic system creating emotional states.

The thesis is the first to study how the neural responses are modulated when attending IAPS pictures with another person. From a cluster-based permutation test, a decrease of the LPP ($p=0.04$) is found when jointly attending the pictures, which reflects a decrease of the arousal state. Source reconstruction localized the differences to the left frontal superior gyrus, the left frontal midline gyrus, the left occipital midline gyrus, the right temporal superior gyrus and the right temporal midline gyrus, which are areas associated with regulation of the emotional state and the MNS system. A time-frequency analysis showed that the presence of another person increased the attention towards negative pictures ($p=0.06$) reflected as decreased alpha power.

Resume

Denne afhandling beskriver et neurovidenskabeligt studie, der undersøger hvordan menneskets opfattelse af emotionelle billeder ændres af en anden persons tilstedeværelse. Vil man blive mere opmærksom på de emotionelle billeder, og vil de opfattes som stærkere eller svagere? Disse spørgsmål bliver undersøgt ud fra et 2×3 $within - subjects$ eksperiment, hvor de to faktorer er den sociale betydning (Alene og Sammen) og det emotionelle indhold af billederne (Positivt, Negativt, Neutralt).

Afhandlingen viser i overensstemmelse med tidligere studier, at det emotionelle indhold af billederne påvirker hjerne aktiviteten. Fra en ERP analyse, differentierer $the\ LPP$ bearbejdningen af emotionelle og neutrale billeder. Dette skyldes en øget tiltrækning af neuroner til bearbejdning af det emotionelle indhold. Lokaliseringen af strømkilderne viste øget aktivitet i den venstre frontale midtlinje gyrus for positive sammenlignet med neutrale billeder. Den venstre frontale midtlinje danner netværk med det limbiske system, der danner følelser.

Afhandlingen er det første studie, som undersøger hvordan den neurale aktivitet ændres, som følge af en anden persons tilstedeværelse, når man bearbejder emotionelle billeder fra $IAPS$. En *cluster-based permutation test* viste et signifikant fald af $the\ LPP$ (p=0.04) grundet tilstedeværelsen af en anden person. Dette reflekterer et fald af den ophidselsestilstand, der opstår pga. emotionelle billeder. Forskellen er lokaliseret i den venstre frontale superior gyrus, den venstre frontale midtlinje gyrus, den venstre occipitale midtlinje gyrus, den højre temporale superior gyrus og den højre temporale midtlinje gyrus. Disse områder er associerede med regulering af ens følelser og $the\ MNS$ system. En tids-frekvens analyse viste, at tilstedeværelsen af en anden person øger ens opmærksomhed af negative billeder (p=0.06).

Preface

This thesis was prepared at the Department of Applied Mathematics and Computer Science at the Technical University of Denmark in fulfillment of the requirements for acquiring a M.Sc. in Medicine and Technology. The work began February 7, 2012.

Acknowledgements

First, I would like to express my gratitude to my supervisor Professor Lars Kai Hansen at DTU Compute for providing guidance, interesting feedback and encouragement throughout the whole progress. A special thanks to Post. Doc Carsten Stahlhut for being patient, contributing with theoretical discussions and ideas, but also helping out with the experiments and Matlab issues. I would also like to give Ivana Konvalinka a special thanks for an extraordinary help with the experiment and valuable contribution to the interpretation of the results. A thanks to Center for Visual Cognition at Copenhagen University for providing facilities. At last, a thanks to Sophie, Ditte, Camilla and Mille for helping and participating in the experiments. Furthermore, an extra thanks to Mille for proofreading the thesis.

Lyngby, 31-July-2013

Nicolai Mersebak

Contents

List of Abbreviations and Symbols

Abbreviations

AAL	Anatomical Automatic Labeling
ACC	Anterior Cingulate Cortex
BEM	Boundary Element Method
ECG	Electrocardiogram
EEG	Electroencephalogram
EMG	Electromyographi
EOG	Electrooculography
EPSP	Excitatory PostSynaptic Potential
ERP	Event Related Potential
ERS	Event-Related Desynchronization
ERS	Event-Related Synchronization
FIR	Finite Impulse Response
IAPS	The International Affective Picture System
ICA	Independent Component Analysis
IIR	Infinite Impulse Response

IPSP Inihibitory PostSynaptic Potential

LPP Late Positive Potential

MCP Multiple Comparison Problem

MENT The Mentalizing System

MNE Minimum Norm Estimate

MNI Montreal Neurological Institute

MNS Mirror-Neuron System

MSE Mean Squared Error

PFC Prefrontal Cortex

SNR Signal to Noise Ratio

TOM Theory Of Mind

Symbols

α Level of Significance

δ Dirac Delta Function

λ Regularization Parameter

$\Phi(\mathbf{r})$ Scalp Surface Potential

ψ The Complex Morlet Wavelet

Σ Noise Covariance

σ_{noise} Standard deviation of Gaussian noise

A Mixing Matrix

C Number of Cycles in Wavelet

CT Cluster Level Test Statistics

D Data Matrix

E White Gaussian Noise

F Forward Field

H_0 Null Hypothesis

H_1 Alternative Hypothesis

j	Samples Within a Cluster
K	Number of Sources
L	Cost Function
M	Number of Samples
N	Number of Channels
P	Power
p	Monte Carlo p-value
S	Sources
T	t-test statistic
U	Estimate of the Signals, X
W	Unmixing Matrix
X	Recorded Signals
Z	Estimate of the Sources, S

Chapter 1

Introduction

The human brain is complex and despite our increased knowledge due to modern modalities like EEG, MRI, CT and PET, our understanding of the brain remains very limited. The field of neuroscience is broad, yet the study of social cognition has been previously neglected. It has only recently become of great interest [109]. Social cognition covers cognitive processes such as encoding, storage and perception of information that help to create an understanding among individuals of the same species [8].

Social interaction is an essential part of human function and the daily life. Lack of social skills can be devastating for the daily functions of the individual and can result in their rejection from the society [53]. Despite the importance of social skills, the underlying neural mechanism is still poorly understood. In addition, because it is known that neurological diseases like schizophrenia and autism affect the ability to interact socially, a better understanding of social cognition could improve the current knowledge of such diseases [53]. The area is very complex to analyze and test as social interaction includes several aspects such as perception, action, attention, which is often analyzed separately. The study of social interaction requires simulation in an experimental environment rather than through more natural social interaction [18].

Even though the interest in the field of social interaction has increased, a "simple" process of how the presence of another person affects the perception of emo-

tional scenes remains unanswered [105]. Until now, the literature (elaborated in Section 1.2) has been focusing on social interaction using experiments originating from game theory [16, 19, 20, 42] or from action-perception paradigms such as follower/leader or coordination [39, 71, 117]. Recently, however, Richardson et al. examined this interesting statement [105]:

> *"By focusing on this minimal social context (knowing that another person is seeing the same images), we can explore the shifts in perceptual processes that occur in response to the presence of others, prior to communication, joint action or cooperation taking place"*

Several studies have shown that the neural mechanisms of processing positive, negative and neutral pictures[1] differ [44, 60, 69]. In the thesis, affective pictures are referred to include both positive and negative pictures. In relation to social cognition, two important questions need to be answered:

1. *Are neural responses pertaining to emotional scenes different when in the presence of others?*
2. *Are affective pictures perceived as more or less extreme when the experience is shared?*

To the knowledge of the author no one has looked at the neural mechanisms behind these questions.

Richardson et al. [105] used an eye tracker[2] to analyze which pictures the participants looked at (gaze), when four images (one negative, one positive and two neutral) were presented simultaneously. They investigated whether the gaze pattern changed as the participants were told that another person was looking at the same pictures. The participants were not able to see or to interact with each other. Moreover, they did not have knowledge about the other person's gaze. The social context was minimized by participants sitting in opposite corners of the room and being told by the screen whether they looked at the same images (joint condition) or not. The distribution of the gaze pattern was modified in the joint condition analyzed by an eye tracker. The participants were more attracted in the joint condition, meaning a higher total looking time, at negative images compared to positive and neutral ones.

[1] Examples of positive pictures are erotic images or babies, while examples of negative pictures are mutilated bodies or "threat" images like spiders and snakes. Neutral pictures might be a cup or a pencil.

[2] An eye tracker captures the eye movement of a participant and can among others be used to detect where on the screen the participant is looking.

Because eye-tracking cannot reveal the level of arousal nor how or when any increased attention is developed, EEG is used to study the underlying neural sources. Therefore, the next step is to investigate similar modifications of attention using EEG to shed light on the underlying neural mechanisms. Utilizing EEG could give a deeper understanding of the potential modulation of attention and emotional perception in joint attention scenarios. Sharing experiences, such as videos or images, is a large part of social interaction. Schilbach et al. [109] state *that being jointly attended can have an impact on the perception of an object and its value, not only on the perception of the other person.* Understanding these potential modifications would improve the understanding of the effect of the mere presence of others on emotional processing and regulation.

1.1 The Human Brain

The following section provides a basic summary of human brain function and anatomy based on the work by Seeley et al. [113]. The brain consists of four major divisions, which are the brainstem, the cerebellum, the diencephalon and the cerebrum as shown in Figure 1.1. The brainstem works as the pathway between the cerebrum and the spinal cord and controls reflexes, whereas cerebellum's major function is the control and learning of motor skills. The diencephalon includes the hypothalamus which controls the endocrine function of the brain and the thalamus that projects the majority of sensory inputs to cerebrum.

The last division is the cerebrum. The cerebrum is divided into the right and left hemispheres by the medial wall. Each hemisphere is divided into a frontal lobe, parietal lobe, occipital lobe and temporal lobe as seen in Figure 1.1a. The function of the frontal lobe includes voluntary movement, motivation and aggression. The parietal lobe receives the majority of sensory information except for visual input, which is received by the visual cortex in the occipital lobe. The temporal lobe is associated with memory, judgment and abstract thinking. The outer surface of cerebrum consists of gray matter and is called cortex. It is a folded structure, where the fissures are called sulcus and the ridges are called gyrus. The white matter is called cerebral medulla and is the layer between the cortex and basal nuclei. The limbic system is seen in Figure 1.1b and covers parts of both the cerebrum and diencephalon. Amygdala and thalamus are parts of the limbic system and play important roles in the perception of emotional input.

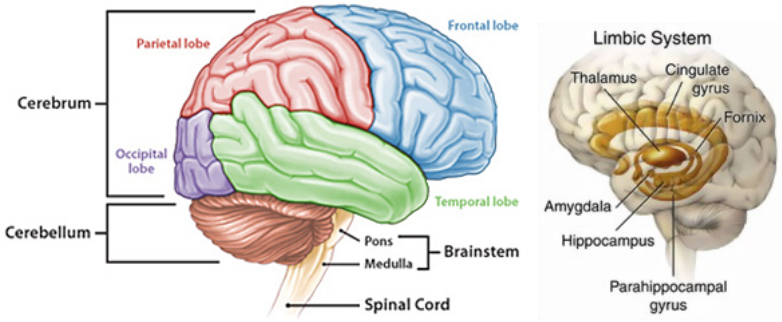

(a) **(b)**

Figure 1.1: The figure shows a) the location of the four lobes in Cerebrum and b) the limbic system, showing the location of amygdala and thalamus. The image is obtained from [2].

1.1.1 Perception of Affective Visual Stimuli

The processing of a visual stimuli is a very complex process and is still not fully understood. Moreover scientists do not agree on how the processing works and especially the roles of thalamus and amygdala [98]. Generally explained, a human exposed to a visual stimulus will transfer the information from retina via the optic nerves to the lateral geniculate nuclei of thalamus, which via thalamic neurons projects the information to the visual cortex in the occipital lobe. The visual cortex transforms the information into a mental image and depending on the information projects it to the target part of the brain [113]. Passoa and Adolphs, [98], discuss the role of thalamus and amygdala in affective visual processing. At one point, one hypothesis was that an unconscious processing of affective visual stimuli bypasses the cortex with a path from thalamus to amygdala. However they [98] propose that the processing of affective stimuli and emotion is more complex than the first hypothesis claims and that the cortex has a larger contribution. The role of amygdala originates from its broad connectivity with the cortex and serves more as a convergence zone, where it both receives and projects information from and to the visual cortex.

From a meta analysis of neuroimaging studies of functional grouping in emotion, [69], it was found that certain regions were consistently activated across studies of emotion and affect. Regions of the visual cortex and visual association cortex at the occipital and temporal lobe were grouped as a function and showed consistently activation in both the early and late processing. The activity of the group was enhanced with increasing emotional content due to neural projections from the limbic system. The prefrontal area also showed consistent

activations and is suggested to generate emotions in a network with the limbic system, amygdala, the visual cortex and the visual association cortex. Amygdala showed consistently activation and is proposed to play a role in both visual and emotional processing. However, the precise role of amygdala still remains unclear [69, 93].

1.2 Literature Review

The literature review is divided into two sections. The first part summarizes findings of *Event Related Potential, ERP* and brain oscillation studies using affective pictures to elicit processing of emotional stages mainly based on [67, 93]. The second part reviews recent findings in two-brain studies and serves as an introduction to the field of social cognition, primarily based upon [72, 109]. Both reviews are important as the thesis combines these two areas.

1.2.1 Affective Picture Processing

The literature in the field of affective picture processing has increased for the last decade using both ERP analysis [93] and analysis of brain oscillations [61]. Modulations of pictures are based on two dimensions. The valence dimension defines the pictures in a scale from pleasant to unpleasant, where the arousal level defines the picture in a calm/excited scale [74]. The review of ERP studies will be divided into findings of an early time window from 0 to 300 ms relative to image onset and a late time window after 300 ms. Furthermore, studies concerning the brain oscillations will be divided into oscillation bands of specific frequency content: the theta band (4-7 Hz), alpha band (8-12 Hz) and beta band (13-30 Hz). Even though the gamma band is interesting and negative valence pictures have shown an increased gamma activity [89], the thesis limits the analyses to the theta, alpha and beta bands.

Modulated ERPs:

In the time window (0 - 300 ms), the early sensory processing affects the modulation of the ERP components and is associated with the valence content of the picture [93]. Pictures with a positive valence are distinguished from negative and neutral pictures [34, 60, 97]. Kiel et al. [60] investigated positive, negative and neutral pictures, where the early negative component, N1, was enhanced[3] for positive pictures at the occipital site. At the fronto-central sites, the positive

[3]Enhancement of the N1 component means a larger negative amplitude.

pictures had a lower negative mean amplitude in the interval from 150 to 300 ms [97]. The review of Olofsson et al. [93] notes large variability across the studies within the early time window with many studies not finding any differences between the pictures. Furthermore, they report that some studies find a larger response for negative pictures compared to positive and neutral ones [93].

The same review, [93], notes very consistent results across the literature in the late time window (>300 ms), where the arousal level distinguishes affective and neutral pictures. A larger response to affective pictures compared to neutral is reported as an increasing positive potential for affective pictures around 400 to 700 ms after image onset. This positive potential in the late latency window is a consistent finding between neutral and affective pictures [93], where the arousal state is correlated with a long lasting stronger response. This effect is found as a positive wave at both the centro-parietal and fronto-parietal sites [60, 61, 94, 97, 107, 108] and as a negative wave at the temporal and occitpital sites [60, 97].

To sum up, the early time window is mostly affected by the valence level of the picture, while the arousal level modulates the ERPs in the late picture processing.

Modulated Oscillatory Brain Activity:

Low frequency oscillations in the theta band have mainly been associated with encoding of new information with *Event-Related Synchronization, ERS*[4] , during successful encoding [62, 65, 66]. From a review by Klimesch [63], it is suggested that an increase in theta power more generally reflects an increase in the attentional demand, task difficulty and cognitive load.

Aftanas et al. [10], showed that the valence dimension in picture presentation distinguished affective from neutral pictures with an increase in theta power from 200 to 500 ms after picture onset. Increased theta power for affective pictures is found in hippocampal[5], which is connected with increased frontal and prefrontal theta power in the first 600 ms after picture onset [68]. It is consistent with the review by Klimesch [63], as affective pictures have a higher cognitive load and tend to improve the memory performance [38].

The alpha band is the dominating frequency band in EEG signals and the most studied, but the precise function of alpha oscillations are still to be defined

[4]ERS means increased power as more neurons are synchronized and therefore create a larger potential.

[5]Hippocampal is a region in the brain that belongs to the limbic system, and plays an important role in, e.g. memory forming [113].

[63, 64]. However, an alpha *Event-Related Desynchronization, ERD*[6] has consistently been interpreted as increased engagement in the stimulus and thereby increased attention [64, 67, 68]. Alpha ERD is seen when affective pictures are presented in contrast to neutral pictures over the occipital [35] and parietal [68] electrode sites suggesting a higher activation of the visual processing. The function of the alpha band has been proposed to be divided into a lower and an upper alpha band. The lower band is spatially widespread with a less clear function related to general attentional demands. The upper band is more spatially widespread and functionally related to semantic memory processing [63].

Literature concerning modulation of beta oscillations, due to affective picture presentation, is lacking as most studies have been focused on theta, alpha and gamma oscillations. G*ü*ntekin et al. [51] found a significant difference with an increased beta activity for negative pictures compared to positive and neutral ones in the early time window. Another study, [103], found that both positive and negative emotions had increased beta activity.

1.2.2 The Social Brain and Interacting Brains

The brain activity underlying social cognition is as mentioned still poorly understood, despite the importance of it as a human being. The earliest findings report that brain lesions in the prefrontal area resulted in social impairment and changes in personality despite unchanged IQ, language etc. Likewise, damage of amygdala has showed that recognition and judgment in a social context were impaired [8]. Hence, these areas were thought to be involved in social cognition.

Social interaction is defined by Sebanz et al. as [112]:

> *"We propose that successful joint action depends on the abilities (i) to share representations, (ii) to predict actions, and (iii) to integrate predicted effects of own and others' actions"..."Joint attention creates a kind of 'perceptual common ground' in joint action, linking two minds to the same actualities."*

A theory to explain crucial processes involved in social interaction is the *Theory Of Mind, TOM*[7]. TOM plays an important part in social interaction as it refers to the ability to distinguish between self and others by believing that others have their own thoughts, intentions and beliefs. The ability to socially

[6] ERD means less synchronization of the neurons and therefore a decrease of power.
[7] TOM is just one of many theories, see [8] for a further elaboration.

interact is highly dependent on ones ability to understand others' intentions, thoughts and beliefs. Successful interaction is not only dependent on understanding each others' actions at the moment but also peoples ability to predict future actions [48, 124]. If a prediction during social interaction is violated, the superior temporal sulcus is activated suggesting its role in updating the predictions and understandings of the other person's action [18, 43, 49]. The ability to understand and predict others' action are linked to two systems the *Mirror-Neuron-System, MNS*, and the *Mentalizing System, MENT*.

The main regions of MNS include the premotor and parietal cortex [112, 121] and have the primary function as a common coding framework of perception and action. Activation of MNS has been reported when observing and executing an action, implying that the MNS is a sensorimotor network. The MNS is only activated if the observed action is recognized [53, 47].

The MENT has the purpose of understanding others' thoughts, intentions and beliefs. The ability to understand these, are derived from our own expectations. The *Anterior Cingulate Cortex, ACC*, has been shown, from a game, to be an important region in making an accurate estimate of others' thoughts, intentions and beliefs [19, 20]. The orbitofrontal area has shown to play a role during cooperation [14], but in general it is also associated with evaluating uncertainty of outcomes [16]. The orbiofrontal area is a subdivision of the medial *Prefrontal Cortex, PFC* that is continuously active and in connection to the temporo-parietal junction during social interaction and more specifically decoding of others' thoughts, intentions and beliefs [18]. As presented earlier, several areas of the brain have been associated with social interaction, despite the fact that researchers, until recently, only have investigated brain activity from isolated individuals [53].

In contrast to the above theory that social interaction can be explained by the activity of a single brain and certain areas, a different way of understanding social interaction is by studying two persons engaged in a mutual interaction with each other. This bidirectional information flow sees the interaction as a larger and more dynamic process, which cannot be explained solely from an observing and imitating point of view [53, 72, 109]. Two interacting people create a shared environment that affects the interacting persons, where one's input will be the output of the partner making a perception-action loop. In addition, each person still tries to understand and predict the actions, beliefs and intentions of the other interacting partner.

An important factor to create sufficient estimates of the other's action is the gaze of the interacting partner. Mutual eye gaze plays an important role in our ability to socially interaction and is an important part of the perception-action loop [73]. It is also known that infants develop and learn through mutual eye gaze and is

the foundation of the first social interaction. Because our predicted intentions of the interacting partner are often based on memory of similar situations in past, facial expressions, gestures and eye contact all play an important role in recognizing the present social situation.

One's motivation towards social interaction is still uncertain, but has been suggested to be connected to the reward system [109]. Schilbach et al. [110], suggest that humans feel rewarded when sharing experiences, which motivates them to interact. By examining the eye gaze, they found that there was a difference between following someones eye and leading the eyes towards a jointly attended object. The ventral striatum, a region associated with being rewarded, was activated when the subjects led the gaze.

Recently, studies in neuroscience have moved away from studying the isolated brain to use the method hyperscanning, defined as simultaneously measuring two or more brains [72]. Several studies use the hyperscanning method to investigate the neural mechanisms of social interaction, where experiments originating from game theories such as Prisoners's Dilemma [19, 42][8], the Chicken's game [14][9] or a card game [16, 20] have been used. Although the studies found active regions (amygdala, ACC, PFC and fronto-orbital regions) similar to ones studying the isolated brain, these met criticism [109].

First, the experiments do not capture a true interaction scheme since the experiments are turn based implying that the participants are either receiving or sending information. Real social interaction is more co-regulated than turn based [109]. Secondly, the areas found are known to have multiple functions questioning the true reason for the increased activity [72]. Another experimental paradigm used with hyperscanning is the synchronization of hand movement [39]. Here participants were told to imitate each others' hand movement. The results showed synchronization between the two brains in the right centro-parietal regions in the alpha-mu frequency band[10]. It supports the concept that the alpha-mu frequency band in the right centro-parietal region was also found as a neural marker complex for social coordination [117]. The neural marker complex consists of two components, phi_1 and phi_2, that were active as the participants either had ineffective or effective synchronization.

[8] Prisoner's Dilemma is a game with two participants, each having two choices: cooperate or defect. If both players cooperate, they will both have a small win, if only one cooperates, the cooperator has a big loss and the defector has a big win. If both defects they both have a small loss [19].

[9] The Chicken game includes two players driving against each other. The players can now stop or continue giving in total three outcomes: both cooperates (stops) giving both of them a small win, one cooperate and one defects (continue) resulting in a big loss and a big win. If neither player gives up, they both have a big loss [14].

[10] The alpha-mu frequency band is 10-12 Hz and describes a sensorimotor rhythm.

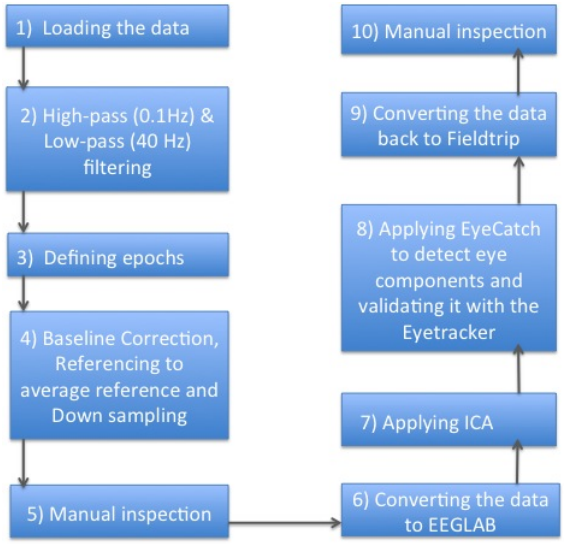

Figure 1.2: The figure outlines the steps used in the preprocessing pipeline.

Most recent, Konvalinka et al. [71] examined, from a dual-EEG experiment, a simple action-perception loop in a finger tapping experiment. Participants aligned their finger tapping beats with either an auditory feedback from a computer (non-interactive) or from another person (interactive). During tapping suppression of 10 Hz and 12-15 Hz neural oscillations were found in the interactive condition compared to non-interactive. Suppression was found at the sensorimotor, right-frontal and fronto-central electrode locations. The results are consistent with [90, 117] suggesting that the alpha-mu rhythm is thought to be a part of MNS activity.

1.3 The Data and Pipeline

The data in the thesis is a 64 channel recorded scalp EEG from 13 females at the Center for Visual Cognition at Copenhagen University. The experimental design is a 2×3 within-subjects design with *the social context* and *the emotional picture content* as the two factors. The two social conditions are defined as *Alone* and *Together*, meaning that the participants are viewing the pictures alone or with another person. The three picture conditions are *positive*, *negative* and *neutral* which define the valence and arousal level of each picture group.

The experimental design allows a sanity check by reproducing the results in the

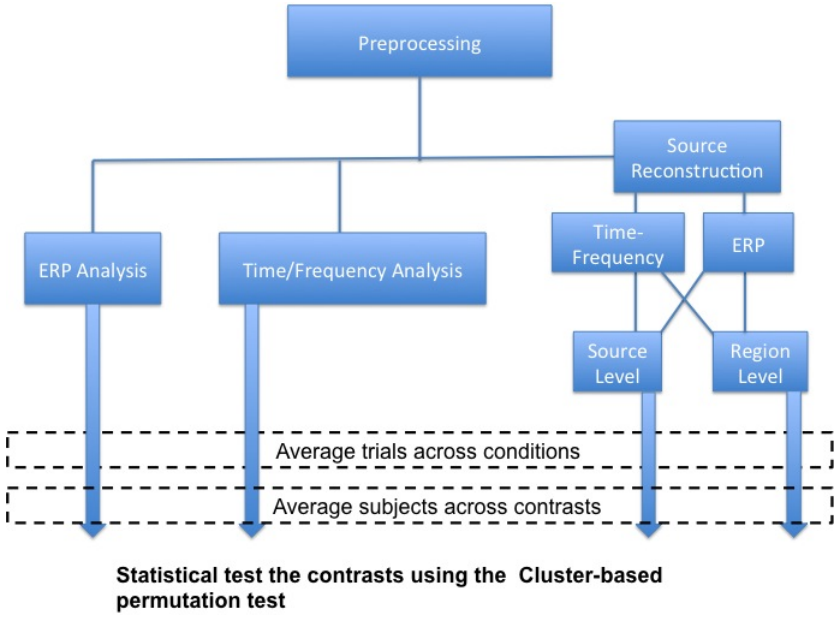

Figure 1.3: The figure outlines the different analyses conducted in the thesis.

literature concerning affective picture processing, and secondly an analysis of the social context.

As the data is self-produced, it is necessary to conduct a sufficient pipeline to denoise and prepare the data prior to the analysis. Figure 1.2 shows a schematic overview of the preprocessing pipeline conducted in the thesis, while Figure 1.3 shows the different analysis applied to the data.

1.4 Problem Definition

The aim of the thesis is to conduct and analyze a social EEG study serving as a preliminary work for future studies recording EEG from multiple subjects to see brain-to-brain interactions. The main problem is to simplify the design while bringing social cognition into an experimental environment, and to ask the right questions in order to quantify the effects.

The nature of EEG signals require a detailed and considered preprocessing pipeline [92]. Great effort and much time was spent on creating an appropriate

pipeline with the purpose of denoising the signals with a minimum of neural signal distortion. The extended INFOMAX *Independent Component Analysis, ICA* algorithm [58] was applied on the data in order to remove *Electrooculography, EOG* artefacts. Wrongly removing components can introduce artificial components in the data as some brain activity is removed. It takes many years of experience to manually distinguish ICA components as EOG and brain activity components, therefore several automatic and semiautomatic methods have been developed [25]. The newest state-of-the art method is EyeCatch, which is based on spatial correlation with templates defined through data mining over thousands of ICA components [25]. To the knowledge of the author, the method has not yet been used in the literature, therefore the thesis will validate the performance of EyeCatch using an eye tracker.

In the thesis, the data is analyzed in three different ways:

1. A traditional ERP analysis.
2. A complex Morlet wavelet decomposition for a time-frequency analysis.
3. Source reconstruction using the *Minimum Norm Estimate, MNE.*

The statistical tests are performed using the non-parametric cluster-based permutation test. In neuroscience, *Multiple Comparison Problem, MCP* is a common problem, where the thesis investigates the non-parametric cluster-based permutation test to solve the MCP using both simulations and real data. The test will from now on be denoted as a cluster-based permutation test. The test will be applied on both channel, region and source level. The author has no knowledge of existing literature applying the cluster-based permutation test on source or region[11] level.

To conduct the pipeline and analysis, a Matlab, [84], based software package for advanced analysis of EEG, Fieldtrip [95], is used, except for the use of ICA and EyeCatch. These are performed in EEGLAB [36], which is another Matlab, [84], software package.

[11] The AAL atlas, with 116 brain anatomical regions, is used in this thesis [119].

1.5 The Outline of the Thesis

Chapter 2 introduces the basic concepts concerning the origin of electroencephalogram. It then outlines general challenges prior to an EEG recording and a description of possible noise sources.

Chapter 3 explains the theory behind the preprocessing steps including filter design and ICA. The last part of the chapter explains the three analyzing methods: the ERP analysis, the time-frequency analysis and source reconstruction using the MNE.

Chapter 4 explains the non-parametric cluster-based permutation test. Furthermore, a simulation study is conducted to investigate crucial parameters of the test.

Chapter 5 describes the experimental design and the pipeline conducted in the thesis to prepare the data prior to analysis.

Chapter 6 serves as an independent chapter, where the performance of EyeCatch is validated with an eye tracker. The method and results of the validation are presented in this chapter including a discussion.

Chapter 7 presents the main results in the thesis. The first part concerns the baseline in the data. The second part shows the results of comparing the processing of positive, negative and neutral pictures. Finally, results due to the social context in the experiment, are presented.

Chapter 8 discusses the results from Chapter 7 including a general discussion of the cluster-based permutation test.

Chapter 9 summarizes the discussion and concludes with the goals set forth in the thesis followed by a perspective on future work.

Chapter 2

Background - Understanding the Electroencephalogram

This chapter serves as an introduction to the basics of the EEG and is divided into two sections.

1. The first section gives a brief introduction about the origin and the characteristics of an EEG signal and is based on [92, 113]. In order to compare results across EEG studies, several parameters have to be defined, e.g placements of the electrodes and the choice of reference. The section is based on [92, 79].

2. The last section deals with the poor *signal to noise ratio, SNR* in EEG recordings as many different and often high energy noise sources distort the EEG signals [118].

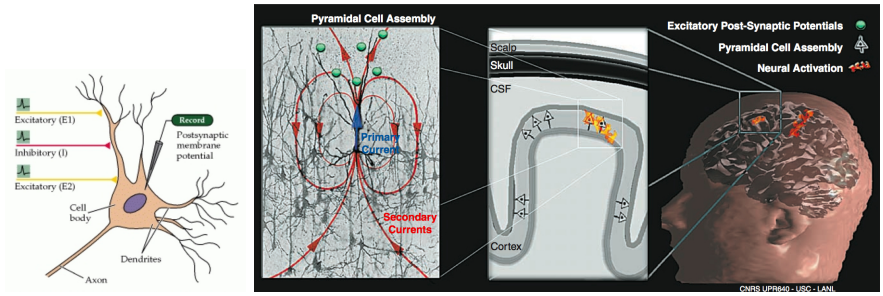

(a) (b)

Figure 2.1: Figure a) shows how the postsynaptic potential is a summation of all ESPS and IPSP. The figure is obtained from [102]. Figure b) illustrates the alignment of the dipoles and how a scalp potential is created. The figure is obtained from [22].

2.1 Electroencephalogram

As mentioned in Chapter 1, an external stimulus is transmitted from the retina through the thalamus to the visual cortex. This path is very complex and includes thousands of neurons. The transmission of a signal between neurons is done through a structure called a synapse. The neuron that carries the signal has its axon at the synapse, where the receiving neuron has its apical dendrites. Action potentials and postsynaptic potentials are the two types of electrical activity in the brain. The postsynaptic potential arrives from *Excitatory Postsynaptic Potentials, EPSPs* and *Inihibitory Postsynaptic Potentials, IPSPs*. EPSPs result in a positive electrical charged cellbody and a negative electrical charged apical dendrites, while IPSPs have the opposite effect. The electrical difference between the cell body and the apical dendrites creates a dipole. The receiving neuron is affected by many neurons simultaneously, working as either an EPSP or an IPSP. It is the summation of these that controls if an action potential is triggered [92].

The electrodes used to measure the electrical potentials in the brain can be scalp or intracranial electrodes [92]. Recordings obtained with intracranial electrodes are out of the scope of the thesis and will therefore not be explained. The largest contribution to the scalp recordings is believed to originate from cortex. A single electrode measures an electrical potential originating from a tissue area spanning over hundred millions to billions neurons. It is therefore not the ESPSs and IPSPs from a single synapse that generate the potentials, but many local synaptic sources that due to spatial adjacency all contribute to the measured

signal.

The folded structure of the brain complicates the summation of all the dipoles, because summation of the dipoles are angle dependent. Dipoles of the opposite direction (180 degrees) will cancel each other. Small cancellations will be present already from an angle of 90 degrees [79]. The alignment of the dendrites is therefore an important factor prior to having a measurable signal. The dendrites are often arranged parallel, meaning that the local synaptic activities add up their dipole potential by forming a dipole layer. A dipole layer is a formation of activity of many synapses that are parallel with synchronized activity. It must consists of approximately 60.000.000 neurons ($\sim 6cm^2$ tissue area) that are synchronously active in order to produce a scalp potential. Axons are orientated more randomly implying that action potentials at the axons have a much smaller contribution to scalp potentials. Additionally, action potentials are not as synchronized as post synaptic activity [92].

The tissue from the generated dipole potential to the scalp electrodes is inhomogeneous, where each different layer[12] has individual resistances and conductivity characteristics. It makes it difficult to locate the precise sources of the EEG signal [92]. The electric potentials therefore provide a large-scale spatial resolution but a very high temporal resolution, making it possible to obtain fast modulations of the postsynaptic potentials. The activity can be divided into two categories: modulations at a short-time scale (milliseconds) and modulations at a large-time scale (seconds to minutes). The short-time modulations arrive mostly because of external stimulus, for example when a picture is presented. The large-time modulations are called spontaneous potentials and are for instance the patterns observed during sleep [92].

The recorded EEG signal can be described according to their frequency content[13] as seen in Table 2.1. The amplitude of EEG signals depends on the previous discussed factors, but are in the range of 0.1 to 100 μV.

2.1.1 EEG Recording

In order to compare EEG studies accurately and make it reproducible, the standardized international 10/20 system has been developed. It has been used for half a century and most newer systems like 10/10 and 10/5 have been developed from it[14]. The system describes the electrode placement with respect to certain anatomical landmarks over the head surface [59]. The landmarks used

[12] Brain tissue, cerebrospinal fluid, skull and scalp tissue.
[13] The range of each frequency band can differ slightly depending on the literature.
[14] The 10/10 and 10/5 systems are used with higher channel density.

EEG rythm	Frequency band [Hz]
delta	1-4
theta	4-8
alpha	8-12
beta	12-30
gamma	>30

Table 2.1: The table shows the EEG rythms and their corresponding frequency content [92].

are *nasion, Nz*, *inion, Iz*, *Left Preauricular Point, LPA* and *Right Preauricular Point, RPA*. Nz is the notch area between the eyes and Iz is the lowest point in the back of your head. LPA and RPA are the peaks at the left and right tragus located in the ear. Two distances between landmarks (Nz/Iz and LPA/RPA) are measured to ensure that the electrode headcap is correct placed. The middle of each distance defines the intersection between the two measurements and is used as reference point that usually corresponds to a specific electrode depending on the used system. An example of a widely used electrode cap is Biosemi's 64 channel headcap [1]. The layout is seen in Figure 2.2, where Cz is used as a reference point when preparing the participants for the experiments. Using this approach for each participant in an experiment, will maximize the homogeneity across the subjects [59]. The 10 and 20 refer to the distance, 10/20 percentage of the total front–back/right–left distance of the skull, between adjacent electrodes in the system. Jurcak et al. [59] discuss that there are two sources to intersubject variability. First, they argue that the landmarks definitions are ambiguous. Second, the scalp and cortical anatomies differ across subject. The 10/10 system which is derived from the 10/20 labeling system is used in the thesis.

To improve the electro-chemical surface between the tissue/skin and the electrode, gel is used between the headcap and participant's skin before a recording. The electrode consists of Ag/AgCl to make a stable and sufficient contact with the skin. The quality of the contact between electrode and skin is measured with input impedance, which is recommended to keep below 25 kΩ. [79]. Other settings of the EEG equipment to ensure a first quality EEG recording is the sampling rate and online filtering. According to Nyquist sampling theorem, [75], the sampling rate needs to be twice as high as the highest frequency. The online filtering often consists of both a low-pass and a high-pass filter with a cut off frequencies, depending on the experiment.

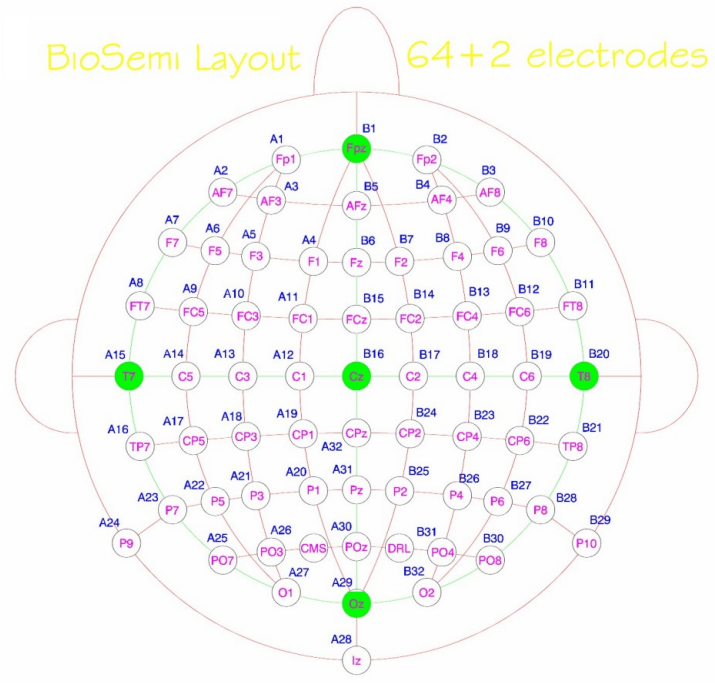

(a)

Figure 2.2: The figure shows the channel layout for the used Biosemi 64 channel headcap in the thesis [1].

2.1.2 The Reference

The obtained signal at a single electrode was previously presented as the summed dipole current. The measured signal is actually the difference between the electrode and a reference electrode. The choice of reference electrode is not simple and can depend on the recording system [92]. The reference electrode and the electrode placement system are two important factors to consider before comparing studies. The ideal reference would be a reference placed at a distance infinitely away from the recording electrodes. Because the localization of the sources are unknown, it is not appropriate to use a distant reference point. It implies that the reference electrode also will be a recording electrode in an EEG recording [92]. The recorded EEG signal is therefore intuitively highly dependent on the chosen reference. Here three widely used methods are presented:

1. The bipolar recording uses an average reference from six adjacent electrodes. The mean of six potential differences between the electrode, n, and six surrounding electrodes will be the final recorded potential at electrode n [92].

2. A second choice is the linked-mastoid reference. The idea is to create an artificial reference with a potential corresponding to the average of the two mastoids. The disadvantage is the dependency of sources at three different locations (the two mastoids and the recorded electrode) [92]. The potentials at the mastoids are often measured with external electrodes.

3. A third solution is to use the average reference. The scalp potential at the average reference, $\Phi(\mathbf{r}_{avg})$, is calculated as [92]

$$\Phi(\mathbf{r}_{avg}) = \frac{1}{N}\sum_{n=1}^{N}\Phi(\mathbf{r}_n) - \frac{1}{N}\sum_{n=1}^{N}x_n, \tag{2.1}$$

   where N is number of channels, $\Phi(\mathbf{r}_n)$ denotes the scalp surface potential at channel n and x_n is the measured potential at channel n. The first term on the right hand side is the average of the scalp surface potential. It is assumed that the current leaving the head through the neck is minimal, which implies that the head can be considered as a closed volume. Due to the current conservation theorem [92], the scalp surface potential must be zero and the term can be ignored. Using this assumption, the scalp potential at the reference will be equal to averaging the measured potentials at all electrodes. An increasing number of electrodes decreases the error of the assumption about considering the head as a closed volume. A sufficient number of electrodes is 64-128 [92]. Besides the numbers of used

electrodes, it is important to have a uniform distribution of the electrodes to make a valid average reference.

The perfect reference when recording an EEG experiment does not exist, since all methods have drawbacks and assumptions. In the thesis, the average reference is used.

2.1.3 The Noisy EEG Signal

A noise free EEG signal is an illusion. Increasing the SNR is very important and necessary before the signals can be analyzed, since the EEG activity often has less power than the noise [92]. The potential sources of noise in an EEG signal are divided into exogenous artifacts and endogenous artifacts. Selected methods to increase the SNR is described in Chapter 3.

2.1.3.1 Exogenous artifacts

Exogenous artefacts originate from external sources, where the three most common are presented.

1. Line noise is an external noise source and is seen as a 50 Hz component[15] and can be reduced with both online and offline filtering. Active shielding is the use of special electrode cables in the amplifier circuit, so the EEG lead is shielded. Usually, the recordings are obtained in an electrically and acoustically shielded EEG cabin lowering the probability of line noise [118]. Spurious electrical noise from sources like elevators, engines etc. can also be present, but an EEG cabin will often prevent such noise.

2. Movement of the electrodes as a result from body movement is an often seen noise source also called jumps squids or spikes. Their characteristics are often quick amplitude changes in a short time interval [118].

3. Measuring with metallic electrodes can introduce a DC component in the EEG signal. The DC component can distort the baseline in the signal. The DC offset can be removed by subtracting the mean of entire trials also called baseline correction in the time domain.

[15] Line noise is 50 Hz noise in Europe and 60 Hz in USA [92].

2.1.3.2 Endogenous artifacts

Endogenous artefacts originating from the human body are often more difficult to remove. There are mainly four types of sources to endogenous artifacts:

1. *Electrocardiogram, ECG* artefacts are caused by the electric activity from the heart and have a large inter-subject variability mostly due to anatomical and physiological differences. If an electrode is placed directly above a blood vessel, prominent ECG artifacts will most likely be present. An ECG artefact is a well defined shape, why a template based subtraction can be used. ICA has also shown to be a great tool to separate the ECG artefact from the signal [118].

2. *Electromyographi, EMG* artefacts are mostly due to muscle movements of the jaw implying that the energy is localized at the temporal lobes. McMenamin et. al [85] state that the majority of EMG artefacts is in the higher frequencies with a peak around 100 Hz, but that EMG artefacts have been detected to as low as 2 Hz. Generally, it depends on the muscle groups producing the artifacts and the contraction intensity. ICA has shown to be effective to detect EMG artefacts [36].

3. EOG artefacts are caused by eye movement such as vertical and horizontal saccades and blinks. EOG artefacts are characterized within the lower frequency range mostly from 1-20 Hz, but it is not uncommon that they reach up to 54 Hz [91]. Generally, there are three different variations of EOG artefacts, 1) the corneo-retinal dipole, 2) blinks and 3) spike potentials. The corneo-retinal dipole is produced during a saccade, where the orientation of the eyeball is changed causing the retina and cornea to produce a dipole as they are negative and positive charged, respectively. Blinks are causing artefacts because the eyelid slides over the cornea and short-circuiting the inter circuit between the forehead and cornea. Spike potentials are seen right before a saccade. Microsaccades are defined as saccades with an angle below one and is reported to distort the signal in the gamma range [70, 46].

   EOG artefacts are the most difficult arefacts to remove as their spectral range overlaps the theta, alpha and lower gamma band [91]. There are several methods proposed to remove EOG artefacts. Simple thresholds methods[16] have been used because of the spikes introduced by EOG [118]. However using a threshold method often results in rejecting the trial. Linear regression has also been widely used, but require external EOG channels in the set up. The linear regression method assumes a

[16] For example using the amplitude, standard deviation, min/max value, amplitude difference between adjacent data points [118].

linear relationship between EOG and EEG channels, where the only common activity is EOG activity. In reality, EEG activity will also have an impact on the EOG channels [118]. More advanced methods include Principle Component Analysis and ICA, where ICA is used and elaborated in Chapter 3.

4. The respiratory system and sweat can affect the input impedance on the electrodes introducing low frequency noise around 0.1-0.5 Hz [118].

2.2 Summary

This chapter outlined how an EEG signal occur, what the scalp electrodes actually measure and discussed the importance of choosing a proper reference and electrode measure system. It is all important prior to making and conducting an EEG experiment. In the last part, several noise sources that often are present in an EEG signal were presented, in order to understand the next chapter, which deals with the theory behind the applied methods to remove noise.

Chapter 3

Theory

This chapter serves to explain the theoretical background of the methods used to analyze the data and is divided into two sections.

The first section deals with the preprocessing of the data to increase the SNR and to prepare the data for analysis, and includes:

1. The purpose of preprocessing and the consequences of applying different filters [75, 79].
2. The use of ICA and the method EyeCatch with the purpose of removing EOG artefacts [58, 81].

The second part of the chapter explains the three methods used to analyze the data.

1. The first method is a traditional ERP analysis, where the data is analyzed in the temporal dimension timelocked to onset of the stimulus [79].
2. The second method is a time-frequency analysis using the complex Morlet wavelet transformation [116].

3. Finally, the underlying neural sources of the recorded scalp EEG is modelled using the MNE [22].

The method to statistically test the data is omitted here, but will be elaborated in Chapter 4.

3.1 Preprocessing

As explained in the previous chapter, EEG signals are often contaminated with noise originating from different sources. Preprocessing the EEG data is therefore a very crucial and important step before analyzing the data. In all preprocessing steps, different trade offs have to be taken into account as removal of noise also will distort the neural sources [79, 92].

The overall goal of preprocessing is to decrease the amount of noise while minimizing the distortion of the neural signals, and thus increase the SNR defined as, [75],

$$SNR = \frac{P_{signal}}{P_{noise}}, \tag{3.1}$$

where P_{signal} denotes the signal power and P_{noise} is the noise power, where power is defined as: $P_f = \lim_{T\to\infty} \frac{1}{T} \int_{-\frac{T}{2}}^{\frac{T}{2}} |f(t)|^2 dt$, over the period T.

3.1.1 Filter Design

The purpose of applying filters is to remove spectral components, which are not of interest in the analysis. The use of filters does not come without a cost as it will distort the data. However, because of low SNR in the raw signal, it is often a necessary step in the preprocessing. The task is therefore to optimize the filter in order to minimize the modulation of the brain signals while removing noise. It includes making decisions about filter causality, filter order and cut-off frequencies.

Causality means that the filter only depends on the past and the present, and will therefore introduce a linear phase delay of the filtered signal [75]. Introducing a phase delay is often unwanted in an ERP analysis as the precise latency of

the ERP components is important. An acausal filter introduces a nonlinear phase delay as the filter also uses knowledge of the future signal. However, the nonlinear phase delay can be avoided by applying the filter twice (forwards and backwards) defining it as a zero-phase shift acausal filter. An *Infinite Impulse Response, IIR,* zero-phase shift acausal Butterworth filter is an often used filter in EEG studies [7, 79, 106, 118].

The choice of filter order has an influence on the level of attenuation and the transition at the cut-off frequency. Generally, a larger filter order implies a steeper cut-off, but also increases the oscillations near the cut-off frequency called ripples. Therefore, the lowest filter order, while making an appropriate filtration is desired to decrease these oscillations [75]. In general, *Finite Impulse Response, FIR,* filters have higher sidelobes than IIR filters with same number of filter coefficients [101]. Furthermore, IIR Butterworth filters provide a less steeper cut-off, meaning a longer transient time but less ripples [106].

A low-pass filter is often used to remove high frequency noise such as line noise and the majority of EMG artefacts depending on your frequency of interest[17]. The only concern is to keep an appropriate distance between the cuf-off frequency and the highest frequency of interest [106, 122].

High-pass filters are of more concern in ERP studies. It is reported by Acunzo et al. [7] that an acuasal high-pass filter introduces a bias in the early ERP components[18] as a consequence of the zero-phase shift (applying the filter twice). This is especially present if the used cut-off frequency is higher than 0.1 Hz. It is therefore recommended to avoid using high-pass filter unless much low frequency noise is present. If the latter is present, then the cut-off frequency should be set as a low as possible with a maximum of 0.1 Hz [79].

On the basis of the previous discussion, a zero-phase shift acausal IIR Butterworth filter is preferred in the thesis both as a low- and a high-pass filter. The settings of the used filter are elaborated in Chapter 5.

3.1.2 Independent Component Analysis and EyeCatch

ICA is best known from *"the cocktail party problem"*, where two persons are talking simultaneously while two microphones are recording a linear combinations of the two voices. By applying ICA, the two sources can be separated into two new "microphones" (ICA components) each only obtaining one voice [26].

[17] Recall from Section 2.1.3, that EMG artefacts are located at high frequencies.

[18] More specific, it is a modulation of the C1-component, which is the first visual component in a respond to a visual stimuli [7].

In the thesis, the purpose of ICA is to separate the recorded signal into noise and neural sources and thereby denoising the EEG signal. The algorithm used in this thesis is the extended INFOMAX introduced by Jung et al. [58], which is based on the original INFOMAX algorithm developed by Bell et al. [23]. In the original algorithm, the sources are assumed to have a super-Gaussian distribution, which is extended to vary between a super-Gaussian and a sub-Gaussian distribution. A super-Gaussian density has a sharper peak[19] and a longer tail than a standard normal distribution and is described in Equation 3.17. The idea behind this distribution is that EEG signals, including EOG, EMG etc, are usually few samples that produce a strong signal, meaning that most of the time these sources have close to zero activity [58]. The strictly sub-Gaussian distribution is described in Equation 3.19 and describes a distribution of periodic signals. Looking at a simple sinusoidal signal, the probability for values at the top or the bottom of the sinusoidal is higher than values in between. It is shown that some EEG sources, e.g. line noise, are better described if the ICA components can be distributed as sub-Gaussian [58].

The following derivation of the extended INFOMAX ICA algorithm is done from a maximum likelihood approach based on the work by MacKay et al. [81]. The recorded signals, $X(N \times M)$ can be explained to time point t, as

$$x_t = As_t, \tag{3.2}$$

where A (N $\times$ N) is an unknown mixing matrix, that linearly mixes the sources S (K $\times$ M) . N is the number of channels, M is the number of time points (samples) and K is the number of sources. In this section, it is assumed that $N = K$, where N will be used as both the total number of channels and sources. From Equation 3.2, x_t and s_t are defined as $x_t = x_1(t), ..., x_N(t)$ and $s_t = s_1(t), ..., s_N(t)$ respectively. Furthermore, it is assumed that noise is absent.

The goal is to estimate an unmixing matrix $W = A^{-1}$ to recover the source signals. It is done by finding the maximum likelihood of the observed data matrix, $D = \{x_t\}_{t=1}^{M}$, given A

$$p(D|A) = \prod_{t=1}^{M} p(x_t|A). \tag{3.3}$$

The probability of the recorded signals and the sources, given the unknown

[19]Sharper peak refers to a less flat top than a standard normal distribution.

mixing matrix is

$$p(D, \{s_t\}_{t=1}^{M}|A) = \prod_{t=1}^{M} p(x_t|A, s_t). \tag{3.4}$$

Using the rules $\int p(A, B|C)dB = p(A|C)$ and $p(A, B|C) = p(A|B, C)p(B)$ in Equation 3.4 gives an expression for the left hand side in Equation 3.4

$$p(D|A) = \int p(x_t|A, s_t)p(s)ds_t. \tag{3.5}$$

The probability of D, is only known when $x_t = As_t$, which can be written with the use of the dirac delta function, δ, as

$$p(D|A, s_t) = \delta(x_t - As_t). \tag{3.6}$$

Assuming that the sources are independent implies [26]

$$p(S) = \prod_{n=1}^{N} p_n(s_n). \tag{3.7}$$

Inserting Equation 3.6 and 3.7 into Equation 3.5 gives

$$p(D|A) = \prod_{t=1}^{M} [\int \delta(x_t - As_t)p(s_t)ds_t]. \tag{3.8}$$

Since knowledge about the sources are limited, it is necessary to define them as $s_t = A^{-1}u_t$ from Equation 3.2, where u_t is an estimate of x_t. Furthermore, using the relation $ds_t = du_t \frac{1}{\det(A)}$ in Equation 3.8 yields

$$p(D|A) = \prod_{t=1}^{M} [\int \delta(x_t - u_t)p(A^{-1}u_t)\frac{1}{\det(A)}du_t]. \tag{3.9}$$

Given the nature of the δ-function[20], Equation 3.9 can be reduced to

$$p(D|A) = \prod_{t=1}^{M} p(A^{-1}x_t)\frac{1}{\det(A)}. \tag{3.10}$$

Using the logarithm function in Equation 3.10 and the relationship of $\log(\det(A)) = -\log(\frac{1}{\det(A)})$ gives the maximum log-likelihood function

$$\log p(D|A) = -\log\det(A) + \sum_{t=1}^{M} \log p(A^{-1}x_t). \tag{3.11}$$

Recall, that the unmixing matrix, W, is defined as the inverse of A. Inserting this relation and taking the derivative of Equation 3.11 with respect to W results in

$$\frac{\partial}{\partial W}\log p(D|A) = \frac{\partial}{\partial W}\log\det(W) + \frac{\partial}{\partial W}\sum_{t=1}^{M}\log p(Wx_t). \tag{3.12}$$

The first term gives $\frac{\partial}{\partial W}\log\det(W) = W^{-1}$ from Equation 13 in [81]. The second term is calculated by making the substitution $z_t = Wx_t$, where z_t is an estimate of the s_t. It yields

$$\sum_{t=1}^{M}\frac{\partial}{\partial z}\log p(z_t)\frac{\partial z_t}{\partial W} = \sum_{t=1}^{M}\frac{\partial}{\partial z}\log p(z_t)x_t. \tag{3.13}$$

Introducing the non-linearity from [76], $\varphi(z)$, as

$$-\frac{\partial}{\partial z}\log p(z) = -\frac{\frac{\partial}{\partial z}p(z)}{p(z)} = \varphi(z) \tag{3.14}$$

[20] δ is only defined when $u_t = x_t$ [75].

and inserting it into Equation 3.12 gives

$$\frac{\partial}{\partial W}\log p(D|A) = \sum_{t=1}^{M}\varphi(z_t)x_t + W^{-1}. \tag{3.15}$$

The derivation of the learning algorithm that maximizes the log-likelihood with respect to W in Equation 3.15, is omitted in this thesis, but can be obtained in [23]. In Equation 7.11 in the study by Amari et. al, [12], it is showed that taking the natural gradient will optimize the algorithm. The final learning algorithm is

$$\Delta W \propto [I - \varphi(Z)Z^T]W. \tag{3.16}$$

Recall that Z is an estimate of S. The next step is to make an assumption about the distribution of the estimated sources, $p(z)$. The following is shown from a single estimated source, z. The super-Gaussian distribution is defined as [76]

$$p(z) \propto p_G(z)\text{sech}^2(z), \tag{3.17}$$

where $p_G(z)$ is a standard normal distribution, $\mathcal{N}(0,1)$ and sech is defined as $\text{sech}(z) = \cosh(z)^{-1}$. Using Equation 3.17 and the definition of the non-linearity ϕ results in

$$\varphi(z) = z + 2\tanh(z), \tag{3.18}$$

where the full deviation is shown in Equation A.3.

Until now, it has been assumed that the sources are distributed as having super-Gaussian distribution. The extended INFOMAX deals with sources distributed both as super-Gaussian and sub-Gaussian. The strictly sub-Gaussian density is defined as

$$p(z) \propto \frac{1}{2}(N(\mu,\sigma^2) + N(-\mu,\sigma^2)), \tag{3.19}$$

where the standard deviation and mean are one [76]. Inserting it into Equation 3.14 gives

$$\varphi(z) = z - \tanh(z), \tag{3.20}$$

where the whole deviation is shown in Equation A.5.

Inserting the results for all source estimates, Z, and for both distributions in the learning algorithm in Equation 3.16 results in

$$\Delta W \propto \begin{cases} [I - \tanh(Z)Z^T - ZZ^T]W & : \text{supergaussian} \\ [I + \tanh(Z)Z^T - ZZ^T]W & : \text{subgaussian} \end{cases}$$

ICA is only valid if it is assumed that each is trial temporal independent, which can be achieved by the experimental design (cf. Chapter 5). Likewise, it is assumed that the number of sources is equal to the channels, where in reality the number of sources contributing to the scalp potential is unknown [118].

3.1.2.1 EyeCatch

The most difficult part in using ICA is to determine which ICA components to reject. It takes several years of experience to correctly classify ICA components, and the process is very time consuming to perform manually. Rejecting an ICA component wrongly will result in removal of neural activity and will in the worst case introduce artificial components to the signal. ICA components contaminated with EOG artefacts will be denoted as eye components.

Recently, automatic or semiautomatic methods have been developed to determine, which ICA components to reject [86, 123]. The newest method EyeCatch [25], is based on spatial correlation between predefined templates and the spatial projections from the unmixing matrix W. Thus, it calculates the maximum spatial correlation between an input scalp map and 3425 eye component templates. A database of ICA components from 80.006 data sets were spatial correlated with 35 predefined eye components. Based on the highest correlations and visual inspection 3425 ICA components from the database were chosen as the predefined templates. These templates are used to detect eye components in new data sets.

EyeCatch showed a great performance comparing it with 11 experts. The area under the Receiver Operator Characteristic curve was 0.993 indicating high sensitivity and specificity [25]. EyeCatch is applied based on its performance and the large population (80.006 data sets). In addition, as the author is not an expert in detecting eye components, it is believed that EyeCatch can provide a better accuracy than the author. However, it is important to notice that EyeCatch is not a perfect algorithm.

EyeCatch is, to the knowledge of the author, the newest method for automatic detecting eye component and has not yet been used in the literature. Therefore, the performance of the method is validated by an eye tracker before applying it. This is elaborated in Chapter 6.

3.2 Event Related Potential Analysis

In an EEG experiment, a participant is presented to a fixed stimulus which is repeated a large number of times. A trial or *epoch* is a time interval locked to the presented stimulus. In the thesis, an epoch is defined as 1.5 seconds before onset of the image and 2 seconds after the image giving an epoch of 3.5 seconds.

The rationale of an ERP analysis is that the neural sources, due to the presented picture, is a time-locked activity (event-related activity) in the epoch in contrast to other ongoing brain and non-brain activity. On the basis of this idea, averaging over multiple trials will serve as a filter operation that cancels all except the event related brain activity. The phase of the ongoing brain activity, that is not related to the stimulus, will differ for each frequency and latency across trials. It means that summing over a number of epochs with random phases, the ongoing activity will be canceled out. Therefore, the trial averaging will not only filter non time-locked events but also non phase-lock events [80]. A drawback of an ERP analysis is the absence of the trial-to-trial variability information in the recorded EEG signals. Both the within-subject variability and the between-subject variability are known to be high in ERP studies, why many trials and subjects are needed.

The components of interest depend on the experimental design and the hypothesis, where this thesis is limited to visual stimulus. Two time windows, an early and late time window, will be used in the thesis consistent with similar studies [60, 93, 97]. Earlier findings within these time windows and the corresponding cognitive functions were explained in Chapter 1. Below is a short presentation of which ERP components that exist in the early and late time windows.

1. **Early time window [0-0.3 s]:** In the early window, the ERP components (C1, P1 and N1) are present. The first visual ERP component, C1, peaks at 80-100 ms with onset at 40-60 ms poststimulus and is located at the posterior midline electrode sites associated with primary visual cortex. It is often difficult to distinguish C1 and P1 as they have temporal overlap. P1 is located at the occipital lobe with onsets between 60-90 ms and peaks around 100-130 ms. The first negative peak, N1, is sometimes divided up into an early and late N1 subcomponent. The early one peaks at 100-150 ms and is located at parietal cortex, where the occipital lobe is the origin of the late N1 subcomponent that peaks around 150-200 ms [79].

2. **Late time window [0.3-1 s]:** In the late time window, three components are of interest: the P300, *Late Positive Potential, LPP* and the slow wave. The P300 and the slow wave is together sometimes referred to as the LPP and starts as a positive wave from 300-400 ms after stimulus onset and continues throughout the picture presentation [78, 93]. The P300 is a positive peak in the interval from 250 to 350 ms depending on the experiment and is most prominent at the central sites. The P300 is often followed by a positive slow wave, which is seen from 400 ms after image onset and continues depending on the duration of the presented stimulus [93].

3.3 Time-Frequency Analysis

The purpose of a time-frequency analysis is to provide additional information to the ERP analysis. As the oscillatory neural activity is non-stationary, the time-frequency analysis is an important tool providing time varying spectral changes [24]. The traditional method is to compute the short-time Fourier transform of windowed segments of the signal, where it is assumed to be stationary. The width of the window used, determines the temporal and spatial resolution of the time-frequency analysis, and introduces a trade-off [118]

$$\triangle f \triangle t \geq \frac{1}{4\pi}, \tag{3.21}$$

where $\triangle f$ and $\triangle t$ are the frequency and temporal resolution respectively. A long time window results in a poor time resolution for high frequencies, where a short time window results in an insufficient frequency resolution. For example, a frequency component of 2 Hz has a wavelength corresponding to 0.5 seconds.

It means that using a time window in the analysis of 0.5 seconds results in a very poor estimate of the frequency component as only one cycle will be present.

In contrast to the short-time Fourier transform, the wavelet transform provides an alternative to optimize the trade-off, by letting the width of the window be dependent on the frequency band. For low frequencies, the wavelet transform uses a long time window, where it uses a narrow time window for high frequencies [24, 118]. The rationale is that high frequencies vary more rapid than low frequencies in time and a higher temporal resolution is therefore necessary [88]. Figure 3.1 visualizes the differences between using the wavelet method and the standard short-time Fourier transform with a fixed window.

The complex Morlet wavelet transformation, $\psi(t, f)$, is a Fourier transform with a Gaussian window function, and is defined by Tallon-Baudry and Bertrand as [116]

$$\psi(t, f) = \frac{1}{\sqrt{\sqrt{\pi}\sigma}} \exp(i2\pi f t) \exp(-\frac{t^2}{2\sigma^2}). \tag{3.22}$$

Here σ determines the width of the Gaussian window function in time and determines the length of the time window for one frequency, f. The advantages of the wavelet transformation is the constant number of cycles, C, given by

$$\sigma = \frac{C}{2\pi f}. \tag{3.23}$$

It is now seen that increasing the frequency, f, shortens the time window through a smaller standard deviation of the Gaussian window function, σ. The choice of C will still have an influence between the spectral and temporal resolution as an increase of σ imply a higher spectral resolution at the expense of the temporal resolution [88, 95]. By a convolution of the complex Morlet wavelet in the time domain with the signal at channel n, $x(t)_n$, it gives the power at time, t, around frequency, f: $P(t, f)_n = |\psi(t, f) * x(t)_n|^2$ [116]. Different wavelets can be used, where the Morlet wavelet is chosen as it has been found very applicable for EEG data analysis [55, 61, 95, 116].

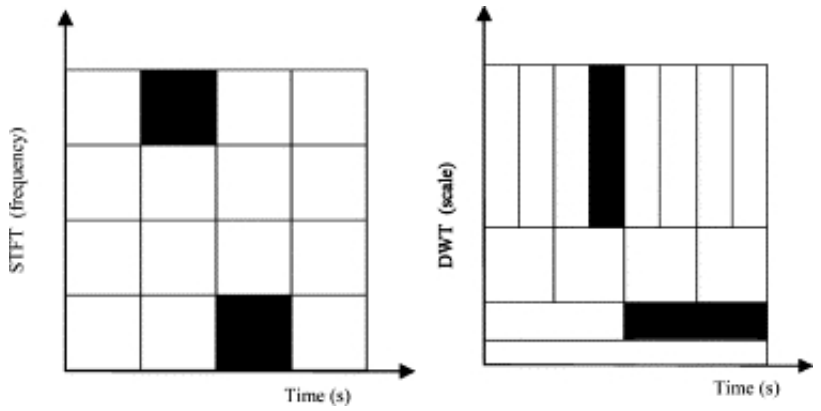

Figure 3.1: The figure shows the differences in the time-frequency domain between the short-time Fourier transform (left figure) and the Morlet wavelet transformation (rigth figure). The image is obtained from [57].

3.4 Source Reconstruction

Source reconstruction is the method of estimating the underlying sources (dipoles) that creates the recorded scalp potential. In order to estimate the sources, the connection between sources and channels need to be defined, which is called a *forward field* [22, 115]. The forward field is modelled from a given headmodel and Maxwell Equations, where the latter is used to describe the physics of EEG. The derivation of Maxwells Equations is omitted here, but is shown by Baillet et al. [22].

The function of the head model is to describe the geometrics (e.g. brain layer conductivity) of the head. Figure 3.2 shows the headmodel used in the thesis. It is a template included in Fieldtrip [96], which is based on the *Boundary Element Method (BEM)*. The BEM assumes homogeneity and isotrophy within each region, where the surface boundaries for the brain, skull and scalp are extracted from a MR scan. The assumption of homogeneity and isotrophy is a simplification, and it contradicts with the knowledge of a real brain [22][21]. Further elaboration of how the head model is constructed is given by Oostenveld et al. [96]. The scalp potentials can from the forward field and the unknown

[21]The Finite Element Method does not assume homogeneity and isotrophy, but is very time consuming to use and is therefore deselected. It is elaborated in [17].

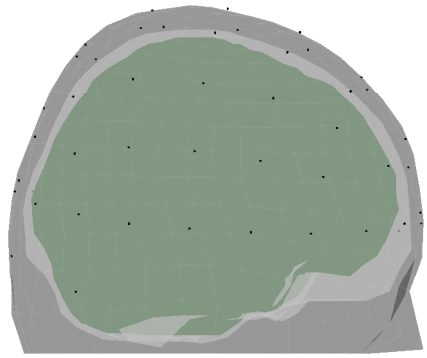

Figure 3.2: The figure shows the template of the BEM head model, [96], where the green area is the brain, the light grey is the skull and the dark grey is the scalp. The small black dots are the locations of the 64 EEG channels.

sources be modelled as

$$X = FS + E, \tag{3.24}$$

where X $(N \times M)$ is the measured potential, F $(N \times K)$ is the forward field model relating the sources to the channels, S $(K \times M)$ is the underlying sources and E is white Gaussian noise matrix with same size as X. Recall from Section 3.1.2 that N is the number of channels, M is the number of time points and K is the number of sources. Notice that unlike Section 3.1.2, the number of sources is not equal to number of channels, and is only representing neural sources. Equation 3.24 is often referred to as *the forward problem*. Estimating the sources from the forward model and scalp potentials is referred to as *the inverse problem* [22].

Several methods have been proposed to solve the inverse problem [115], where the MNE [52] is used in the thesis. The inverse problem is severely underdetermined as $K \gg N$. As the dipole orientation is constrained to be the local surface normal, the inverse problem is linearly with only the amplitudes as unknown.

Because the problem is severely underdetermined, a regularization parameter is needed to restrict the range of solutions and to avoid overfitting [22]. How to determine the regularization parameter is elaborated later in this section. Using Bayes theorem to solve the problem yields

$$p(S|X) = \frac{p(X|S)p(S)}{p(X)}, \tag{3.25}$$

where $p(S|X)$ is the posterior probability of the sources, S, given the recorded data, X. $p(X|S)$ is the conditional probability of the data given the sources and $p(S)$ is the prior distribution of the sources reflecting the known statistically properties of the sources. It is shown, [22], that maximizing the posterior estimate gives a Tikhonov regularization problem also known as ridge regression [22, 37]. The Tikhonov regularization problem is defined as [22]

$$L(\lambda) = \min_S(\|\Sigma^{-\frac{1}{2}}(X - FS)\|_F^2 + \lambda\|S\|_F^2), \tag{3.26}$$

where L is the cost function, λ is the regularization parameter controlling the range of solutions and Σ is the noise covariance matrix. $\|\cdot\|_F$ denotes the Frobenius norm. In general, the first term measures the fitting to the data, where the second term ensures the regularization of the solution.

The deviation of Equation 3.26 to the estimate of the sources is shown from one time point, t, implying that Equation 3.26 can be rewritten as

$$L(\lambda) = \min_S(\sum_{t=1}^{M} \|\Sigma^{-\frac{1}{2}}(x_t - Fs_t)\|_2^2 + \lambda\|s_t\|_2^2) \tag{3.27}$$

Equation 3.27 can be expanded to

$$\begin{aligned} L(\lambda) &= (x_t - Fs_t)^T\Sigma^{-1}(x_t - Fs_t) + \lambda s_t^T s_t \\ &= x_t^T\Sigma^{-1}x_t - 2s_t^T F^T\Sigma^{-1}x_t + s_t^T F^T\Sigma^{-1}Fs_t + \lambda s_t^T I s_t \\ &= s_t^T(F^T\Sigma^{-1}F + \lambda I)s_t - 2s_t^T F^T\Sigma^{-1}x_t + x_t^T\Sigma^{-1}x_t. \end{aligned} \tag{3.28}$$

Taking the derivative of L with respect to s_t yields

$$\frac{\partial L}{\partial s_t} = 2(F^T\Sigma^{-1}F + \lambda I)s_t - 2F^T\Sigma^{-1}x_t = 0. \tag{3.29}$$

Isolating s_t is achieved by moving the second term to the right hand side and taking the inverse[22] of the term in the brackets

$$s_t = (F^T\Sigma^{-1}F + \lambda I)^{-1}F^T\Sigma^{-1}x_t. \tag{3.30}$$

Using The Woodbury Identity lemma[23] [99] gives

$$s_t = \lambda^{-1}F^T(F\lambda^{-1}F^T + \Sigma)^{-1}x_t = F^T(FF^T + \lambda\Sigma)^{-1}x_t. \tag{3.31}$$

The regularization parameter controls the fitting of the source reconstruction. As the regularization goes towards zero, the second term in Equation 3.26 becomes negligible. From Equation 3.26, it is seen that having zero regularization implies that the minimum is $X = FS$. Thus, besides a possible residual term, zero regularization means a full fitting solution. However, letting the regularization term going towards infinity, the first term in Equation 3.26 vanish. It implies that the second term in Equation 3.26 is minimized, when $S = 0$.

In order to find the optimal value of the regularization parameter, the parameter is determined for each subject by a cross validation approach. Thus, the model is first trained on a training set and afterwards tested on a test set. The regularization parameter is then found with respect to minimize the *mean squared error, MSE*, of the test set [26]. In the thesis, the MSE is defined as

$$MSE = \frac{\sum_{n=1}^{N}\sum_{t=1}^{M}(X(n,t) - U(n,t))^2}{\sum_{n=1}^{N}\sum_{t=1}^{M}X(n,t)^2}, \tag{3.32}$$

where *X(n,t)* and *U(n,t)* are the true and estimated potential respectively at channel n to time t.

[22] This operation is straight forward as it is a squared matrix.
[23] $(P^{-1} + B^TR^{-1}B)^{-1}B^TR^{-1} = PB^T(BPB^T + R)^{-1}$ [99].

In Chapter 5, an example is shown of how the parameter is determined, and Figure 5.7 shows the MSE of the training- and test set vary as a function of the regularization. An estimate of the regularization parameter can be calculated in the white Gaussian noise case[24] by the largest value of the singular value decomposition of the matrix FF^T [22, 77].

3.5 Summary

In this chapter, the theory behind the methods used in the thesis was elaborated. The first part described the importance of choosing a proper filter depending on the purpose of the study. Next, ICA was elaborated in details to give the reader an understanding of the method. The thesis uses the ICA to remove EOG artefacts, but also as a part of the validation of the EyeCatch method in Chapter 6. In the last part, the theory of three different analyzing methods were described. With an understanding of the three methods, the next step is to test the hypotheses statistically, which is elaborated in the next chapter.

[24]The white Gaussian noise case implies $\Sigma = I$.

Chapter 4

Cluster-Based Permutation Test

This chapter explains, the non-parametric cluster-based permutation test used throughout the thesis to test different hypotheses statistically, and is based on the work by Maris et al. [82]. The cluster-based permutation test is complex to explain and understand, and is not as well-known as the other methods used in the thesis. Therefore, important concepts and simulations are defined in order to ease the reader's understanding of the test. As the test is an essential part of the thesis, it is assigned to its own chapter.

The chapter is divided up into three sections.

1. First section defines the MCP and outlines the motivation behind the test.

2. The test is then elaborated step by step, supported by a small simulation to visualize the procedure.

3. In the last section, a more detailed simulation study is presented to investigate and discuss important parameters of the test.

4.1 Multiple Comparison Problem

In neuroscience, the MCP is a common problem. As the spatiotemporal location of the differences between two conditions are rarely known, multiple tests need to be computed. If it was known beforehand, in which spatiotemporal sample the effect of the experiment would be, a simple t-test would be sufficient to test the null hypothesis. Testing a hypothesis, four different outcomes are possible. The hypothesis can be correctly rejected or correctly accepted. The two errors are false positive and false negative, and are denoted *Type I error* and *Type II error* respectively. The precise definition of the Type I error[25] is giving as

Definition 4.1 *The Type I error is the probability under the null hypothesis of falsely concluding that there is a difference between the experimental conditions* [82].

In hypothesis testing, the p-value is the chance of making a Type I error [45]. Before testing a hypothesis, a level of significance is chosen reflecting how large a probability of making a Type I error is accepted prior to rejecting the hypothesis. Often, the level of significance is chosen to be 0.05 or 0.01 meaning that the probability of making a Type I error is either 5 % or 1 % respectively. For example, conducting a test with a significance level of 5 % means that the hypothesis is rejected with a 5 % chance of making a Type I error. However, testing multiple tests of the same null hypothesis increases the probability of making a Type I error, and the p-value is longer equal to the probability of making a Type I error. This p-value and the level of significance can therefore not be compared. This issue is the MCP and is defined as

Definition 4.2 *The Multiple Comparison Problem is due to a large number of statistical comparisons, where it is not possible to control the Type I error rate by means of the standard statistical procedures that operate at the level of a single sample* [82].

The main reason for using the cluster-based permutation test is to solve the MCP and thereby control Type I error and to keep a valid level of significance. It is done by testing all samples in one single comparison through the clustering approach.

Other methods have been proposed to solve the MCP, where in particular the Bonferroni inequality [56] has been widely used. The Bonferroni-corrected p-value is defined as α/J, where α is the critical significance value from which the

[25] The Type I error is also called the family-wise error rate or false alarm rate.

null hypothesis is rejected, and J is the number of total samples. The data structure in the thesis is [spatio × temporal] or [spatio × spectral × temporal], meaning that the number of tests (one for each sample) will be very large. Bonferroni inequality method will in such case be very conservative. It can be illustrated with a simple example, where significance level is 0.05 and the data consists of 64 channels and 1200 time samples, giving 76.800 samples in total. The Bonferoni-corrected critical value would in this example be $^{0.05}/_{76.800} = 0.0000007$. Including the frequency dimension would imply an even lower critical value showing the criticism of using the Bonferroni inequality method to solve the MCP [82].

4.2 Cluster-Based Permutation Test

The cluster-based permutation test will be explained on the basis of a data structure of [spatio × temporal], where each point[26] will be referred to as a sample. Two types of designs will be used in the thesis, a *between trials* for a single subject and a *within subjects* for multiple subjects, where the former design is used to explain the method.

The cluster-based permutation test is used to test the null hypothesis, H_0, which is defined in Definition 4.3.

Definition 4.3 *The null hypothesis at subject level is defined as all m conditions have same probability distributions [82]:*

$$H_0 : f(D_1) = ... = f(D_m), \tag{4.1}$$

where $f(D_1)$ and $f(D_m)$ are the probability distributions for condition 1 and condition m respectively. Furthermore by rejecting H_0, one concludes that the probability distributions are modulated by the experimental design [82].

Definition 4.3 is only valid under the assumption of statistically independence between the trials in the experiment. In practice, it means that the EEG signal has to return to baseline before the next trial is initiated.

The cluster-based permutation test consists of three major steps. First the clusters need to be formed, then the corresponding cluster level test statistic needs to be calculated, and finally the clusters are tested against an estimated

[26] One channel and one time point.

permutation distribution. From the data described in Simulation 4.4, and the work done by Maris et al. [82], the following steps will explain, in details, the procedure of conducting a cluster-based permutation test to solve the MCP.

Simulation 4.4 *The first simulation is used to visualize the procedure of the cluster-based permutation test. The data simulates an epoch of 600 samples from one channel with two experimental conditions defined as Condition 1 and Condition 2. Each condition has 50 trials and the averaged signal of the conditions are seen in Figure 4.1a.*

1. The total data-set (Simulation 4.4) consists of 100 trials, where *the true observation* is defined as the separation of the data into Condition 1 and Condition 2 with each 50 trials. The two conditions are seen in Figure 4.1a. For each sample [channel $\times$ time points] the independent two sided t-test statistic is calculated with a given significance level defined as *cluster alpha*[27]. Figure 4.1b shows the t-test statistic for each sample with a significance level of 5 % (cluster alpha = 0.05) seen as the red vertical line.

2. Samples, whose t-values from step 1 exceeded the cluster alpha (the red line in Figure 4.2a), are potential candidates to be included in a cluster. The cluster alpha is a controllable parameter that reflects how sensitive the test is. Section 4.3 examines through simulations the influence of this parameter.

3. It is now possible to form the clusters on the basis of temporal and spatio adjacency. Temporal adjacent timepoints exceeding the threshold in step 2 will form a cluster in the temporal dimension. The sign of the cluster is maintained as it has importance for the analysis, e.g. which condition exhibits the highest amplitude or consists of most power. Figure 4.1c shows the five clusters formed from the simulated data. It is seen that the clusters are aligned with the visual difference between the two conditions.

   The clustering of channels (spatial dimension) are done on the basis of a neighbor structure defining which channels that are neighbors. It is done by the euclidean distance[28], where a *max distance* is given as input to define the maximal distance between two channels that are neighbors.

4. By taking the sum of the t-test statistics, T, in each cluster, $CT = \sum_{l=1}^{j} T_l$, the cluster level test statistics, CT, are calculated[29]. j denotes the number of samples within the cluster,

[27] The notation cluster alpha is used to be consistent with the code implemented in the Fieldtrip framework.

[28] There are different methods to define the neighbors, e.g. from a pre-defined neighbor structure.

[29] An alternative is to calculate the number of samples in each cluster, however the sum

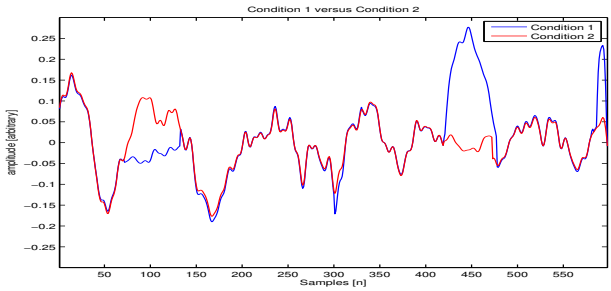

(a)

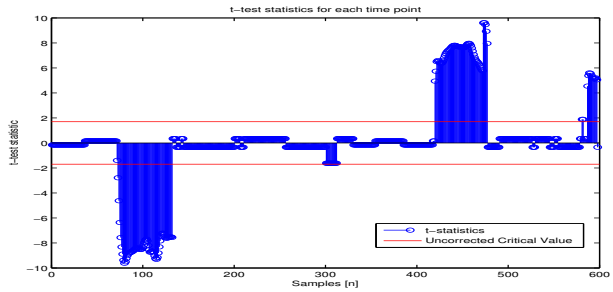

(b)

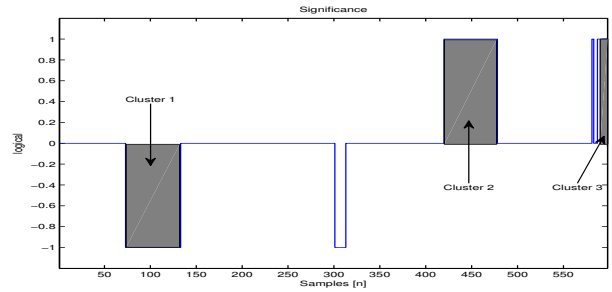

(c)

Figure 4.1: The figures show the idea behind forming the clusters from the "true observation". In figure a) the two signals correspond to the two conditions. There are three clear differences, from sample 50-150, 420-480 and the last 40 samples. In figure b) the t-test statistic for each sample is seen with the corresponding uncorrected critical value, which is the parameter *cluster alpha*. Figure c) shows that five clusters are formed, where the grey color indicates that they are significant. Samples within the white clusters were found significant from the t-test, but insignificant by the cluster-based permutation test. Notice that the clusters are both positive and negative, and that it is possible to have several significant clusters in one test.

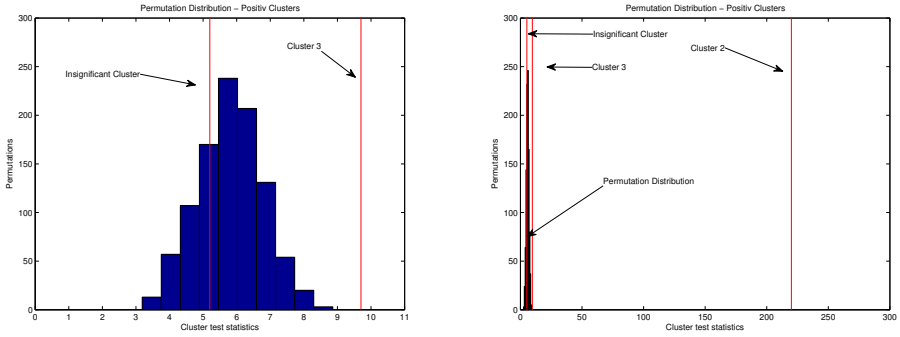

(a) **(b)**

Figure 4.2: The figures show the permutation distribution for positive clusters and the corresponding three *positive* clusters from Figure 4.1. It is seen that Cluster 2 and 3 are significant.

5. The next step involves the creation of the permutation distribution of which each of the five clusters in Figure 4.1c are tested against. The trials from each condition is combined with a single set of 100 trials. The data is then randomly separated, independently on the conditions, into two new subsets of each 50 trials. This new subset is a *random permutation*. This operation is valid as the null hypothesis states that all trials are drawn from the same distribution independently on the experimental condition, cf. Definition 4.3.

6. Step 1-4 are now repeated with the random permutation in order to find clusters and their corresponding cluster level test statistics. The cluster with the *largest* absolute cluster level test statistic value is selected and used to establish the permutation distribution.

7. By repeating step 5 and 6 *k-times* a *k-sample* distribution, called the permutation distribution, is established. 1000 random permutations were used for the simulated data and the corresponding permutation distribution is shown in Figure 4.2.

8. The clusters formed from the true observation are now tested against the permutation distribution from the previous step, in order to obtain the permutation p-value for each cluster.

of the t-values approach is used throughout the thesis. For an elaboration of the different approaches see [54].

Since, it is practical impossible to obtain the true permutation p-value[30], a Monte Carlo estimate of the p-value is made instead, based on k-permutations. k is often chosen to 1000 for a significance value of 5%. The Monte Carlo p-value explains how many random permutations that have a higher cluster level test statistic than the original one(s) from the true observation. It is calculated as

$$p = \frac{1 + \sum_{i=1}^{k} I(CT_i \geq \hat{CT})}{k+1}, \tag{4.2}$$

where k is the number of permutations, $\hat{CT}$ is the true cluster level test statistic and I is a logic function counting one if CT_i is larger than $\hat{CT}$ and zero otherwise. It follows from the Equation 4.2 that the minimum Monte Carlo p-value is $\frac{1}{k+1}$ [40]. Figure 4.2b shows the two significant positive clusters, one positive insignificant cluster and the permutation distribution of 1000 permutations.

4.2.1 Extensions of the cluster-based permutation test

Until now, the data is assumed to be [spatio × temporal]. Dealing with 3D data [spatio × spectral × temporal], the number of calculated t-values increases, but the procedure remains the same as the previous steps. A sample is now defined as one channel, one frequency bin and one time point. The clustering of the samples in the time-frequency domain within one channel is visualized in Figure 4.3. Samples with grey color illustrates samples that exceed the cluster alpha as described in Step 2, where the white pixels were below. Determination of neighboring channels is identical to the 2D data approach.

Until now, the test has been explained from a single subject *within trial* experiment point of view. Using the method to test a hypothesis on group level, *within subject* experiment, the sample level statistics are now a dependent t-test instead of independent t-test, as the samples are subject specific [82].

The subject specific averages for the r'th subject are defined as a pair (D_{r1}, D_{r2}) with D_{r1} being the averaged of the trials belonging to Condition 1 and D_{r2} for Condition 2.

It also changes the null hypothesis in Definition 4.3 to

[30] Obtaining the true permutation p-value would require to make a permutation distribution of all possible permutations.

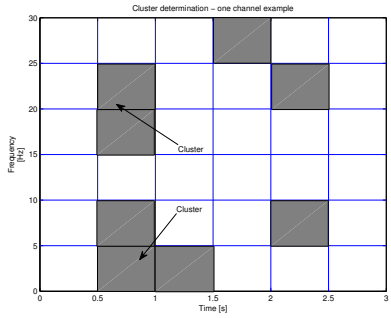

Figure 4.3: The figure shows how a cluster is formed for data with both the spectral and temporal dimension. The example is shown for one channel. Squares with grey color corresponds to the samples that exceeded the uncorrected critical value (threshold for the t-test statistic on sample level), corresponding to the parameter cluster alpha.

Definition 4.5 *The null hypothesis on group level is defined as the marginal distributions for all conditions m within each subject are equal:*

$$H_0 : f(D_{r1}, D_{r2}) = f(D_{r2}, D_{r1}) \tag{4.3}$$

Rejecting the null hypotheses, therefore implies that the marginal distributions for D_{r1} and D_{r2} are different due to modulation of the experimental design [82].

The permutation distribution is now conducted by randomly permuting the subject specific averages within each subject instead of randomly changing the trials [82]. For an experiment with three subjects and two conditions the true observation would be (D_{11}, D_{12}), (D_{21}, D_{22}) and (D_{31}, D_{32}). A random permutation could be: (D_{11}, D_{12}), (D_{22}, D_{21}) and (D_{31}, D_{32}), where (D_{22} and D_{21}) have swapped order, which is valid due to the definition of the null hypothesis on group level, cf. Definition 4.5.

It is important to notice, that it is only possible to obtain a weak control of the Type I error as the channels not are completely independent of each other. Therefore, the null hypothesis is actually a global null hypothesis. It means that if a significant difference between two conditions are found in one channel, it is not possible to conclude that the difference is not present in other channels as well [82].

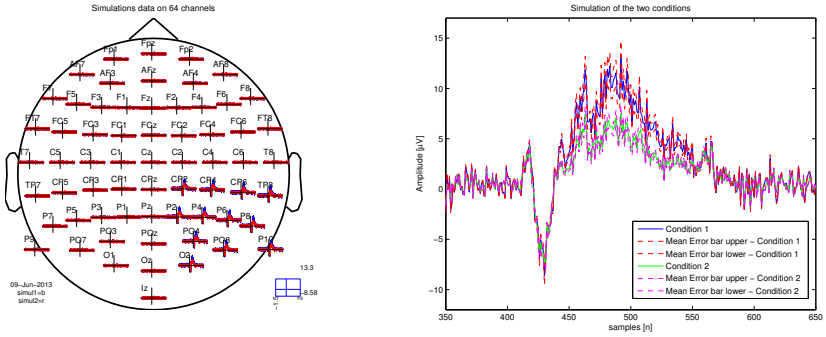

(a) **(b)**

Figure 4.4: The figures show the simulated data, where a) shows that the two signals are present in 12 channels at the right centro-parietal and right parietal-occipital area. Figure b) shows the two averaged signals of 120 simulated trials with the correspoding mean error bar. The blue signal is Condition 1, where the red color reflects Condition 2.

4.3 Simulation

The purpose of the simulations is to investigate the influence of cluster alpha and how the amount of samples manipulates the significance of a cluster. Two time windows are used, a large window consisting of all samples and a narrow window consisting of the samples from 400 to 600. The simulated data is defined in Simulations 4.6 and is seen in Figure 4.4.

Simulation 4.6 *The simulated signal is created from a real ERP response to a visual stimulus. The difference is simulated from sample 440 to 550 as seen in Figure 4.4 with added white noise, N(0,*σ_{noise}*). *σ_{noise}* depends on varying SNR value defined as*

$$\sigma_{noise} = \frac{\hat{x}^2}{M \cdot SNR}, \tag{4.4}$$

where M is number of samples in the simulated signal, $\hat{x}$, and σ_{noise} is the standard deviation of the added noise.

Each condition is simulated with 120 trials, each multiplied with a random num-

ber ranging from zero to one introducing variability across the trials. For the spatial dimension, the simulated differences between the two conditions are located in 12 channels in the right centro-parietal and right parietal-occipital area as seen in Figure 4.4a. The other 52 channels consist of white noise.

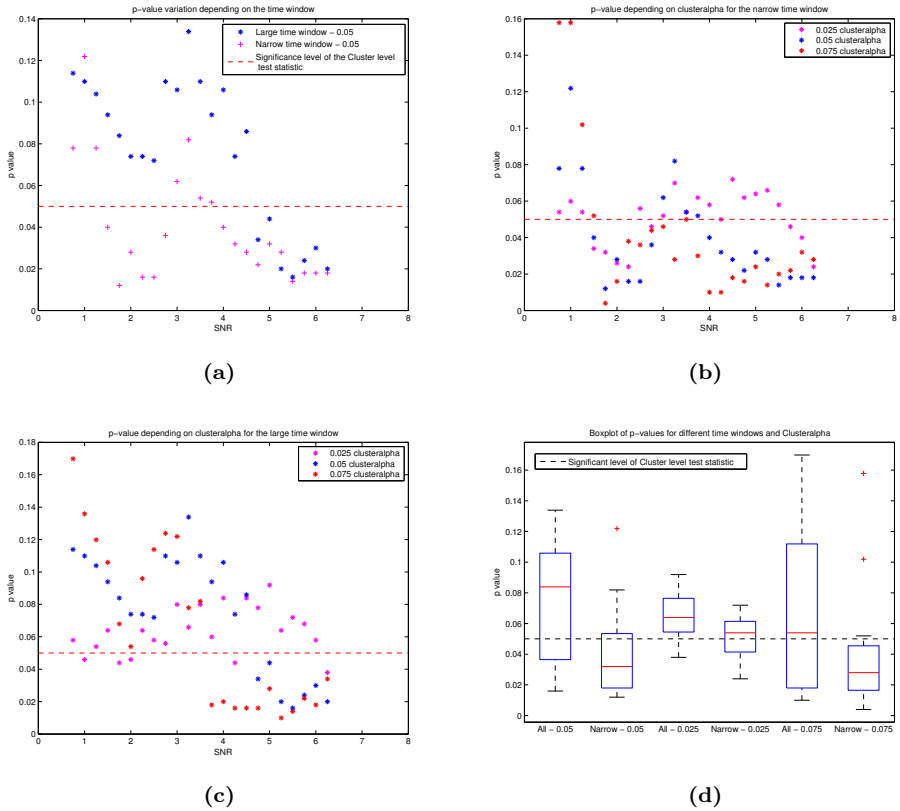

Figure 4.5: The figures show the results from the simulation study. In figure a) it is seen that narrowing the window in the test will decrease the p-value and make it less sensitive to noise. Figure b) and c) show how the p-value for the cluster is changed as the parameter *cluster alpha* varies. Lowering the value will make it less sensitive to noise. However, a large difference between two conditions are needed to make it significant. Increasing the cluster alpha value makes the cluster very sensitive to noise. Figure d) summarizes the variation of the different parameters and shows that these parameters have an important influence when using this test.

Figure 4.5a shows that by decreasing the SNR, the cluster becomes insignificant meaning that the simulated difference is vanished due to the added noise. Decreasing the amount of samples to a narrow time window, the same cluster is still significant for a SNR value of 2 in contrast to the large time window. It clearly shows that narrowing the time window in the analysis can change the result of the analysis and the conclusion of accepting or rejecting the null hypothesis. This is however not surprising, as the method has to correct for fewer samples when solving the MCP.

The cluster alpha controls the sensitivity of the test. Increasing the parameter will decrease the threshold of the t-test on sample level in Step 2 (the red line in Figure 4.1b) and thus increase the number of samples exceeding the threshold. Likewise, a decrease of cluster alpha will increase the threshold and the sensitivity implying a decrease of samples exceeding the threshold.

Figure 4.5b and 4.5c show how the p-value varies with three values of cluster alpha (0.025, 0.05 and 0.075) for the narrow and large time windows respectively. A cluster alpha value of 0.025 is more stable against a varying SNR. It is constant around the level of significance. It implies that both the SNR and contrast between the two conditions have to be high before a cluster is found significant. However, in noisy data, this approach could be preferred to find tendencies in experiments. For the high cluster alpha value, the highest variance is seen making it very sensitive to noise. By changing the cluster alpha, it is possible to manipulate the outcome of the analysis. Testing several cluster alpha values introduces another MCP, which also should be corrected.

4.4 Summary

This chapter explained the MCP and why it is necessary to correct for in order to make a proper conclusion for the hypotheses. It presented the cluster-based permutation test as a method to solve the MCP, which was elaborated step-by-step. It was shown, from a simulation study, that changing the time window and the cluster alpha value, it is possible to modulate the result of the test and in the end change whether the null hypothesis should be rejected or accepted.

Chapter 5

Methods

This chapter presents the experimental design, the preprocessing pipeline and data analysis. Reading this chapter will ease the readers understanding of the results in Chapter 7. It is divided into five sections:

1. The first section describes the participants in the experiment.
2. The second section explains the used stimulus and the experimental design, which was changed and improved after the first two participants.
3. Section three provides a description of the EEG and eye tracker systems.
4. The preprocessing pipeline is elaborated step by step corresponding to Figure 1.2.
5. The last section describes how the data analysis methods, explained in Chapter 3, is implemented and used.

This chapter is also dedicated to the work of Ivana Konvalinka and Carsten Stahlhut, as they designed, modified and implemented the experiments, in co-operation with the author.

5.1 Participants

Thirteen females volunteered for the study recruited via the Center for Visual Cognitions facebook site. They all gave written informed consent. The participants were healthy and did not take any form of medication. Furthermore, all had normal or corrected to normal vision.

Many parameters have an influence on the EEG signal when a participant is presented to a picture. The idea is to isolate the parameters which are studied. It is achieved by controlling other parameters as much as possible. Therefore, as women and men rate pictures from the *The International Affective Picture System, IAPS*, differently [27], the participants in the experiment were only females. The ages of the participants ranged from 22 to 31 with an average age of 25. The experiments were conducted over seven days.

5.2 Task and Procedure

This section describes the used stimulus from the IAPS and the changes of the experiment leading to the final experimental design.

5.2.1 International Affective Picture System

The IAPS is a database that categorizes pictures in three dimensions. The first dimension is *valence* varying in a pleasure scale form pleasant to unpleasant. The second dimension is *arousal*, where the pictures are rated in a calm/exciting scale. The last dimension is a *dominance* scale rating the pictures with low or high dominance [74]. The database is widely used in experiments studying emotion or attention [44, 60]. Figure 5.1 shows how different images are rated in the three dimension, which also illustrates the gender differences, which were mentioned previously.

In the thesis, the pictures are divided into three groups and are referred to as positive, negative and neutral pictures. Positive pictures[31] have a high arousal and pleasure scale, where negative images[32] have high arousal ratings but low pleasure score. Neutral images[33] have a low arousal rating and is in the middle

[31] Positive pictures could be erotic pictures, pictures of a happy family or baby pictures.
[32] Negative pictures could be threats like snakes or spiders, but also mutilated bodies.
[33] Neutral images are for example a cup or a pencil.

of the pleasure score. The 240 pictures that were used correspond to a number in the database, which is specified in Appendix B. The dominance scale is not used in the thesis similar to other studies looking at emotion and arousal [35, 38, 60].

5.2.2 The Experimental Design

The experimental design is a 2×3 within subject design with the social context (Alone and Together) and emotional content of the pictures (Positive, Negative and Neutral) as the two factors. For each participant, it gives the following six conditions with each 40 images:

1. Alone with neutral images.
2. Alone with positive images.
3. Alone with negative images.
4. Together with neutral images.
5. Together with positive images.
6. Together with negative images.

The images were pseudo-randomized, but with the two social conditions containing the same mean arousal/valence score across all images. Likewise, the order of the presented images was pseudo-randomized, such that the participants never received an image from the same emotional class more than twice in a row.

The participants were seated 62 cm from a computer screen in an electrically and acoustically shielded EEG cabin connected to the EEG recording system and eye tracker system. The chin was leaned to a stand to brace the head and minimize movements. Furthermore, the stand was fastened to the table, where a keyboard was placed in front of the participant. The other person in the EEG room, during the Together condition, was sitting behind and to the left of the participant.

5.2.3 Improvements of the Experimental Design

The procedure of the first experimental design is seen in Figure 5.3a. It begins with a 3 second long condition message on the screen stating whether the participant is viewing the pictures alone or together. Then, a fixation cross appears

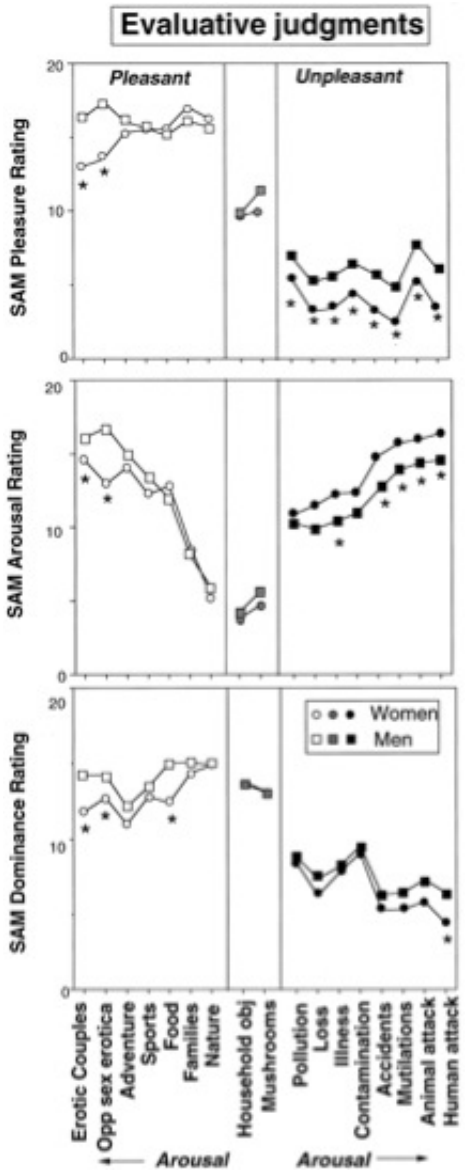

Figure 5.1: The figure outlines the three dimensions that describe the pictures in IAPS. Positive pictures have a high arousal and high pleasure score, where negative pictures have high arousal and low plesure score (unpleasant). Neutral pictures have a low arousal score and a middle pleasure score [27].

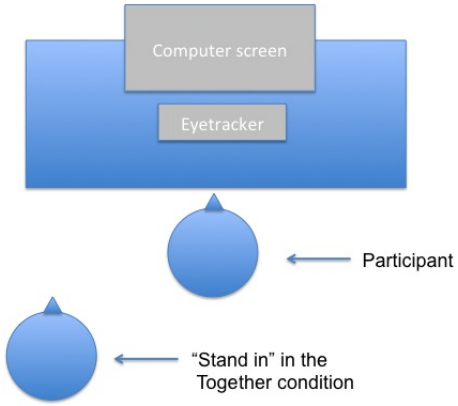

Figure 5.2: The figure shows the experimental setup and how the participant and the "stand in" are sitting relative to each other, in the Together condition.

for 2 seconds, followed by the picture for 2 seconds. After the two seconds, the participant gets a message saying: *press return when ready to continue*. A new trial is then initiated as soon as the participant pressed return.

The following improvements were made going from the first to the final experimental design:

1. A pilot study prior to the actually experiment was conducted[34] to investigate the task and procedure. After the pilot study, the pictures on the screen were scaled down to a height of 12 cm and a width of 16.3 cm, yielding a visual angle of 15 degrees horizontally and 11 degrees vertically, consistent with previous studies [60]. If a picture is large and too close to the participant, the field of vision will be smaller, which could introduce more eye movement.

2. After the pilot, it was suspected that the participants did not pay attention to the condition message stating if the picture was viewed alone or together. The first two participants confirmed this suspicion as they stated that they did not pay attention to the condition message and did not realized whether they viewed the pictures alone or together. The experimental design was therefore changed from writing the social condition to actually having another person seated next to the participant jointly looking at the images. The condition message in the final experimental de-

[34]My co-supervisor was used as a participant.

sign was therefore replaced by a *Get Ready* message. The social condition was changed after the first half of the experiment (120 trials).

3. The trials need to be independent of each other. It is ensured by the condition message of three seconds. The independence of the trials is a necessary assumption before performing the cluster-based permutation test and ICA. Furthermore, it gives the participant the opportunity to blink, cough and make small movements if needed.

4. The duration of the fixation cross was lowered to 1.5 seconds. As mentioned, several repetitions are needed in an EEG study increasing the possibility of participants getting tired. Lowering the duration of each trial will minimize the probability of blinks and the participant getting tired. However, the time interval between the fixation cross and image onset has to be of sufficient length so the EEG signal will reach the baseline prior to image onset.

The experimental design makes it possible to test different hypotheses. The within-subject design has the advantage to increase the statistical power compared to a between-subject experiment. Moreover, the error variance is also decreased as the same subjects are used for all conditions, which is an important factor in the thesis as the number of participants is low.

A disadvantage is the fatigue effect, a negative effect meaning that the mind and motivation from one subject might change during the experiment. It is known that participants can get tired in EEG experiments as many repetitions are required. Therefore when running the second half (either Alone or Together), the motivation and tiredness could change and affect the results. There could also be a practice effect meaning that the participants do not respond as strong to positive and negative images in the end of the experiment compared to the beginning [87]. The fatigue and practice error are of concern as the number of participants is low in the thesis. Therefore, the order of the social context was counterbalanced.

5.2.4 The Final Experimental Design

The experiment was modified with the four previously described items. The procedure for the final experiment is seen in Figure 5.3b. It begins with a message saying: *Get Ready.* Then a fixation cross appears for 1.5 seconds, followed by an image for 2 seconds. After the 2 seconds, the participant receives a message saying: *press return when ready to continue* and a new trial is initiated as soon as the participant pressed return. After 120 images a small break is

given, where the Alone/Together condition is changed by seating or removing the other person. The last 120 images are then presented. The order of the social condition is counterbalanced to block out the parameter of when the other person is present.

After seeing all 240 images, the participants rated 60 images, that they had previously seen, in the scales: pleasant - unpleasant, calmed - aroused.

The procedure for one participant can be summed up as follows:

1. The participant read the information sheet and signed the written consent.
2. The participant received instructions of the experiment.
3. The participant saw examples of pictures similar to the ones presented in the actually experiment.
4. Preparation of the participant (connecting the EEG and eye tracker systems).
5. The participant is seeing the first half of the task (120 images).
6. The social condition is changed, and the next 120 images are presented for the participant.
7. Disconnecting the EEG equipment.
8. The participant rated 60 images.

5.3 EEG and Eye Tracker Systems

This section explains the set-up of the EEG and eye tracker system respectively.

5.3.1 EEG System

EEG was recorded from the participant during the task using a 66 Biosemi "Pin-type" active electrodes with a sintered Ag/AgCl electrode tip (64 channels including CMS and DRL channels) and a Biosemi headcap [1]. The electrodes were placed in the positions of the international 10-10 system described in Chapter 2 with a layout identical to Figure 2.2. It was ensured that the input impedance was kept below 25 kΩ by creating a good contact surface between the

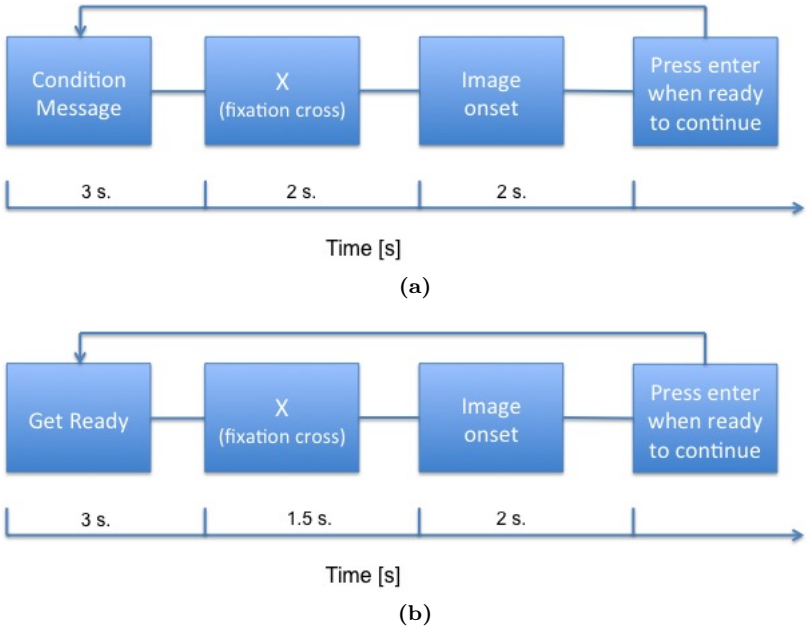

Figure 5.3: Figure a) shows the experimental design of the pilot study. It begins with a 3 second message stating the condition (alone or together) followed by the fixation cross of 2 seconds. Then the image is on for 2 seconds followed by a message saying *press return when ready to continue*. The participant therefore has time to move a little and get comfortable before next trial begins. b) The design of the final study follows the same procedure as the pilot study but with two small changes. The first message is now: *Getready* instead of stating the condition. It is changed because the second person now is seated in the EEG cabin during the first or second half of the experiment. The second change was the duration of the fixation cross which was lowered to 1.5 seconds.

electrodes and skin. This was partly achieved by applying electrode gel in the holes of the headcap. A visual inspection of the input impedance and the signals ensured that noise on the channels was minimized. An ActiveTwo AD-box [1] was used, which was optically coupled to the computer. The sampling rate was 2048 Hz. An analog high-pass filter with cut-off at 0.16 Hz and an analog low-pass filter with cut-off at 100 Hz were used. Event triggers corresponding to conditions were sent to the EEG system at the beginning of each image onset.

5.3.2 Eye tracker System

Eye-tracking was recorded with Eyelink 1000, SR Research Ltd., Mississauga, Canada [5]. It recorded eye movement using monocular pupil tracking at 1000 Hz. The eye position for each subject was calibrated and validated using a 9-point grid procedure. Eye movement was detected with saccades above 0.1 degrees. It was possible to visually validate the quality of the eye tracker during the recording. The eye-tracking recordings were sensitive implying that only few subjects had eye-tracking recordings of good quality. Event triggers also send to the eye tracker in order to align the EEG and eye tracker system. In the thesis, the purpose of the eye tracker is to validate the performance of EyeCatch, which is elaborated in Chapter 6.

5.4 Data Preprocessing

For the data processing and analyzing Fieldtrip[35] [95], a MATLAB[84], software toolbox was used. EEGLAB, [36], another MATLAB [84], software toolbox, was used for applying ICA and EyeCatch.

Figure 1.2 sums up the pipeline for preprocessing, where each step corresponds to the description below.

1 The continuous data is loaded into Fieldtrips environment.

2 Before epoching the data, a high-pass and low-pass filter is applied on the continuous data. Both filters were zero-phase shift IIR Butterworth filters of order four. The cut-off frequencies were 0.1 Hz and 40 Hz respectively. Earlier studies have used a cut off frequency for low-pass filtering ranging from 20 to 40 Hz [71, 30, 32, 60]. The low pass filter is applied to remove

[35] Fieldtrip version 20130124 was used.

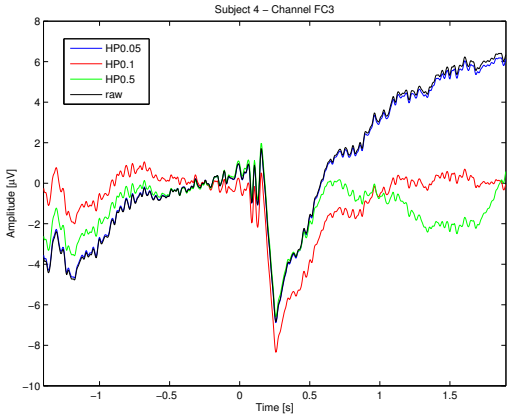

Figure 5.4: The figure shows the ERPs after applying three different filters, for subject 4 at channel FC3. The blue color shows the ERP after applying a high-pass filter with a cut-off frequency of 0.05 Hz. It is seen that the linear drift is still present. The linear drift is removed for the ERP of the red color, which uses a cut-off frequency at 0.1 Hz. The green ERP signal is a high-pass filter with a cut-off at 0.5 Hz, where it is seen that the shape of the ERP is modulated. The yellow ERP shows the signal without applying any high-pass filter.

high frequency noise including EMG artefacts, while making it possible to analyze frequencies in the beta band.

On the basis of the discussion in Chapter 2 several cut-off frequencies for the high-pass filter were tried. As a linear drift was present in some subjects, it was necessary to apply a high-pass filter. Figure 5.4 shows an epoch and three different cut-offs to remove the linear drift. For a cut-off frequency with 0.05 Hz (blue color), the linear drift is still seen where a cut-off at 0.5 Hz (green color) distorts the ERP shape. A cut-off frequency of 0.1 Hz (red color) is chosen as the epoch is undistorted and the linear drift is removed. Furthermore, it is in accordance with the recommendations from [79] as discussed in Chapter 2. The low-pass and high-pass filters were both applied prior to epoching to avoid a windowing effect on the epoched data.

3 The epochs of the data are defined from the event triggers send to the EEG system corresponding to image onset. One epoch (trial) is defined as 1.5 seconds prior to image onset (trigger event) and 2 second after image onset giving a total duration of 3.5 seconds. The time prior to image onset

is important to get an identical baseline for both conditions. Fieldtrip's implemented function that finds the triggers could not be used for this data-set, so a custom made MATLAB script was written by the author and integrated within the framework of Fieldtrip.

4 After epoching, baseline correction was applied on epoch level by subtracting the mean. In the thesis, the averaged reference method was used as the 64 channels were distributed uniformly over the head by the 10/10 labeling system as explained in Chapter 2. At last, the signals were downsampled from 2048 Hz to 256 Hz to lower the computational time when processing the signals. A sampling frequency of 256 Hz is sufficient according to Nyquist's sampling theorem [75] and the frequencies of interest (0-30 Hz).

5 Manual inspection is a necessary and an important step in order to check the quality of the data and remove bad trials and/or channels. However, looking through all the channels and trials is very time consuming, why they were evaluated on the basis of the variance. Figure 5.5 shows the variance for all trials and channels for subject 12, where trial 111 showed a high variance. Before rejecting trial 111 a detailed examination is performed. Figure 5.6 shows the data for subject 12 trial 111. It is seen that some low frequency noise caused the high variance and the trial was therefore rejected. If a channel was detected a bad (high variance), it is replaced by an estimate found from interpolating the average of the nearest channels[36]. Table 5.1 shows an overview of removed trials and channels for each subject.

6 The data was converted into EEGLAB environment as EEGLAB and Fieldtrip use different frameworks. Despite that Fieldtrip has a function implemented to go from Fieldtrip to EEGLAB, several modification were necessary to make, as the function was outdated. EEGLAB is used for ICA and EyeCatch as EyeCatch is not implemented in Fieldtrip.

7 The ICA algorithm used in the thesis is the extended Infomax, which is derived in Chapter 3. The performance of ICA is dependent on the amount of noise in the data and the number of small sources. If these increases, the performance will decrease. It is therefore recommended to perform ICA on as clean data as possible [80]. The extended Infomax algorithm was chosen as it is widely used in similar studies [36]. In addition, the majority of the templates used in the EyeCatch software were also based on the extended Infomax [25]. Examples and discussions of different ICA components are presented in Chapter 6.

8 The EyeCatch software is used as an automatic algorithm to detect EOG artefacts. Chapter 6 elaborates the use of EyeCatch and how the eye

[36]The procedure is done with Fieldtrip's function, ft_sourceinterpolate [95].

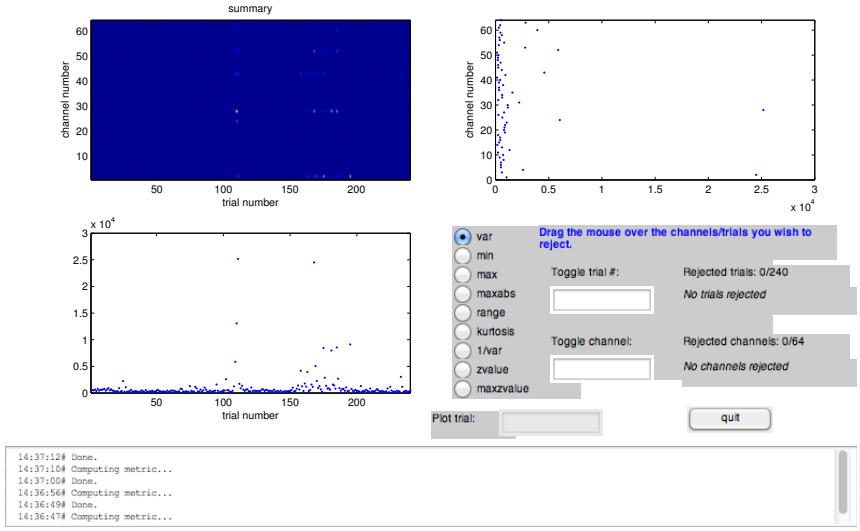

Figure 5.5: The figure shows an example of a visual inspection of subject 12. It is seen that several trials have very high variance. Two of the channels show a high variance, however after a more detailed inspection the channels were not continously bad, why the trials were removed instead of the channels.

Subject	Trials	Channels	ICA comp.
3	47, 62, 63, 83, 84, 107, 141, 152, 237	-	5
4	7, 184	O2 (64)	1, 3
5	2, 7, 54, 59, 87, 99, 103, 111, 117, 121, 122, 128, 197, 222, 235, 237	-	1
6	3, 35, 103, 147, 202, 215, 226	-	3, 6
7	4, 109	-	4, 9
8	2, 46, 48, 83, 121, 157, 195	-	-
9	13, 18, 34, 53, 56, 64, 65, 97, 111, 121, 124, 150, 205, 212, 228	-	5
10	184	-	-
11	85, 219	-	4
12	102, 110, 111, 121, 163, 168, 169, 171, 175, 177, 178, 181, 185, 186, 195, 233	-	8

Table 5.1: The table shows removed trials, channels and ICA components in the preprocessing step. Removed trials and channels are removed on the basis of the variance distributions. ICA components are removed on the basis of EyeCatch similarity score.

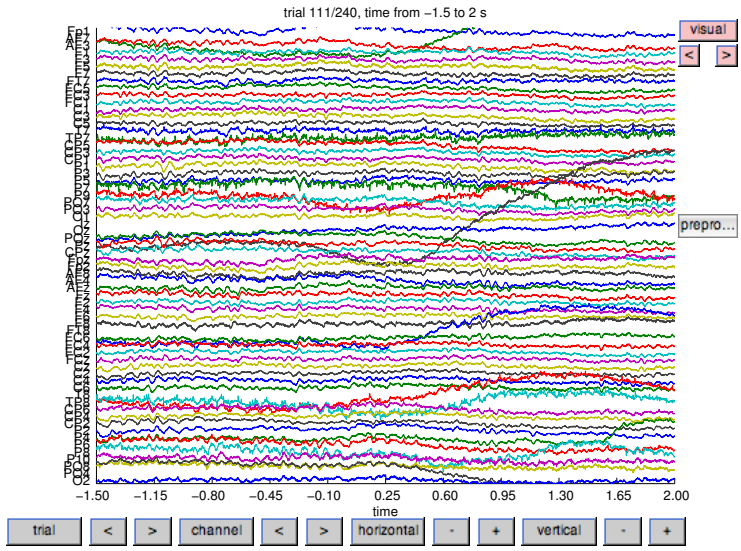

Figure 5.6: The figure shows trial 111 for subject 12. The slow drift starting around -0.10 seconds relative to image onset, is the reason for the high variance in this particular example. Trial 111 was therefore rejected.

tracker was used as a validation tool. Table 5.1 shows removed ICA components for each subject. There was no ICA components that reflected EMG or EKG artefacts.

It is suggested by Kønig et al. [70] that the amount of eye movement can vary between different conditions and introduce a behavioral difference. The eye tracker was therefore also used to check for biases in the data set, originating from eye movements. Figure B.2 shows, for subject 6, 9, 11 and 12, detected eye movements and blinks for the six conditions. No differences are seen between the two social conditions, where affective pictures might tend to consist of more eye movements and blinks.

9 After denoising the data with ICA and removing the detected eye components, the data was converted back to Fieldtrip from EEGLAB as done in Step 6.

10 The data is now assumed to be clean and is ready for data analysis.

Subject 1 and 2 were excluded because of the changed experimental design. Furthermore, subject 13 seemed very uncomfortable during the experiment, which also reflected very noisy data and was therefore also excluded from further analysis. The remaining 10 subjects are used in the data analysis.

5.5 Data Analysis

Figure 1.3 outlines the different analysis methods used in the thesis prior to applying the statistical tests. The theory behind these methods was elaborated in Chapter 3, where the following section describes how the methods were used.

5.5.1 ERP Analysis

For the ERP analyses, the data was averaged across the conditions[37] within each subject followed by an average across the subjects to obtain the group level average.

[37] This average depends on the tested contrast, e.g for the contrast Positive versus Neutral differs from Alone versus Together.

5.5.2 Time-Frequency Analysis

For the time-frequency analysis, the complex Morlet wavelet from Equation 3.3 was used. It offers a good trade off between the spectral and temporal resolution and is widely used in EEG studies [24, 61, 88, 116]. From Equation 3.3, six cycles (C=6) was used, as it is strictly recommended to use a value above five. Different values were tried and manually checked looking at the temporal and spatial resolution. The lowest frequency of interest is 4 Hz giving one cycle a duration of 0.25 s. Increasing the number of cycles would require a longer epoch interval or an increase of the lowest frequency of interest. 30 miliseconds was used as an overlap for the moving window. The time-frequency analysis is applied for each trial before averaging to keep the non-phase locked activity.

The time-frequency analysis was also applied on source level as an interesting result in the alpha band was found. The sources were used instead of the 64 channels for the spatial dimension. For each trial and source, the averaged power in the alpha band was calculated before averaging across the trials.

5.5.3 Source Reconstruction

For the source reconstruction, the headmodel described in Chapter 3 and a source grid of 2015 sources are used. The regularization parameter, λ, in the MNE source reconstruction is an important parameter to chose and is determined from a cross validation approach for each subject. The trials were separated, independent on the conditions, into three sets: a training set, test set and a validation set. The MNE was applied on the training set with a noise-covariance, Σ in Equation 3.4, estimated from -0.4 to -0.1 s prior to image onset. As explained in Chapter 3, an estimate of λ can be calculated from an eigen value decomposition of FF^T. Starting with the estimate of λ as an initial guess, a range of λ values were tried on the training and test set to evaluate the MSE. The training and test errors are seen in Figure 5.7, where Figure B.6 compares, for one trial, the true signal and an estimated version of the signal. The estimated signal is calculated from Equation 3.24.

The optimal λ corresponds to the minimum error of the test-set. The validation set was used to test the performance of each subject, which is summarized in Table B.1. Using the optimal λ from the test set and the noise-covariance from the training set, the MNE was applied on each trial.

Before visualizing the results from the source reconstruction, it is necessary to interpolate the sources on a 3D surface grid, which was done from a template

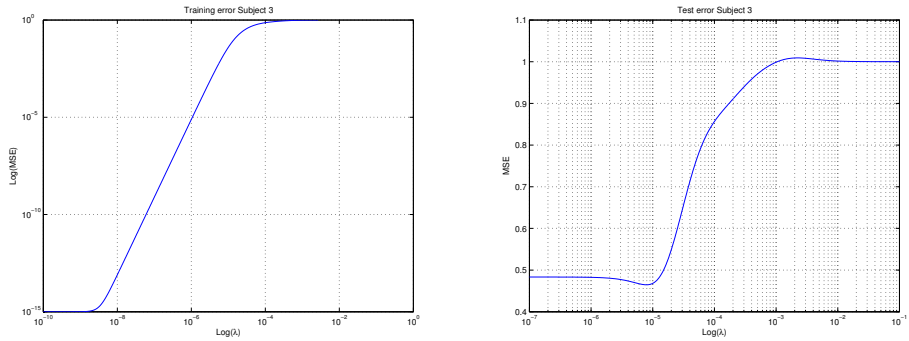

(a) (b)

Figure 5.7: The figures show the MSE for a) the training set and b) test set for subject 3 as a function of the regularization, λ. The minimum MSE for the test set, is the optimal λ value.

brain defined in the *Montreal Neurological Institute, MNI*, space [31]. Using a template for all ten subjects, will off course introduce a small uncertainty as the brain anatomy varies between individuals.

In order to retrieve functional information from the sources, the *Anatomical Automatic Labeling, AAL*, atlas was used [119]. It defines 116 regions that outlines the brain anatomy, e.g. *ThalamusL* which covers the Thalamus in the left cerebral hemisphere. Figure B.7 shows the different regions where each color corresponds to a region [4]. Furthermore, all the 116 regions are written in Appendix B.

5.5.4 Cluster-Based Permutation Test

Applying the cluster-based permutation test, several important parameters need to be defined.

1. A cluster alpha value of 0.05 is used on the basis of the simulations in Chapter 4, and from the study by Maris et al. [82].
2. 1000 permutations were used to conduct the permutation distribution, which is sufficient when using a significance value of 5 % [82].
3. Three different time windows were used. A *large time window* is defined

as the whole epoch[38]. An *early time window* is defined from 0 to 0.3 s. relative to image onset and a *late time window* is defined from 0.3 to 1 s relative to image onset.

4. On channel level, the neighbor structure is defined from a template[39] in Fieldtrip that correspond to a Biosemi 64 channel headcap. It resulted in 3.7 neighbors on average per channel and is visualized in Figure B.4.

   For the test applied on source and region level, the neighbor structure was calculated using the 3D Euclidean distance. The number of averaged neighbors was kept as low as possible with the restriction that all sources or regions had one neighbor. It resulted in 7.7 neighbors on average per channel for the sources and 6.4 for the regions.

It was challenging to apply the cluster-based permutation test on source and region level as the method is not implemented in Fieldtrip nor used in the literature, to the knowledge of the author. In addition, each region needed to be defined by one coordinate set corresponding to the center of mass. A custom made Matlab script was used to calculate the average power/amplitude and the center of mass for each region. The averaged power/amplitude had to be calculated for each sample in each trial resulting in many calculations. It was therefore necessary to use the cluster system at DTU compute.

5.6 Summary

This chapter gave a detailed description of the experimental design and why a visual stimulus from IAPS was used. Furthermore, the advantages and disadvantages of the 2×3 within-subjects experimental design was outlined. All ten steps of the preprocessing pipeline in Figure 1.2 were explained and discussed. The last section of the chapter outlined, how the three analysis methods and corresponding parameter values were used and implemented.

[38] -1.5 to 2 s relative to image onset.
[39] The 2D euclidean distance is used followed by some manually corrections.

Chapter 6

Validation of ICA and EyeCatch using the Eye Tracker

The following chapter is an independent chapter in the sense that it has its own results and discussion. A manually inspection of all ICA components for all participants is very time consuming and it takes many years of experience to manually distinguish eye and brain components. Therefore, several automatic and semiautomatic methods have been used [25]. EyeCatch has, to the knowledge of the author, not yet been implemented in the literature, why the thesis will, with the use of an eye tracker, validate and discuss the performance of EyeCatch. This chapter corresponds to step 8 in Figure 1.2 and is an important step in order to rely on the results presented in Chapter 7.

The chapter is divided up into three sections:

1. The first section describes the method used to validate the performance of EyeCatch.
2. The second section presents the results.
3. The final section discusses the performance of EyeCatch.

6.1 Method

Every time a participant moves the eyes above 0.1°, with respect to a fixation cross in the middle of the screen, an eye movement is detected by the eye tracker. With each eye movement the precise angle and duration is recorded. The duration of each blink is likewise detected. An example of the output data from the eye tracker is shown in Figure B.1.

The eye-tracking data is now epoched similar to an EEG epoch from the fixation cross to the end of the picture presentation as seen in Figure 5.3. The epoched eye-tracking data is assigned an arbitrary value for each sample as

1. If a blink is detected a value of five is assigned to the epoch in that specific sample. For example, if a blink has a duration of 10 samples, each of the 10 samples are assigned with a value of five.
2. If a saccade above 1.28° is detected a value of 1 is assigned to the epoch.
3. If neither a saccade or a blink is detected, the sample will be assigned with a value of zero.

The bottom figures in Figure 6.3 show examples of epoched eye-tracking data. By adding up all the values for each sample in the 3.5 second long epoch, each epoch ends up with an arbitrary number explaining the level of EOG noise. The value of 1.28 is used as it distinguishes saccades from microsaccades. Large saccades are defined at an angle of $\sim 23°$ [70]. However, as no saccades above that value were present, all saccades in the thesis are represented with the same value. Blink artifacts have 5-10 times larger amplitude than saccades, why the ratio between blink and saccades is chosen to be five to one [70].

Since EOG artefacts contain more power than brain activity, as explained in Section 2.1.3, trials with distortion of EOG artefacts should contain more power than "clean" trials. Therefore, by taking the power of each trial for each ICA component and calculating the 90th quantile, each trial of each ICA component is represented by a single value reflecting the power. The 90th quantile is used instead of the maximum power to increase the robustness.

A single trial is now represented by an arbitrary *"distortion"* value from the epoched eye-tracking data and by a single *"power"* value from each ICA components power signal. Pearsons Correlation Coefficient, [45], is used to find the correlation between these two representations. A high correlation means that the eye tracker classify the corresponding ICA component as an eye component.

The correlation between an ICA component and the epoched eye-tracking data is referred to as a *correlation score*.

As elaborated in Chapter 3, EyeCatch calculates a similarity between each ICA component and the templates from the database, where a score above 0.94 means that the ICA component is classified as an eye component. The similarity will be referred to as a *similarity score*.

6.2 Results

As mentioned in Section 5.3.2, the eye tracker was sensitive making the data from the eye tracker unreliable for some participants. Participant 5, 7, 8 and 10 are therefore not included in the results.

The correlation score for the first five ICA components are presented in Table 6.1 with the corresponding p-value[40]. The p-value is calculated using a permutation test with 1000 permutations under the significance level of $\alpha = 0.05$. The last number in each cell in the table represents the similarity score.

Figure 6.1 shows all 64 ICA components for subject 3 and their corresponding correlation and similarity score. Similar results for the other subjects are presented in Appendix B.

ICA component 3, 5 and 13 for subject 3 are used as examples and are presented in details. ICA component 3 is used as the similarity score is high and the correlation score is low. ICA component 5 is an example of when both the similarity and correlation scores are high. ICA component 13 has a high correlation score, but a low similarity score.

Figure 6.2 shows the relationship between the arbitrary distortion values and the power values for ICA component 3, 5 and 13 for subject 3.

As mentioned, ICA component 3 has a high similarity score, but a low correlation score. It means that EyeCatch classified ICA component 3 as an eye component as opposed to the eye tracker. Figure 6.3 shows three trials, where the eye tracker has detected many EOG artefacts, which is not reflected in ICA component 3 (top figures). Figure 6.4 shows three trials where ICA component 3 has a high power value, but a low distortion value from the eye tracker.

ICA component 5 is used as an example where the two methods are consistent.

[40]The p-value is calculated under the null hypothesis that there is zero correlation.

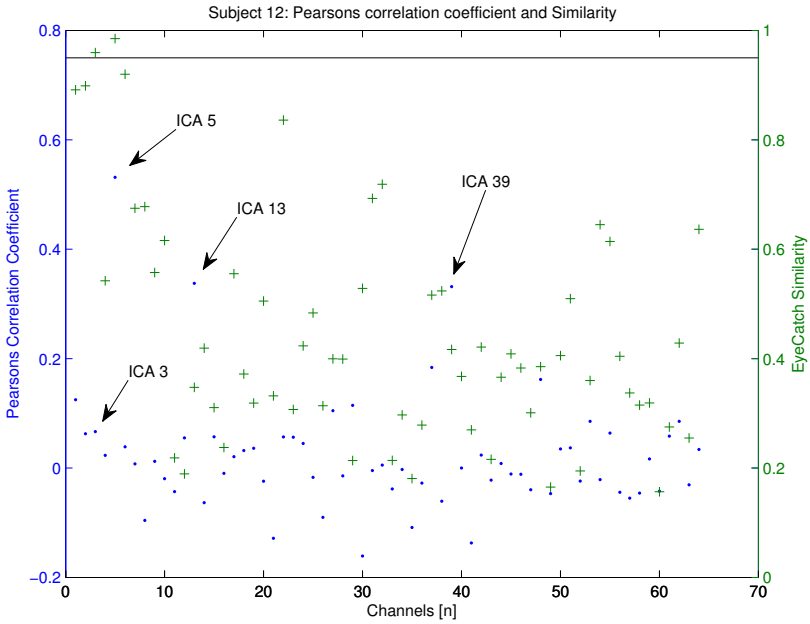

Figure 6.1: The figure shows the correlation between the eye-tracking data and all 64 ICA components for subject 3. The correlation is symbolized with blue dots and the blue y-axis to the left. The figure also presents the similarity score given by EyeCatch for all 64 ICA components. These are marked with a green + and belongs to the green y-axis. The vertical line indicates the threshold (0.94) used for the similarity score by EyeCatch. It is seen, from the green +, that ICA 3 and 5 are exceeding the similarity threshold. ICA component 5, 13 and 39 all show a high correlation coefficient.

Subj	ICA 1	ICA 2	ICA 3	ICA 4	ICA 5	Total
3∗	0.13 p=0.08 sim:0.89	0.06 p=0.2 sim:0.90	**0.07** **p=0.17** **sim:0.96**	0.02 p=0.37 sim:0.54	**0.51** **p=0.001** **sim:0.99**	0.33
4∗	**0.58** **p=0.001** **sim:0.99**	-0.045 p=0.72 sim:0.74	**0.34** **p=0.003** **sim:0.98**	-0.05 p=0.69 sim:0.26	-0.09 p=0.87 sim:0.31	0.56
6∗	0.19 p=0.009 sim:0.90	0.2 p=0.012 sim:0.90	**0.43** **p=0.001** **sim:0.97**	0.09 p=0.07 sim:0.65	-0.05 p=0.83 sim:0.56	0.30
9	0.19 p=0.001 sim:0.93	0.18 p=0.001 sim:0.93	0.019 p=0.35 sim:0.6	0.14 p=0.021 sim:0.5	**0.54** **p=0.001** **sim:0.99**	0.42
11	0.17 p=0.012 sim:0.85	0.14 p=0.02 sim:0.84	-0.08 p=0.87 sim:0.45	**0.32** **p=0.002** **sim:0.99**	-0.03 p=0.65 sim:0.65	0.31
12	0.07 p=0.12 sim:0.87	0.08 p=0.09 sim:0.87	-0.06 p=0.74 sim:0.51	0.08 p=0.22 sim:0.5	0.05 p=0.19 sim:0.79	-0.05

Table 6.1: The table presents the correlation and similarity score for the first five ICA components for subject 3, 4, 6, 9, 11 and 12. The similarity score is denoted with *sim*. Furthermore, the p-value for the correlation score is presented. ICA components highlighted with bold are components classified by EyeCatch as eye components. The last number in the *Total* column shows the correlation between the similarity and the correlation score for all 64 ICA components for each subject. ∗: only the first half (120 trials).

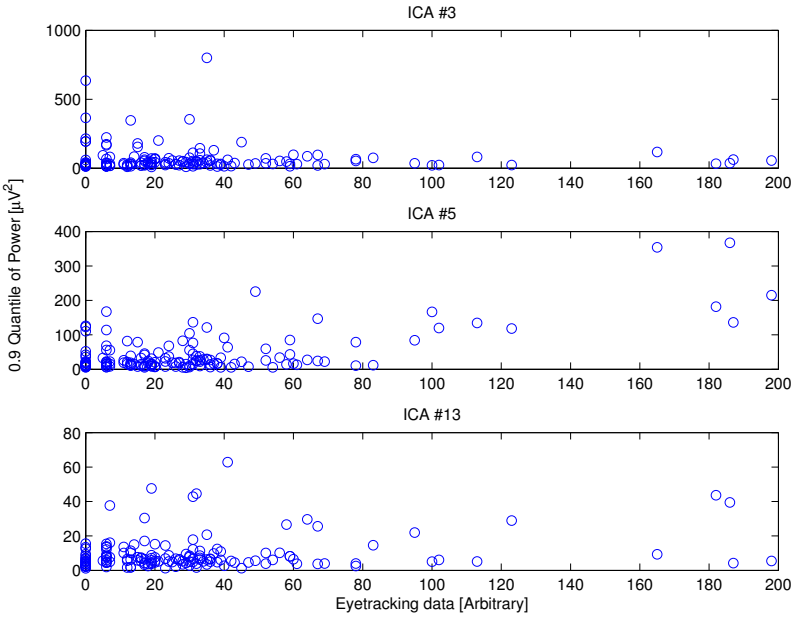

Figure 6.2: The figure shows the relationship between the epoched eye-tracking data and the 0.9th quantile power for ICA components 3, 5 and 13 for subject 3. Each sample (blue dots) represents a trial. The correlation coefficients are 0.07 (ICA3), 0.51 (ICA5) and 0.34 (ICA13) and the similarity score is 0.96, 0.99 and 0.44 respectively. The contradicting result for ICA component 3 is clearly seen in the topplot, as a high value for the eye-tracking data is not resembled in the power score.

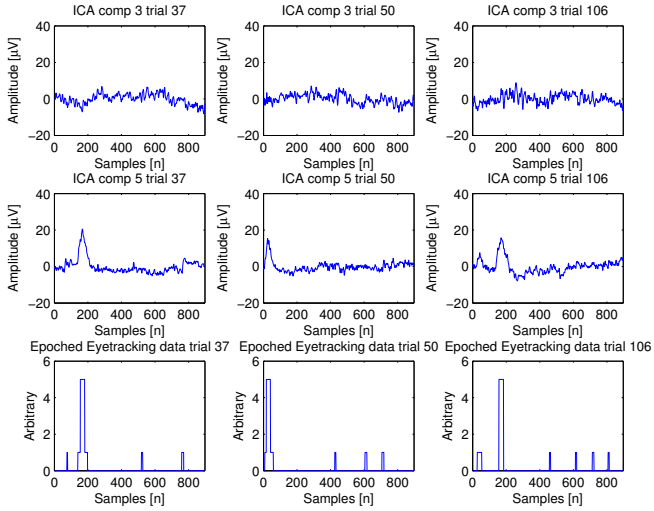

Figure 6.3: The figure shows trial 37, 50 and 106 for subject 3 where the distortion score from the eye tracker is high because of the detected blinks and eye movements. The corresponding time series of ICA component 3 and 5 are also shown. EOG artefacts in ICA component 5 are aligned with the detected blinks and saccades from the eye tracker. This is not the case for ICA component 3.

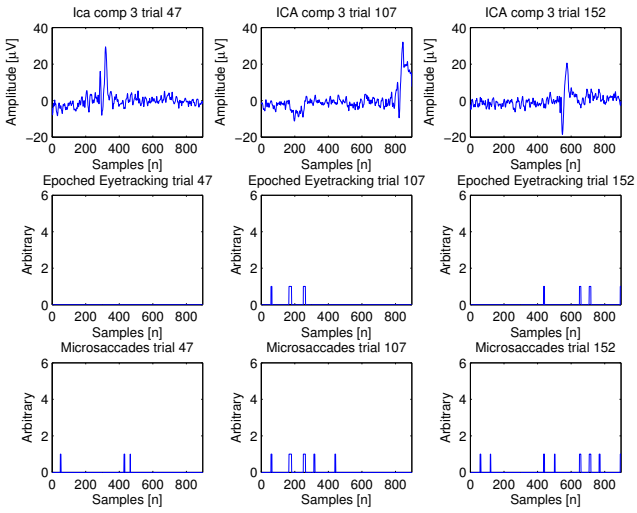

Figure 6.4: The figure shows subject 3 in trial 47, 107 and 152 for ICA component 3 and the corresponding epoched eye-tracking data. The high power score is due to the seen spikes, which is not reflected in the eye-tracking data. The middle plots show the normal epoched eye-tracking data using the threshold of 1.28. The bottom figures show the epoched eye-tracking data without any threshold to see if microsaccades could explain the spikes in the top figures.

The similarity score is 0.99 and the correlation score is 0.51 with a corresponding p-value of 0.001. Figure 6.3 shows how ICA component 5 consists of EOG artefacts and is aligned with eye movements and blinks detected by the eye tracker.

In Figure 6.1, it is seen that ICA component 13 has a similarity score below 0.4, but a correlation score of 0.34. Figure 6.5 compares three trials with a high distortion and power value to see why the obtained correlation is high. It is seen that the detected eye movement and blinks are not aligned with ICA component 13.

The topographies, the average time series and the power spectrum of ICA component 3, 5 and 13 are shown in Figure 6.6 to further inspect if the components are eye components or not. Furthermore, ICA component 2 is shown to visualize a component reflecting brain activity.

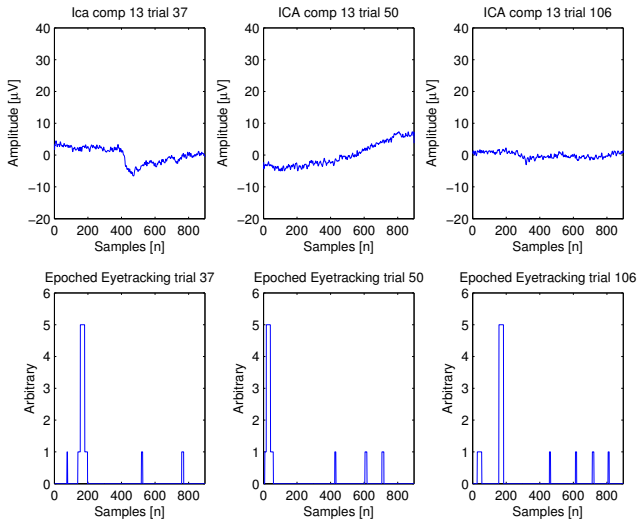

Figure 6.5: The figure shows subject 3 in trial 37, 50 and 106 for ICA component 13 and the corresponding epoched eye-tracking data. Pearsons correlation showed a high correlation score, where the similarity showed a low score. The detected eye movements and blinks are not aligned with ICA component 13. The seen fluctations are not sychronized with the eye tracker.

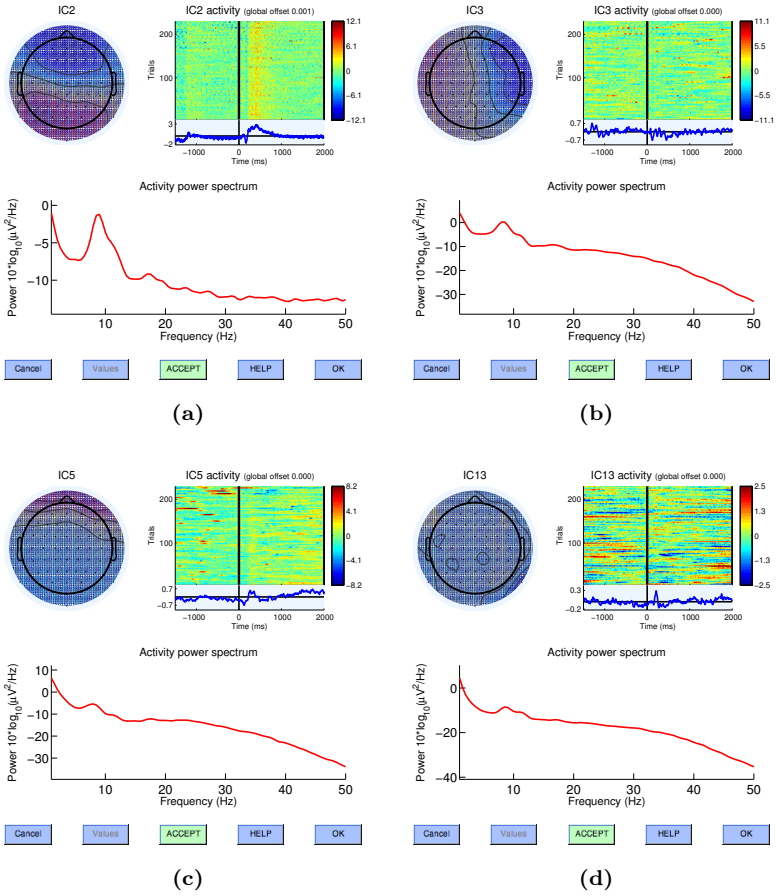

Figure 6.6: The figures show the topographies, power spectrums and average time series for ICA component 2, 3, 5 and 13 respectively. These are obtained from subject 3. Figure a) shows ICA component 2, where it is clear that the activity is aligned with the presented picture (upper right corner). Furthermore, the majority of the power is in the alpha band meaning that ICA component 2 clearly reflects brain activity. Figure b) shows that the power is located in the frontal/temporal area for ICA component 3. The time series do not show any connection to the ERPs from the visual stimuli. The power spectrum shows activation of the low frequencies and in the low alpha band. Figure c) shows ICA component 5, where the power is located in the frontal area with high activation of low frequencies. Figure d) shows the characteristics of ICA component 13. It does not contain much energy compared to the three other ICA components. The power is located at the low frequencies and in the right parital/occipital-parietal area.

6.3 Discussion

For the six subjects, where the eye tracker worked, EyeCatch detected 8 ICA components as eye components, where only one, ICA component 3 for subject 3, was questionable.

ICA component 3 showed a high similarity score and a low correlation score implying that either the eye tracker or EyeCatch was mistaken. If the eye tracker is mistaken, it could be due to eye movement that was below the used threshold of $1.28°$[41], and therefore was not included in the epoched eye-tracking data. However, the bottom figures in Figure 6.4 reject this idea as the eye movements not are aligned with ICA component 3.

The second option is a wrongly detected eye component by EyeCatch. The power spectrum in Figure 6.6b shows that the power of ICA component 3 peaks in the low alpha band. The alpha band is tricky as both EOG artefacts and brain activity have energy in the alpha band [91]. Looking at Figure 6.4, it is clear that the spikes seen in the top figures are not brain activity. EMG artefacts are left out as a possibility as the power spectrum would be distributed over a broader frequency range with more power at the higher frequencies. ICA component 3 could therefore reflect both EOG artefacts and brain activity.

From the EEGLAB turtorial, [3], it is recommended to keep such a component, and run a second round of ICA to see if the ICA algorithm makes a better separation of the underlying sources. Keeping ICA component 3 and rerunning the ICA, the EyeCatch did not detect any components as eye components as the highest similarity score was 0.91. It could imply that the previous ICA component 3 was falsely detected by EyeCatch. However, the seen artefacts in Figure 6.4 are still problematic as they still are present in the data. Therefore, the trials were excluded from the subject 3.

ICA component 5 from subject 3 showed both a high correlation score and high similarity score, indicating that ICA component 5 is an eye component. In Figure 6.3, ICA component 5 showed alignment between EOG artefacts and the epoched eye-tracking data. This is also in accordance with Figure 6.6c, where the power of the signal is localized in the frontal electrodes and in the low frequency band.

ICA component 13 is not an eye component, despite the high correlation with the eye tracker. The power spectrum, topography and the lack of no temporal alignment with detected eye movements, prove that ICA component 13 is not

[41] Saccades below this threshold are usually denoted microsaccades [70].

an eye component.

The results imply that classifying ICA components solely based on the topographies might not be sufficient. ICA component 3 is suggested removed by EyeCatch despite the fact that it most likely also consist of brain activity. It is also reported that the performance of experts[42] manually classifying ICA components increases, when the times series and power spectra are used in a combination with the topographies [70]. Therefore, it is suggested to expand the EyeCatch method to include information about the power spectrum.

Kønig et al., [70], use the eye tracker to classify ICA components by making a variance ratio between "clean" and "noisy" intervals in the ICA components, where the intervals are defined by the eye tracker. Their results are remarkable good, when using a ratio of 1.1, with an area under curve of 0.99. As the method seemed very promising, the method was implemented and tested in the thesis. Using the suggested ratio of 1.1, 55 components were classified as eye components. Increasing the ratio to lower the number of classified eye components, the results were very contradicting when comparing to EyeCatch's similarity score. The experiment in [70] is very controlled with respect to eye movement and is cleaned from other sources in contrast to the data presented in the thesis. This difference could explain why the great performance found by Kønig et al., [70] could not be reproduced.

6.4 Summary

This chapter described a method to validate the EyeCatch with an eye tracker. The eye-tracking data was epoched and compared to the power of ICA components. These were analyzed with Pearsons Correlation Coefficient and compared to the similarity score given by EyeCatch. EyeCatch detected eight ICA components as eye components, where one was a false positive as the component consisted of both eye and brain activity.

[42] Here, the experts are referred to the experts from [70].

Chapter 7

Results

This chapter presents the main results forming the basis of the discussion in Chapter 8. The remaining results are shown in Appendix C.

The chapter is divided into three sections.

1. First, the results concerning the baseline are presented as it varies across the social conditions. The baseline is defined in a window from -0.4 to -0.1 seconds prior to image onset. Therefore, an analysis of the baseline is necessary to provide a sufficient baseline correction before further analysis. However, it might also indicate a difference during the resting state (baseline) between the two social conditions.
2. The second section presents the results concerning the emotional content of the pictures. The section serves as a sanity check by reproducing results about perception of positive, negative and neutral pictures.
3. The last section presents the results concerning the social context. The ERP analysis revealed a difference in the LPP, where the time-frequency analysis showed a difference in the alpha band.

Recall from Chapter 5 that three different time windows are used as input in the cluster-based permutation test: the large [-2:1.5 s], the early [0:0.3 s] and

the late [0.3 1 s] time window, where all times are relative to image onset. In addition, the time-frequency analyses are limited to the three frequency bands: the theta band (4-8 Hz), the alpha band (8-12 Hz) and the beta band (12-30 Hz).

7.1 Baseline

The time-frequency analysis of the baseline showed a difference between the two social conditions in the alpha band. The top figure in Figure 7.1 shows, for channel PO4, that the Alone condition has more power in the alpha band indicated by the red color. In Figure 7.2, it is seen that the difference is most prominent at the parietal/occipital-parietal channel sites.

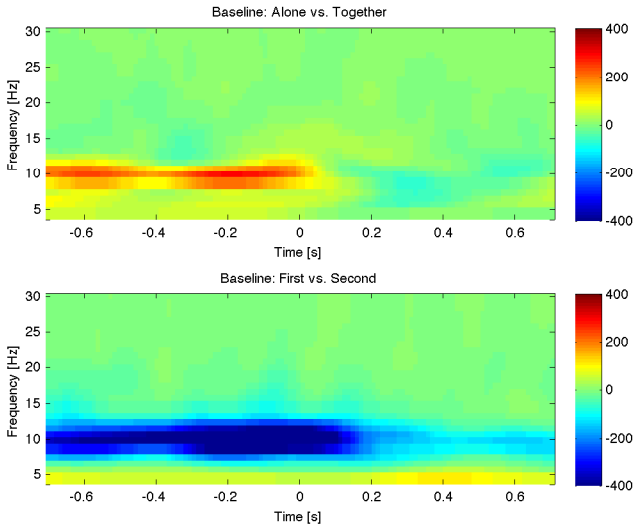

Figure 7.1: The figures show the differences prior to image onset at channel PO4 for Alone/Together (top figure) and the First/the Second half of the experiment (bottom figure). The top figure shows increased alpha activity in the baseline in the Alone condition indicated by the red color. The bottom figure shows alpha suppression in the first half compared to the second half, indicated by the blue color. The differences are calculated as Condition 1 - Condition 2.

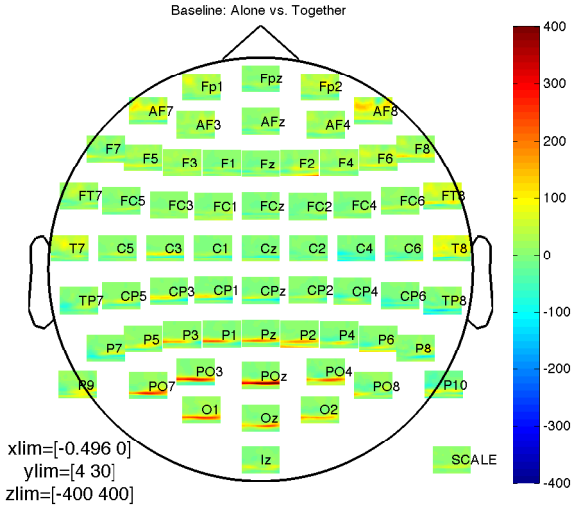

Figure 7.2: The figure shows the raw difference for all 64 channels between the Alone and Together condtion. The time axis is from -0.5 to 0 s relative to image onset and the frequency axis is from 4 to 30 Hz. The spatial distributions are located at the parietal/occipital-parietal sites. The red color indicates more power in the Alone condition.

Recall from Section 5.2.4 that after the first 120 images, the social condition is changed. Therefore, the first 120 pictures will be referred to as the first half of the experiment, where the last 120 pictures will be referred to as the second half of the experiment. The bottom figure in Figure 7.1 shows the difference between the first and second half, where the blue color indicates more alpha power in the second half. In contrast to the baseline difference concerning the social context, the baseline difference here is present in almost all channels, cf. Figure C.1.

To investigate the intersubject variability, the baseline difference between the first and second half are shown in Figure 7.3 for the first nine participants[43] at channel PO4. The figure shows a high intersubject variability, where subject 3, 7, 8 and 9 show a large difference between the first and second half in contrast to subject 4, 5, 6, 10 and 11. Subject 3, 5, 6, 9 and 11 were all in the Together condition during the first half of the experiment.

[43]The last person is not included in order to simplify the visual result. Subject 12 did not show any differences between the first and second half.

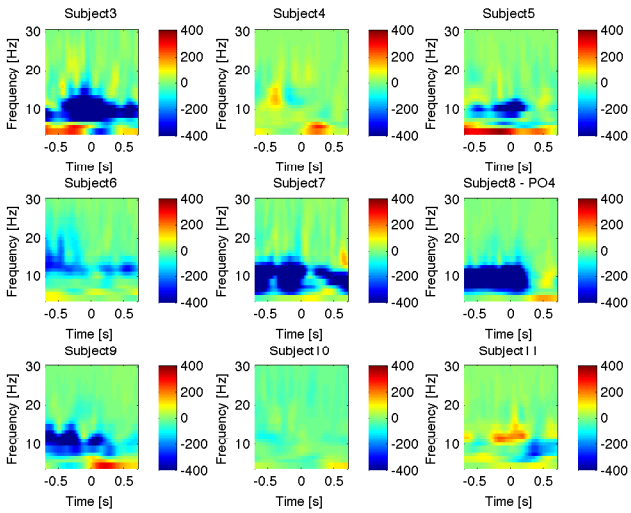

Figure 7.3: The figure shows the raw differences at channel PO4 for the first nine subjects between the first and the second half of the experiment. It shows that subject 3, 7, 8 and 9 had a large increase in alpha power during the second half, where subject 4, 10 and 11 do not show a substantial difference. Subject 3, 5, 6, 9 and 11 were all in the Together condition during the first half.

7.2 Main Factor - Emotional Content of The Picture

This section shows the results concerning the emotional content of the pictures, where the ERP and the time-frequency results are divided up into two sections.

Table 7.1 and 7.2 summarize the results for the ERP and time-frequency analysis respectively, where only few will be presented and discussed. These are written in italic type. The tables are divided into the three contrasts; 1) negative versus positive, 2) positive versus neutral and 3) negative versus neutral. Furthermore, the contrasts are tested when the data is pooled across the social conditions, but also separately within each social condition[44]. Unless otherwise is stated, the results presented are for the pooled data, using the large time window with a cluster alpha of 0.05.

[44]E.g. the contrast viewing negative pictures alone versus viewing neutral pictures alone.

7.2.1 ERP Analysis

7.2.1.1 Early ERP Components

Figure 7.4 visualizes the ERPs for negative (red), positive (blue) and neutral (green) pictures at channel O2 and CPz. At channel O2 in Figure 7.4a, a small difference is seen in the N170 component for positive pictures compared to negative and neutral ones. For channel CPz in Figure 7.4b, the positive pictures exhibit a larger response for both the negative peak at 100 ms and the positive peak at 170 ms.

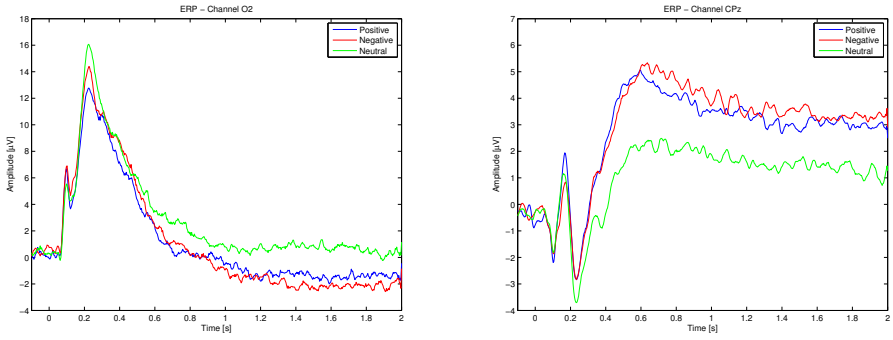

(a) **(b)**

Figure 7.4: The figures show ERPs across all ten subjects for channel a) O2 and b) CPz for negative (red), positive (blue) and neutral (green) pictures. A small modulation, between the positive pictures compared to the negative and neutral ones, is seen at the early latency. A clear difference is developed at the late latency (>300 ms) between the affective and neutral pictures.

Figure 7.5 shows the results of testing positive against neutral pictures. From 150 to 300 ms, a significant negative cluster (p=0.05) is seen at the occipital and parietal-occipital sites. The difference reflects a more positive amplitude for the neutral pictures. No significant differences of the early ERP components were found for the contrasts Negative/Neutral and Positive/Negative when using the large time window. The early time window revealed new significant differences for the contrast Negative/Neutral (Figure C.5a) over the centro-parietal sites from 50 to 200 ms, and for the contrast Positive/Neutral (Figure C.6a) at the frontal sites from 200 to 300 ms. In addition, a significant difference between

positive and negative pictures was found after 100 ms at the fronto-central and frontal sites, seen in Figure C.7.

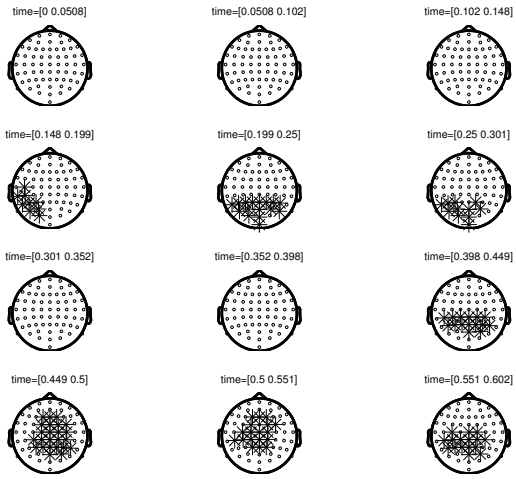

Figure 7.5: The figure shows the results from the cluster-based permutation test for positive versus neutral pictures. The first significant cluster is negative (p=0.05) reflecting a difference in the early picture processing. The difference is located at the occipital-parietal area from 150 to 300 ms after image onset. The second cluster is positive (p=0.02) and shows a difference in the LPP after 400 ms. The difference is located in the centro-parietal and centro-frontal area.

7.2.1.2 Late ERP Components

In Figure 7.4, clear differences are seen between the affective and neutral pictures starting after 300 ms and continues throughout the epoch. A similar pattern is shown for channel FC2 and F1 in Figure C.2.

In Figure 7.5, the second cluster reflects a difference between positive and neutral pictures starting after 400 ms. The difference is located at the central channel sites ranging from parietal-occipital to the frontal sites. The cluster is positive reflecting a stronger response for positive pictures in accordance with Figure 7.4b.

		Time window		
Contrast	Social context	Large:[-2:1.5]	Early:[0:0.3]	Late:[0.3:1]
Neg/Pos	Pooled	-	neg:p=0.03, p=0.03	-
	Alone	-	pos:p=0.03, p=0.05 neg:p=0.05	-
	Together	-	-	-
Pos/Neu	Pooled	*pos:p=0.02, p=0.05*	pos:p=0.006, neg:p=0.02	pos:p=0.002
	Alone	pos:p=0.002, p=0.02	pos:p=0.05, neg:p=0.02	pos:p=0.002, p=0.024
	Together	pos:p=0.008, p=0.03	neg:p=0.04, p=0.03	pos:p=0.04, p=0.04
Neg/Neu	Pooled	*pos:p=0.01, p=0.03*	neg:p=0.002	pos:p=0.004 neg:p=0.04
	Alone	pos:p=0.002, p=0.01	neg:p=0.04	pos:p=0.008, p=0.002
	Together	pos:p=0.03, p=0.03	neg:p=0.01	pos:p=0.02, neg:p=0.03

Table 7.1: ERP analysis: The table shows the results from the cluster-based permutation test, testing the emotional content of the pictures in three different time windows (large, early, late). A significant difference between two conditions is presented with a *pos* or a *neg* reflecting the sign of the cluster with the corresponding p-value. The precise spatial and temporal location are not seen from the table. E.g for the contrast Neg/Neu for the pooled data, a positive cluster is seen with p=0.01 within the large time window. The actual cluster is found from 350 to 500 ms after image onset, as seen in Figure 7.8.

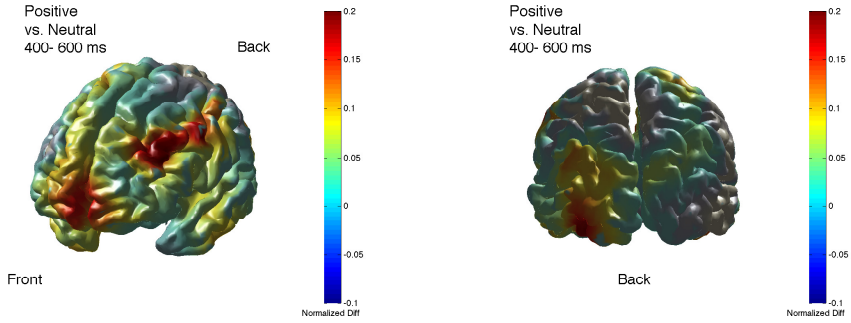

(a) **(b)**

Figure 7.6: The figures show the results of the MNE for the contrast Positive/Neutral pictures in the interval from 400 to 600 ms. It shows the normalized differences, where the red color indicates a stronger signal for positive pictures. It is seen that both the frontal and left prefrontal area together with the occipital lobe is mostly activated. From the AAL atlas, the left frontal gyrus showed high activation, as seen in Figure a).

From the MNE source reconstruction, Figure 7.6 shows the normalized difference between the positive and neutral pictures from 400 to 600 ms. It is seen that the frontal and occipital areas show a stronger response for the positive pictures, indicated by the red color. Localizing the differences using the AAL atlas, the left Frontal Midline Gyrus region showed high activity as seen in Figure 7.7.

Figure 7.8 shows significant clusters testing negative against neutral pictures. A significant cluster (p=0.01) is seen from 370 ms to 480 ms, ranging from parietal-occipital to the parietal channels, reflecting a difference in the LPP. The second significant cluster (p=0.03) begins after 570 ms ranging over the same sites as the previous cluster. Both clusters are positive, meaning that the negative pictures exhibit a stronger response in accordance with Figure 7.4b. The MNE source reconstruction showed a widespread difference with activation of several AAL regions including the left and right Frontal Midline and Inferior Gyrus and left and right Temporal Midline, Inferior and superior Gyrus, which is seen in Figure C.8.

Figure C.3 shows the intersubject variability of the ERPs for channel O2 and CPz. It is seen that the variability across the subjects are much higher than across the conditions. In addition, Figure C.4 shows the variability across all trials for subject 3.

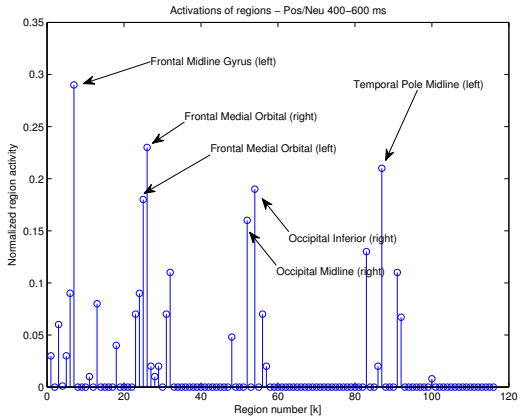

Figure 7.7: The figure shows which AAL regions that showed the highest activity for the normalized difference between the positive and neutral pictures from 400 to 600 ms relative to image onset.

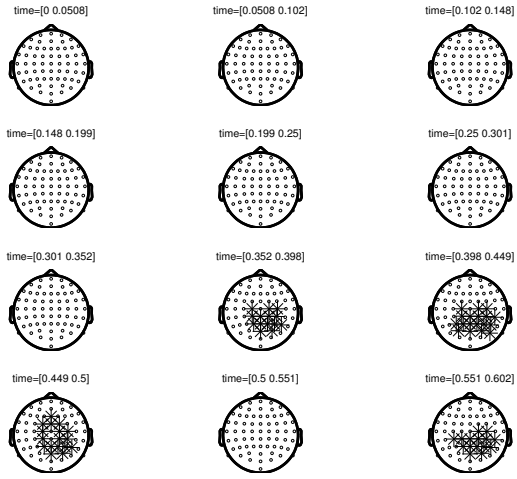

Figure 7.8: The figure shows the results from the cluster-based permutation test between negative and neutral pictures. The figures show two positive significant clusters (p=0.01 and p=0.03) reflecting a difference in the late positive potential, with a higher response to negative pictures.

7.2.2 The Time-Frequency Analysis

The time-frequency showed ERS in the theta band right after image onset, and ERD of alpha oscillations after 200 ms for both positive, negative and neutral pictures. This is seen in Figure C.9, where the bottom figures show the normalized differences between affective and neutral pictures. The red color indicates higher power for affective pictures in the theta band after 200 ms. The blue color indicates less power for affective pictures in the alpha band starting from 600 ms. A similar example is shown for channel O2 in Figure C.10.

Table 7.2 summarizes the statistical results when the late time window is used, as no significant differences were found in the large or early time window.

From Table 7.2, it is seen that for positive against neutral pictures, differences are found in all three frequency bands. These results are not based on the pooled data, but solely when the pictures are viewed alone. The clusters for the theta and alpha bands are seen in Figure 7.9, while the beta band is presented in Figure C.11. The top figures visualize the spatial location with channels marked with $\star$. The bottom figures show the temporal and spectral location of the clusters. The color bar indicates in how many channels a single pixel (time point $\times$ frequency point) is represented. For example, a color with index value of ten means that the pixel is found to be a part of the cluster in ten channels.

		Late latency [0.3-1 s]		
Contrast	Social context	Theta:[4:8 Hz]	Alpha:[8:12 Hz]	Beta:[12:30 Hz]
Neg/Pos	Pooled	-	pos:p=0.02	-
	Alone	-	-	-
	Together	-	pos:p=0.03	-
Pos/Neu	Pooled	pos:p=0.02	-	-
	Alone	*pos:p=0.006*	*neg:0.006*	*neg:p=0.002*
	Together	pos:p=0.05	-	-
Neg/Neu	Pooled	pos:p=0.002	-	-
	Alone	-	-	neg:p=0.02
	Together	pos:p=0.05	neg:p=0.004	-

Table 7.2: Time-Frequency analysis: The table shows significant clusters when testing the picture content in the late time window, for three different frequency bands. The statistical test did not show any significant differences in the early time window, why these are excluded from the table. The interpretation of the table is similar to Table 7.1

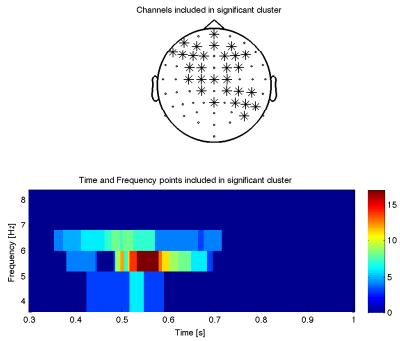

(a)

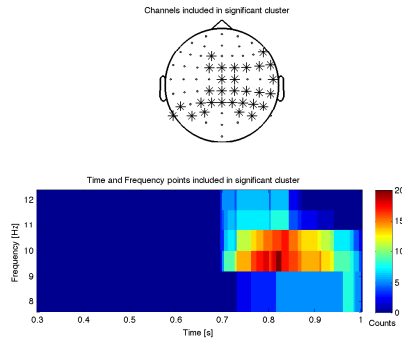

(b)

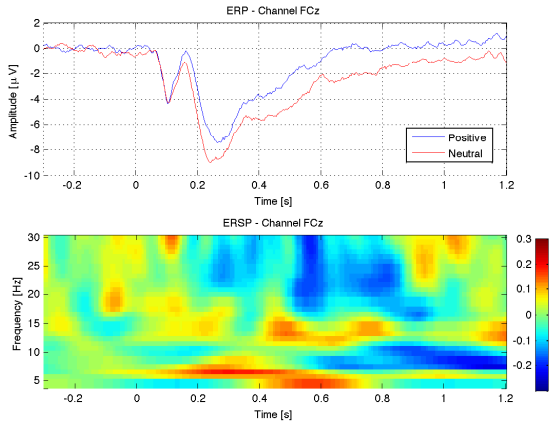

(c)

Figure 7.9: The figure shows significant clusters for the contrast Positive/Neutral pictures in a) the theta band (p=0.006) and b) the alpha band (p=0.006). The top figures visualize the spatial location of the differences with channels marked with $\star$. The bottom figure shows the location in the spectral and temporal dimension. The colorbar indicates the number of channels, a single pixel (time point $\times$ frequency point) is represented in. E.g a color with index value of ten means that the pixel is found to be a part of the cluster in ten channels. Figure c) shows the ERPs and corresponding normalized difference in the spectogram for channel FCz. Here red indicates higher power for positive pictures and blue higher power for neutral pictures. The spectogram clearly shows differences in the three frequency bands: higher theta power and lower alpha and beta for positive pictures.

In the theta band, the significant difference (p=0.006) is seen from 350 to 700 ms around 6 Hz. The spatial location is widely distributed, but mostly located at the centro-frontal area. The cluster is positive reflecting higher theta power for positive pictures.

The significant cluster (p=0.006) in the alpha band, has a later onset after 700 ms with a peak frequency of 10 Hz. The spatial location of the cluster is widely distributed with most of the parietal and right temporal sites included. The cluster is negative reflecting a higher alpha power for neutral pictures.

7.3 Main Factor - Social Context

This section shows the results concerning the social context, where the ERP and the time-frequency results are divided into two sections.

7.3.1 ERP Analysis

Figure 7.10 shows the ERP differences between Alone and Together for channel F2 and PO4 divided into positive, negative and neutral pictures. For affective pictures, a difference in the LPP is seen in contrast to neutral pictures. The Alone condition exhibits a larger amplitude after 600 ms, where the two conditions are very similar for neutral pictures. The differences at the LPP are seen with the mean error bar at channel PO4 in Figure 7.11.

The results from the cluster-based permutation test revealed a significant positive cluster (p=0.04) averaging over all pictures. The positive cluster is seen in Figure 7.12 from 850 to 950 ms in the frontal area meaning a larger response when viewing the pictures alone. As the p-value is close to the level of significance, it is recommended to increase the number of permutations [82]. The number of permutations was increased from 1000 to 5000 to get a more sufficient permutation distribution, however the cluster was still found significant with a p-value of 0.04.

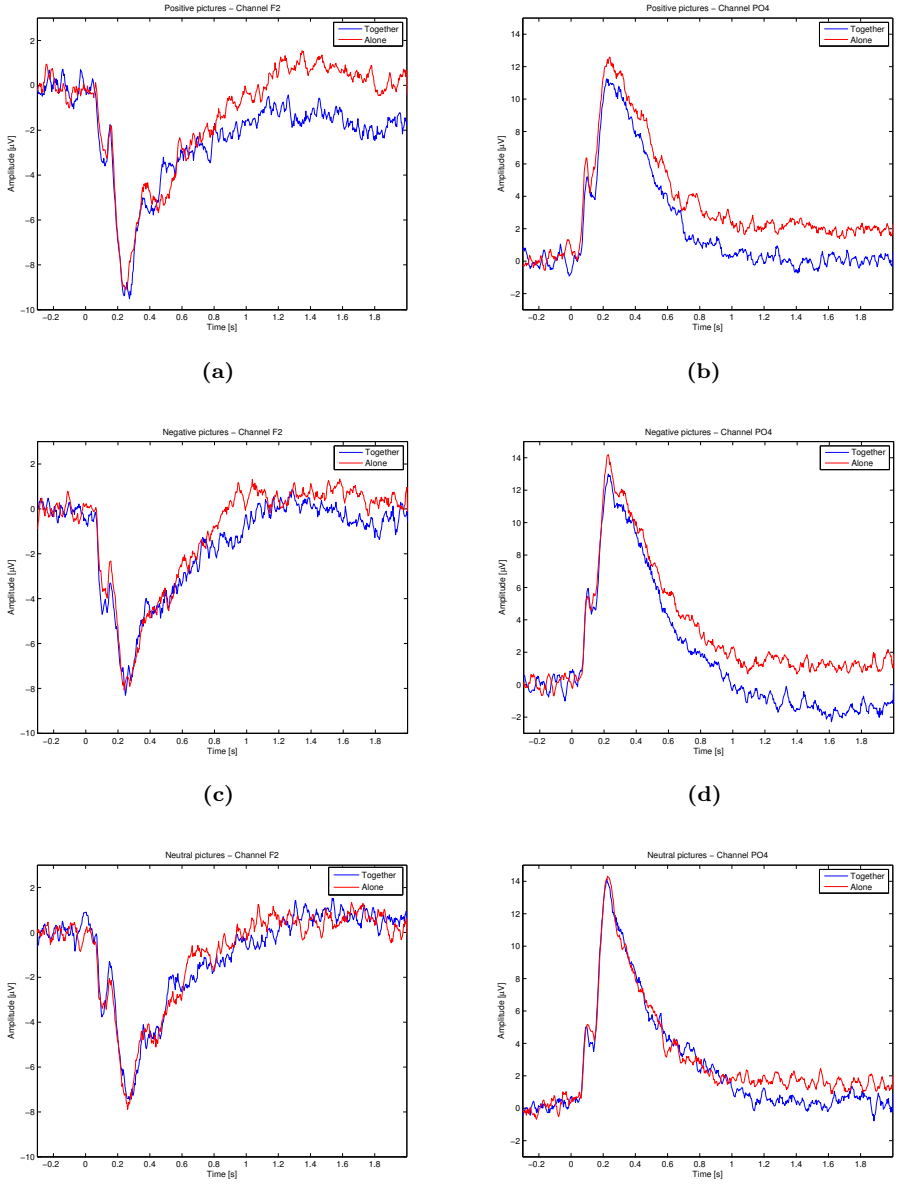

Figure 7.10: The figures show the ERPs at channel F2 and PO4 for the two social conditions for positive (top), negative (middle) and neutral (bottom) pictures, respectively. The blue color indicates the Together condition and the red the Alone condition. A difference in the LPP is seen for affective pictures compared to neutral ones.

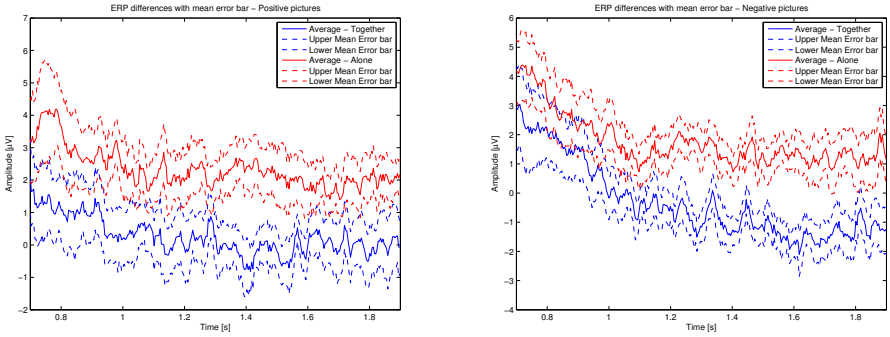

(a) **(b)**

Figure 7.11: The figures show the mean error bar of across the ten subjects for channel PO4 for the contrast Alone/Together. Figure a) shows the positive pictures and b) the negative pictures, where the red color is the Alone condition and the blue color is the Together condition. It is seen that the ERPs and mean error bars for the two conditions are separated.

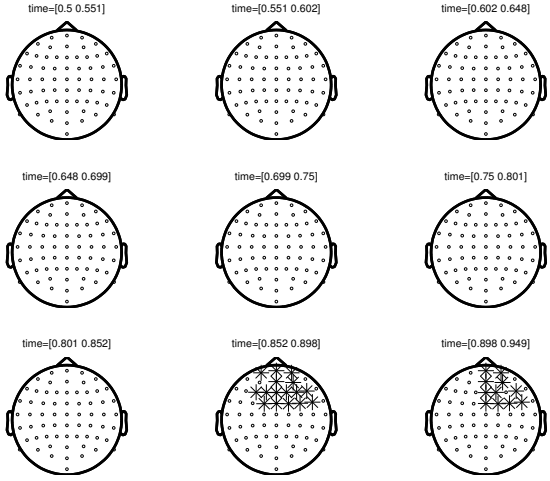

Figure 7.12: The figure shows the results from cluster-based permutation between the social conditions for all pictures combined. A significant cluster (p=0.04) is located in the frontal area from 850 to 950 ms. The cluster is negative, meaning the response is larger for the Alone condition.

The cluster was further investigated by rerunning the test after excluding one participant of the group. Figure 7.13 shows how the p-value varies as each subject is excluded. The permutation number corresponds to the excluded subject, for example permutation number 1 is subject 3, where permutation number 10 is subject 12. It is seen that subject 6, 7 and 10 have an important impact on keeping the cluster below the significance level. This shows the lack of statistical power, as the statistic should not be influenced by removal of just one participant.

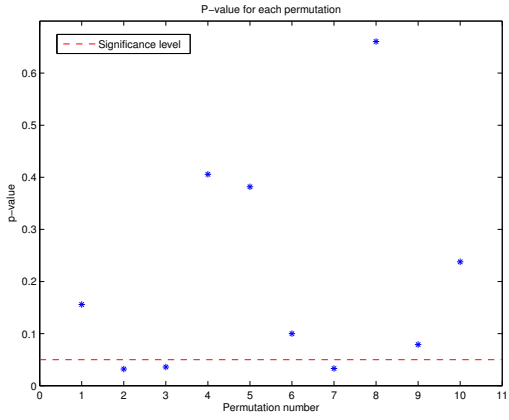

Figure 7.13: The figure shows how the p-value of the found significant cluster from Figure 7.12 varies as one of the subjects are excluded from the group. The permutation number corresponds to the subject excluded from the group prior to the analysis. The red line shows the level of significance. Recall that the original p value for the found significant cluster was 0.04. Subject 6, 7 and 10 (permutation number 4, 5 and 8) have a large impact on the found difference, whereas subject 4, 5 and 9 are slightly lowering the p-value.

In Figure 7.10, it was seen that the difference at the LPP was most prominent for affective pictures. Therefore, a similar cluster-based permutation test was applied using only affective pictures. However, the test did not reveal any significant differences.

The MNE source reconstruction was used to localize the sources that exhibited the differences. Figure 7.14 shows the normalized difference averaged over a time interval from 0.7 to 1.2 s. It is seen that the frontal area is the active corresponding to the found cluster in Figure 7.12. Interesting, the source re-

construction also showed a difference at the parietal-occipital lobe, which was not revealed by the cluster-based permutation test. Relating the sources to the AAL atlas, the following regions showed high activation: left frontal superior, left frontal midline gyrus, left occipital midline gyrus and right temporal midline gyrus. It is shown in Figure C.13.

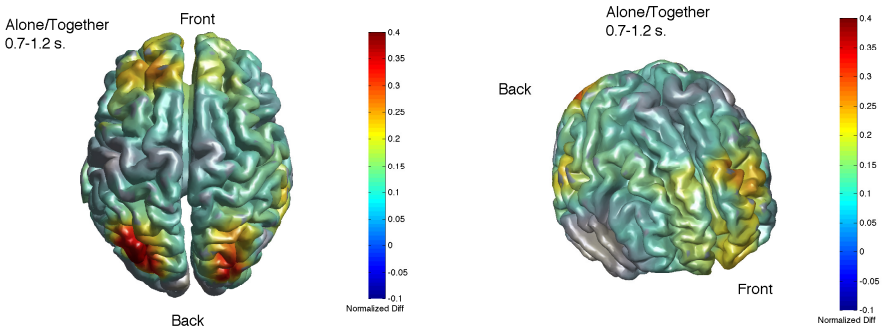

(a) **(b)**

Figure 7.14: The figure shows the MNE result for the normalized difference between Alone and Together from 0.7 to 1.2 s. It is seen that the left frontal and the parie-occipital area are activated. The following regions in the AAL atlas showed high activation: left frontal superior, left frontal midline gyrus, left occipital midline gyrus and right temporal midline gyrus.

The cluster-based permutation test on source level did not reveal any significant for the social contrast. However, it did find a positive cluster with p-value of 0.09 from 700 to 950 ms. The cluster included 807 out of the 2015 sources, which is seen in Figure C.14. Running the test on region level using 116 regions instead of the sources or channels as the spatial dimension, did not reveal any significant differences.

Studying how the social contrast affected the perception of the pictures separately, a positive cluster (p=0.06) close to the significance level was found for positive pictures. The cluster is seen in Figure C.15 at the frontal, centro-frontal channels from 650 to 750 ms. Rerunning the same test using 5000 permutations instead of 1000 increased the p-value to 0.08. No differences were found when testing negative or neutral pictures separately.

It is known that the intersubject variability is high in ERP studies [79], which Figure 7.4 also visualizes. It is likely that the intersubject variability increases,

when studying a more complex situation as the effect of the social context causes. Therefore, a cluster based permutation test was applied on subject level. The purpose was to see if some subjects exhibited the same results. However, the results did not reveal any pattern, which is seen in Figure C.16. From the 2×3 experimental design, the 3 interaction terms[45] were also tested, but did not show any significant differences.

7.3.2 Time-Frequency Analysis

Figure 7.15 shows the spectograms at channel F3 and C4 for negative pictures in the Together condition (top figures) and in the Alone condition (middle figures). The bottom figures show the normalized difference, where a red color indicates more power when viewing the pictures alone. A suppression of alpha power in the Together condition is seen after 200 ms until 1 second.

The spectograms are consistent with the result from the cluster-based permutation test[46] indicating higher alpha power in the Alone condition. Figure 7.16 shows the negative cluster (p=0.06), which ranges from 600 to 900 ms. It is spatially located from left prefrontal area to right centro-parietal area. As the p-value is close to the significance level, the same test was conducted using 5000 permutations, but it did not change the p-value of the cluster.

The source reconstruction analysis did not provide further information about the spatial location of the underlying neural sources of the cluster. The difference was widely spread out as seen in Figure C.18 with several AAL regions activated.

Similar tests were applied for positive and neutral pictures using both the large, early and late time windows, but no clusters near or below the significance level were found. Pooling the data across the pictures did nor reveal any differences in the time-frequency analysis for the social context.

[45] One interaction term is Alone/Together $\times$ Positive/Neutral.

[46] The late time window and the alpha band were used as inputs in the cluster-based permutation test.

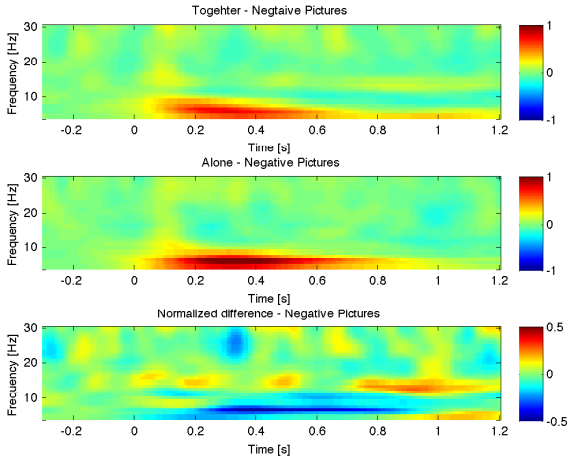

(a)

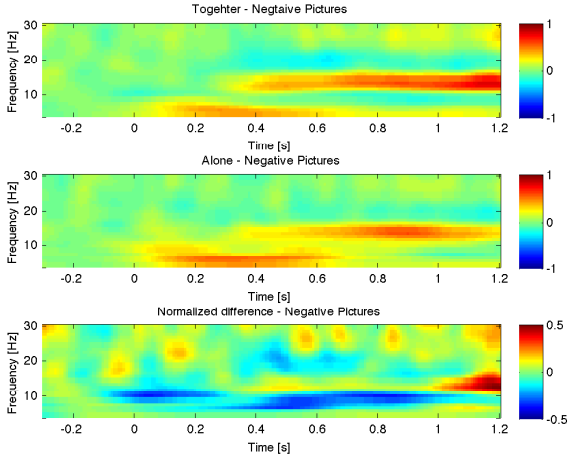

(b)

Figure 7.15: The figures show the averaged spectograms across all ten subjects for negative pictures for channel a) F3 and b) C4. The top figures are the average spectograms for negative pictures in the Together condition, and the middle figures are the spectograms for the Alone condition. The color indicates changes relative to the baseline. The blue color indicates power suppression, where the red color indicates increased power. The bottom figures show the normalized differences for the contrast Together versus Alone. Channel F3 and C4 are included in the cluster shown in Figure 7.16. Consistent with the cluster-based permutation test, alpha suppression are seen in both channels, when viewing the pictures together, indicated by the blue color.

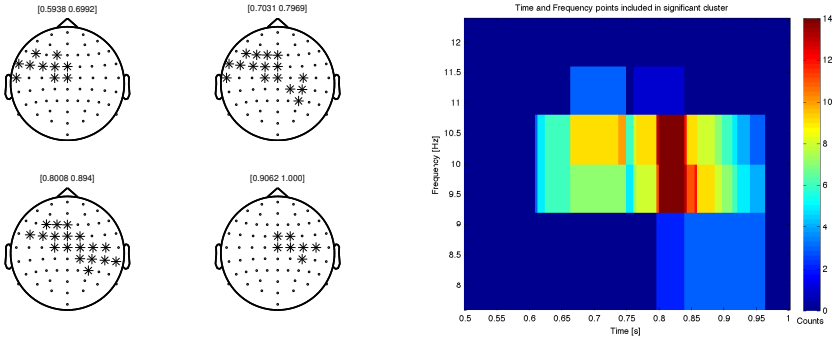

(a) **(b)**

Figure 7.16: The figures show a negative cluster (p=0.06) for the contrast Together/Alone for negative pictures. In figure a) the spatial location of the cluster is seen for four different time steps. It is ranging from the left prefrontal area to the right centro-parietal. In figure b) the temporal and spectral samples of the cluster are seen. The colorbar indicates the number of channels a single pixel (time point $\times$ frequency point) is represented in. E.g a color with index value of ten means that the pixel is found to be a part of the cluster in ten channels. The cluster is found in the alpha band most prominent around 10 Hz from 600 to 900 ms. The negativity of the cluster implies higher alpha power in the Alone condition.

Chapter 8

Discussion

This chapter discusses the main findings presented in Chapter 7. The chapter has the same structure as Chapter 7 to ease the understanding for the reader:

1. The first section provides a discussion of the baseline and prestimulus alpha.
2. The second section compares the results of the emotional content of pictures to similar studies.
3. The third section discusses, how the presence of another person can modulate attention and the level of arousal.
4. The chapter ends with a general discussion of the cluster-based permutation test, taking both the simulation from Chapter 4 and the real data into account. Furthermore, it provides a discussion of the implementation of the cluster-based permutation test on source and region level.

8.1 Baseline

It is well-known that alpha activity is connected to the state of attention of a person [63]. It is therefore not surprising that the alpha power increases during

the second half of the experiment as participants tend to tire. Furthermore, it is important to make clear that the baseline modulation is not related to the emotional content of a picture, as the participants had no knowledge about the upcoming picture beforehand.

The modulation of prestimulus alpha between Alone and Together can be explained in two ways. First, the participants are more attentive during the resting state (baseline), as one might feel more alert by the presence of another person. Second, the modulation could be a coincidence as a high intersubject variability in the baseline is present (cf. Figure 7.3). In theory, the effect of being Together or Alone in the first half should have been blocked by the experimental design, as the order of being Alone or Together is counterbalanced. However, the experiment included only 10 participants, which means that the large intersubject variability still could have an effect. The result also shows why counterbalancing the order of conditions is so important.

The differences between Alone and Together are located at the parietal and occipital sites, where the differences due to the order are present at all channels, cf. Figure 7.2 and C.1. In addition, prestimulus alpha has shown to play a role in a visual discrimination task. Increased alpha power in the baseline decreased the ability to detect a difference in gray levels between two discs [120] and decreased the performance of short time memory [83]. Both findings indicate prestimulus alpha as a measure of awareness prior to image onset. It is also shown that memory performance increases when another person is present [104, 105]. These results would support the idea of decreasing alpha power in the baseline for the Together condition.

It is difficult to conclude, if the prestimulus alpha difference between Alone and Together is a result of participants being more alert or an effect of the high intersubject variability.

8.2 Main Factor - Emotional Content of the Pictures

This section will discuss results from the ERP analysis divided up into the early and late time window. Next, the time-frequency results are discussed with respect to the theta and alpha band.

8.2.1 ERP Results

Early ERP modulations: The positive pictures were distinguished from neutral pictures within the latency of 150 to 300 ms in the parietal and occipital lobe, which is consistent with the literature [60, 97, 100]. It has been proposed to be allocation of attentional resources [60, 97, 100], where the limbic system enhances activation in the visual cortex when emotional pictures are presented [69]. The limbic system is connected to the prefrontal cortex during generation of emotions [69], which would explain the found significant cluster at the frontal and prefrontal sites when testing with the early window, cf. Figure C.6a.

An alternative explanation of increased activity for affective pictures compared to neutral ones, is the complexity of the picture as the neutral pictures in general are less complex [69, 93]. A study by Bradley et al. [28] compared simple and complex affective pictures, and found a difference at the early ERP components. However, studies comparing affective and neutral pictures while keeping the picture complexity equal, studies have still found differences at early ERP components [28, 69].

Late ERP modulations: The cluster-based permutation test showed significant differences between affective and neutral pictures after 350-400 ms. The results are consistent with similar studies [28, 60, 97, 111], and reflect enhanced attraction of attentional neural resources for processing the emotional content. In addition, when comparing the spatial location of the cluster with the one in the early time window, the cluster is more widely distributed and not very located at the occipital and parie-occipital sites.

A recent study by Liu et al. [78] showed that by combining fMRI and EEG, the differences between positive and neutral pictures are located to medial PFC, where the differences between negative and neutral pictures are located at the midline parietal cortex. Amygdala and visual cortices show increased activity when processing affective pictures. In the thesis, the source reconstruction revealed increased activity in the left frontal midline gyrus for positive compared to neutral pictures. Left frontal midline gyrus is located in the left prefrontal cortex including the left dorsolateral prefrontal cortex. The dorsolateral prefrontal cortex has been associated with processing emotions [33, 50]. In addition, it has been suggested that the left dorsolateral prefrontal cortex is connected to positive emotions, where several areas in the right prefrontal cortex has been associated with processing negative emotions [33]. For the negative compared to neutral pictures, several areas showed activation in both the right and left prefrontal area and in regions at the right temporal lobe. A recent study by Aldhafeeri et al. [11] also showed activation of the temporal lobe for negative pictures and a review by Kobe et al. [69] noted the right temporal cortex to be

a part of the visual association group which shows activation in both the early and late visual processing.

Amygdala has been identified as a key structure during perception of affective pictures compared to neutral ones [50], however the source reconstruction did not show any activation of amygdala. One reason for this could be that amygdala is a deep structure, which is difficult for the source reconstruction.

8.2.2 Time-Frequency Results

Theta oscillations: Figure 7.9a shows increased theta power for positive pictures compared to neutral ones[47] from 350 to 700 ms. The effect is mostly located at the frontal electrode sites, which could indicate increased theta oscillations from hippocampal in the limbic system. It is similar to earlier studies that report a difference from 200 to 500 ms [10] and within the first 600 ms [68]. The hippocampal structure is related to the memory, where increased theta oscillation is positively correlated with memory performance and encoding of new information [62]. Increased theta oscillation has been shown during processing of emotions and has been proposed to play a role for the connection between amygdala, hippocampal and prefrontal cortex [41].

Alpha oscillations: The significant difference between positive and neutral pictures is mostly located at the parietal electrode sites with lower alpha power for positive pictures similar to earlier findings [35, 68]. The difference begins after 700 ms, which is in the interval of LPP. It is consistent with Cesarei et al. [35] who suggest a functional association between the LPP and alpha ERD. In Table 7.2, it is seen that alpha ERD differences are not consistently found for the different combinations[48] compared to findings in the LPP, cf. Table 7.1. Cesarei et al. [35] report similar that the modulations of the LPP are more consistent as the intervariability is greater in the alpha modulation. In the thesis, the alpha band is defined from 8 to 12 Hz, where there is evidence of interpersonal variability of the alpha band [63]. The high interpersonal variability could be the reason for the more consistent findings in the ERP analysis compared to the time-frequency analysis. Defining subject-specific frequency band prior to the time-frequency analysis might decrease the high variability.

The alpha modulation between negative against positive pictures is an interesting finding, as it was only expected to find differences between affective and neutral pictures. The result suggests, that the subjects were more attended to

[47] The difference presented is for pictures solely in the Alone condition.

[48] Different combinations refer to the different tests, where both the pooled data and data separated in the Alone and Together conditions are used.

positive pictures. This is in contrast to men, as they are more aroused by erotic (positive) pictures, where females are more attentive to threats and mutilated bodies (negative) pictures [27]. As only female subjects were used, the opposite result was expected.

8.3 Main Factor - Social Context

The significant cluster for the contrast Together/Alone begins after 850 ms and reflects a higher response in the Alone condition within the LPP. The result might reflect a higher arousal state when viewing the pictures alone as LPP is connected to arousal [111].

Interestingly, the difference is visually most prominent for affective pictures as seen in Figure 7.10. In addition, neutral pictures are not believed to create an arousal state. Therefore, it is reasonable to believe that the effect of the social context only should modulate the signals for affective pictures. If the difference was caused by a non-event related activity (e.g. noise), it would also be present for neutral pictures. It is supported by Figure 7.11 that shows the mean error bars for the ERPs of the affective pictures, where the two social conditions still are separated. It is therefore strongly believed that the effect is caused by the social context. However, excluding the neutral pictures in the cluster-based permutation test did not enhanced the difference. Removing one third of the trials decreases the statistical power and affect the cluster-based permutation test during both the formation of the clusters and the permutation distribution.

The presence of another person has previously been shown to lower the arousal state measured by a decrease in heart rate [29], such that

> *"In the past few years, several studies examining effects of social presence manipulations on blood pressure and heart rate responsivity to laboratory stressors have been presented (1-6). Many of these studies demonstrate that the presence of a person who behaves in a supportive manner has the effect of attenuating cardiovascular responses to psychological stress".*

One possible explanation is that people might share the arousal load, and hence distribute the emotional effect. Another possibility could be that they are more controlled when the other person is in the room, and hence suppress the emotion. In the thesis, the second person did not behave in a supportive manner. However, the study [29], does not outline what supportive manner precisely

means nor tested if any difference is seen between the presence of a supportive person and a passive person.

From the MNE, *the left frontal superior gyrus, the left frontal midline gyrus, the left occipital midline gyrus, the right temporal superior gyrus and the right temporal midline gyrus* were the most activated AAL regions from the normalized difference from 0.7 to 1.2 s. The prefrontal cortex has consistently found to play an important role in late processing of emotional pictures and in regulation of the emotional state [11, 41], which might support the idea of emotion suppression. It is interesting that the temporal superior gyrus and prefrontal cortex are activated as it is consistent with studies of social cognition [8, 9, 53]. Adolphs [9] proposes a model of social cognition that includes the two areas, which also are connected to the MNS [53]. However, the same areas were activated for affective against neutral pictures as described earlier. This shows the aforementioned criticism, in Section 1.2.2, from isolated studies of social cognition, in that specific areas are social areas despite the fact that the same areas are active for non-social stimulus.

The time-frequency analysis showed a trend[49] of decreased alpha power when jointly viewing negative pictures, compared to being alone. The difference in the alpha band means that the participants were more attended towards the negative pictures with the presence of the other person. Richardson et al. [105] found that participants shifted their attention[50] towards negative pictures in contrast to positive or neutral pictures when viewing the pictures together. Thus, the participants became more attended to negative pictures when jointly seeing the pictures. However, they showed that the difference is enhanced if the participants had a shared goal, belief or task implying joint engagement. Therefore, they propose that a shared exposure without being jointly engaged is not enough to produce a difference in cognitive effects, despite that the attention was shifted towards negative pictures when they shared the pictures passively. It is important to notice that the participants in [105] were told by a message on the screen whether they were looking at the same or different pictures[51]. Recall from Chapter 5 that the experimental design was changed from giving a message to actually having a person inside the EEG cabin, because the participants did not pay enough attention to the presented messages. Having a person next to you, rather than only believing another person is seeing the same image as yourself, could enhance the effect of jointly looking at the pictures.

Richardson et al. [105] propose that the increased attention in the Together condition reflects an increase of generally alertness due to the presence of another

[49] Recall that the cluster-based permutation test found a cluster with p-value of 0.06.

[50] In the study [105], attention was measured as total looking time obtained by an eye tracker.

[51] The two participants were sitting back to back in opposite corners of the same room.

person. This hypothesis is supported by the difference in the baseline, where the Alone condition showed a higher alpha power. However, it does not explain why the increased attention only is seen for negative pictures. They explain the increased attention towards the negative pictures as an enhancement of the pre-existing bias meaning that people in generally is more engaged towards negative pictures.

A second hypothesis is proposed by the same study, [105], that viewing the pictures together align the emotions between the interacting persons, which would enhance the attention towards the pre-existing bias for negative pictures. This contradicts the results in this thesis as the ERP analysis showed a decrease of the arousal level in the Together condition reflected by a decrease in the LPP.

The presented results concerning the social context suggest that the arousal state is decreased, but that the attention is increased when jointly looking at the negative pictures. As mentioned earlier, Cesarei et al. [35] propose that the LPP and alpha ERD is connected, which contradicts the results in the thesis. They do, however, suggest that this connection needs to be studied further, including different cognitive processes. It raises the question of how the arousal state and attention can be disentangled from each other as LPP reflects arousal and alpha ERD reflects increased attention.

8.4 Cluster-Based Permutation Test

It was shown in the simulations that it is possible to manipulate the significance of a cluster by changing the time window in the analysis and/or the cluster alpha parameter[52]. Going from the large time window to the early time window revealed new significant clusters in the real data. The significant difference between negative and neutral pictures starting from 50-100 ms (Figure C.5a) was only present when using the early time window in contrast to the large. To the knowledge of the author, the current literature that uses the cluster-based permutation test does not provide information about the used cluster alpha parameter nor the used time window. Testing a hypothesis with several cluster alpha values or time windows introduces another MCP, which in theory should also be corrected.

It was shown that it is possible to apply the cluster-based permutation test on source and region level. However, prior to sufficiently perform the tests, an appropriate neighbor structure is necessary. In the thesis, the 3D euclidean distance was used to define the neighbor structure, which is a simplification

[52]Recall that the cluster alpha is the threshold when testing on sample level, cf. Chapter 4.

of the real source structure. The rationale is that two sources may appear as disconnected (e.g. being on two sides of a sulcus) whereas, given the poor spatial resolution, they belong to the same spatial blob. An improvement would be to use the geodesic distance as seen in Figure B.5 or define the neighboring structure from functional connections between the sources. It might explain the reason that the clusters on source level included so many sources, e.g. 809 sources out of 2050 as seen in Figure C.14. In addition, the MNE is known to have a poor performance as all the sources are distributed to the entire brain [115].

The low subject number in the thesis has its influence on the results from the cluster-based permutation test. Figure 7.13 shows how dependent the results are on a single person (e.g. subject 10 - permutation number 8). Increasing the number of subjects will increase the statistical power and lower the influence of the interpersonal variability. The interpersonal variability is visualized in Figure C.3b, where e.g. subject 3 and 9 show a strong negative response(200-250 ms after picture onset) in contrast to the rest of the subjects for both neutral, negative and positive pictures.

Chapter 9

Conclusion

In the thesis, a social neuroscience study was conducted in order to investigate how the presence of other human beings can affect one's attention and state of arousal when looking at emotional pictures.

The experimental design made it possible to reproduce earlier findings of how the neural mechanisms differ the processing of positive, negative and neutral pictures. In the early processing, it was shown that positive pictures were distinguished from negative and neutral pictures at the parietal and occipital sites associated with visual cortex consistent with similar studies [60, 97, 111]. At the late processing stage affective pictures showed an increase of a LPP mainly over the central sites compared to neutral pictures, which is also consistent with earlier studies [35, 60, 93]. The MNE source reconstruction showed high activation of the left frontal midline gyrus for positive pictures compared to neutral ones. The left prefrontal cortex has previously been shown to be connected to the processing of positive emotions [33]. The time-frequency analysis also showed consistent results compared to earlier findings with increased theta power and decreased alpha power for affective pictures [35, 62, 68].

By reproducing these results, it can be concluded that the used preprocessing pipeline was successful implemented with the applied analysis methods. During the preprocessing, the performance of the method EyeCatch was validated, with the use of an eye tracker. It was shown that one out of eight ICA components

was a false positive. Expanding the EyeCatch to include the frequency spectrum could improve the performance.

The cluster-based permutation test was of certain interest and was therefore investigated using both simulation and real data. The parameter *cluster alpha* was shown to have an important influence on the conclusion of whether to accept or reject the null hypothesis. Furthermore, it was shown using both simulation and the real data, that it is possible to manipulate the results by changing the time window in the cluster-based permutation test. The importance of these parameters complicates the fact that studies using the method in the literature are not reporting which values they are using and why they are used.

The cluster-based permutation test was also applied on source and region level. However, the tests did not show any significant differences, which is probably due to the insufficient defined neighbor structure. The 3D euclidean distance was used to define the neighbor structure, and it is proposed that using the geodesic distance would improve the tests. Another important factor could be the used source reconstruction method as it is shown to have a poor performance distributing the sources to the entire brain compared to newer and more advanced methods [115].

The analysis of the social context showed that the presence of the another person increased the attention when viewing negative pictures. It was consistent with Richardson et al. [105] who showed an increased attention towards negative pictures when the pictures are viewed jointly. Furthermore, the baseline showed increased attention prior to image onset. This could reflect a tendency toward general increased alertness due to the presence of another person. In the ERP analysis, the alone condition exhibited a larger LPP, which is associated with a higher aroused level. The decreased aroused level due to the presence of another person is proposed to be a sign of controlling one's emotion or sharing the emotional load. From the source reconstruction, the sources creating the difference were located at regions in the left prefrontal and right temporal area. These areas have been associated with processing information concerning social cognition [9, 53].

It can be concluded, that due to the high intersubject variability in the data and the differences being close to the significance level, more subjects are needed to increase the statistical power and to confirm the two findings. Furthermore, the presented study is the first of its kind and should be used as inspiration and as a preliminary work for future studies.

9.1 Future Work

One essential limitation of the thesis is the lack of statistical power due to the low number of participants. Although that results were reproduced using only ten participants, the results concerning the social context were very close to the significant level and dependent on single participants. The intersubject variability is known to be high in ERP studies and was also shown in the thesis, cf. Figure C.3 and 7.13. It indicates that more participants are needed before drawing a final conclusion. Furthermore, the social context complicates the analyzed neural mechanisms, which most likely increases the intersubject variability, requiring an even higher number of subjects.

In addition to recruit more participants, it would also be desirable to add a second experiment, where the participants after viewing the pictures had a task. Richardson et al. [105] propose that the effect of being jointly attended is enhanced if the participants are engaged in the same task, because this requires to process the meaning of the image. A memory task could therefore be added with the hypothesis that being jointly attended and engaged would increase the memory performance. As mentioned, decreased prestimulus alpha has been shown to increase the performance [83, 120], which was found in the Together condition.

In a future study, it would also be highly relevant to add third social condition, in which a person is present in the EEG-cabin but is not jointly looking at the images. It could answer whether the results were due to the subjects being jointly looking at the pictures or the fact that another person is just present in the room. If this condition showed a decrease in alpha power compared to the Alone condition, it would indicate that simply having a person in the same room increases the alertness.

To support the finding of decreased arousal level when jointly looking at the pictures, it could be interesting to measure the pulse and see if the pulse varied between the seeing the pictures alone or together. Likewise, it would be of interest to study the ratings that the participants made of the 60 images. First, these could be compared to the IAPS database ratings to see if the ratings were consistent. Secondly, these could be compared to the neural mechanisms (for example to see the arousal differences between positive and negative pictures).

The increased attention towards negative pictures when jointly looking at pictures could be further investigated by dividing the negative pictures up into threats and mutilated bodies. The source reconstruction found areas that are associated with the MNS. It could be interesting to see if the difference would be enhanced for the mutilated bodies compared to threats. It would shed light

on whether this increased attention is due to negative pictures in general or pictures concerning humans (e.g. mutilated bodies), which already activates the MNS.

In future studies, it would be interesting to do multiple EEG recordings (5-10 subjects) simultaneously while jointly attending a video to study the inter-personal dynamics since this can capture co-regulated couplings. It is suggested by Konvalinka and Roepstorff [72], that studying inter-personal dynamics instead of intra-personal dynamics might help us understand the underlying neural mechanism about social cognition. Several studies have used coherence and granger causality to capture inter-personal dynamics [13, 15, 14, 19, 21, 114]. For the present paradigm, coherence and functional connectivity could be used to find connection between arousal/emotional brain areas. It would also be interesting to study large groups and see whether group size had an effect on processing emotional scenes.

The cluster-based permutation test was tested on source and region level, which is highly desirable because the advantage of test is the ability to include many time points and spatial points (regions, channels or sources). Prior to applying the test, it is necessary to define a proper neighbor structure, e.g. by the geodesic distance or a functional structure. A better source reconstruction method would also improve the ability to locate the neural sources. Due the limited time, it was not possible to try these improvements . However, it would as mentioned be very relevant in a future perspective.

Appendix A

Mathematical Derivations

A.1 ICA

This appendix presents excluded mathematical derivations of ICA, which was presented in Chapter 3.

Recall that

$$\varphi(z) = -\frac{\frac{\partial}{\partial z}p(z)}{p(z)} \tag{A.1}$$

For the super-Gaussian it yields

$$\varphi(z) = -\frac{\frac{\partial}{\partial z}P_G(z)\text{sech}^2}{P_G(z)\text{sech}^2} \tag{A.2}$$

Defining $\mathcal{N}(0,1) = \exp(-\frac{z^2}{2})$ and taking the derivative gives

$$\varphi(z) = \frac{-1}{p_G(z)\text{sech}^2(z)}(p'_G(z)\text{sech}^2(z) + p_G(z)(\text{sech}^2(z))')$$

$$= \frac{z\exp(-\frac{z^2}{2})\text{sech}^2(z)}{\exp(-\frac{z^2}{2})\text{sech}^2(z)} + 2\frac{\exp(\frac{z^2}{2})\tanh(z)\text{sech}^2(z)}{\exp(-\frac{z^2}{2})\text{sech}^2(z)} \tag{A.3}$$

$$= z + 2\tanh(z).$$

For the sub-Gaussian it yields

$$\varphi(z) = -\frac{\frac{\partial}{\partial z}\frac{1}{2}(N(\mu,\sigma^2) + N(-\mu,\sigma^2))}{\frac{1}{2}(N(\mu,\sigma^2) + N(-\mu,\sigma^2))} \tag{A.4}$$

Defining $\mathcal{N}(0,1) = \exp(-\frac{z^2}{2})$ and taking the derivative gives

$$\varphi(z) = \frac{z\exp(-\frac{(z-1)^2}{2}) - \exp(-\frac{(z-1)^2}{2}) + z\exp(-\frac{(z+1)^2}{2}) + \exp(-\frac{(z+1)^2}{2})}{\exp(-\frac{(z-1)^2}{2}) + \exp(-\frac{(z+1)^2}{2})}$$

$$= z\frac{\exp(-\frac{(z-1)^2}{2}) + \exp(-\frac{(z+1)^2}{2})}{\exp(-\frac{(z-1)^2}{2}) + \exp(-\frac{(z+1)^2}{2})} - \frac{\exp(-\frac{(z-1)^2}{2}) - \exp(-\frac{(z+1)^2}{2})}{\exp(-\frac{(z-1)^2}{2}) + \exp(-\frac{(z+1)^2}{2})}$$

$$= z - \tanh(z). \tag{A.5}$$

Appendix B

Method

This appendix presents information about the task and procedure and settings about the eye tracker, cluster-based permutation test and the source reconstruction.

B.1 Task and Procedure

The following 240 pictures were used from the IAPS database:

[1019;1022;1033;1050;1051;1120;1200;1201;1202;1205;1220;1240;1270;1271;1274;
1275;1300;1304;1310;1321;1930;1931;1932;2036;2038;2039;2045;2050;2055;2057;
2070;2071;2075;2080;2091;2101;2102;2104;2107;2150;2151;2152;2153;2154;2155;
2156;2158;2160;2165;2170;2190;2191;2214;2215;2216;2221;2222;2396;2398;2411;
2435;2441;2480;2488;2491;2493;2495;2499;2500;2506;2511;2512;2513;2518;2530;
2550;2570;2595;2749;2811;2850;3000;3001;3005;3010;3015;3016;3019;3030;3051;
3053;3059;3060;3061;3062;3063;3064;3068;3069;3071;3080;3100;3101;3102;3110;
3120;3130;3131;3140;3150;3168;3185;3195;3225;3250;3261;3266;3400;3530;4490;
4520;4531;4533;4538;4542;4550;4559;4561;4572;4575;4604;4606;4607;4608;4609;
4611;4612;4624;4625;4626;4628;4641;4643;4647;4650;4651;4652;4656;4658;4659;
4660;4664;4666;4670;4672;4677;4680;4687;4690;4693;4698;4800;4810;6150;6190;
6231;6244;6260;6263;6300;6312;6313;6350;6510;6520;6550;6555;6560;6570;7002;

7003;7004;7006;7009;7010;7012;7014;7017;7019;7020;7025;7030;7031;7035;7038;
7040;7041;7045;7050;7052;7055;7057;7058;7059;7060;7062;7078;7080;7090;7100;
7110;7130;7150;7175;7179;7185;7233;7235;9070;9253;9405]

B.2 The Eye Tracker

Figure B.1 shows an example of how the eye-tracking data looked like. The example shows the data for one trial.

```
MSG     4291338 TRIALID 11
MSG     4294366 RECCFG CR 500 2 1 L
MSG     4294366 ELCLCFG MTABLER
MSG     4294366 GAZE_COORDS 0.00 0.00 1023.00 767.00
MSG     4294366 THRESHOLDS L 74 219
MSG     4294366 ELCL_PROC ELLIPSE  (5)
MSG     4294366 ELCL_EFIT_PARAMS 1.01 4.00  0.15 0.05  0.65 0.65  0.00 0.00 0.30
MSG     4294367 !MODE RECORD CR 500 2 1 L
START   4294368         LEFT    EVENTS
PRESCALER       1
VPRESCALER      1
PUPIL   DIAMETER
EVENTS  GAZE    LEFT    RATE     500.00 TRACKING        CR      FILTER  2
SFIX L   4294602
EFIX L   4294602        4294846 246       515.6   368.1    9361
SSACC L  4294848
SBLINK L 4294894
EBLINK L 4294894        4294904 12
ESACC L  4294848        4294984 138       518.3   363.7   502.6   360.0    0.50    1533
SFIX L   4294986
MSG     4295867 TRIAL_000011
EFIX L   4294986        4296028 1044      512.3   368.7    9518
SSACC L  4296030
ESACC L  4296030        4296052 24        512.4   368.0   447.0   343.1    2.20     162
SFIX L   4296054
EFIX L   4296054        4297876 268       552.0   424.1    8238
END     4297879         EVENTS  RES       33.23   26.00
```

Figure B.1: The figure shows an example of how the data file from the eye tracker looked like. The string *START* indicates the fixation cross, *TRIAL_*000011 represents image onset and *END* means that the trial is ended. *SBLINK L* indicates the beginning of a blink for the left eye, and *SSACC L* indicates the beginning of a saccades. In this example one blink and two saccades are found for trial 11. The corresponding saccade degree are seen to be 0.5 and 2.20.

Figure B.2 shows the distribution of detected eye movements and blinks for subject 6, 9, 11 and 12 across the six conditions.

Figure B.3 belongs to Chapter 6 and shows the correlation between the eye-tracking data and all 64 ICA components for the remaining subjects. Figure 6.2 shows the corresponding figure for subject 3.

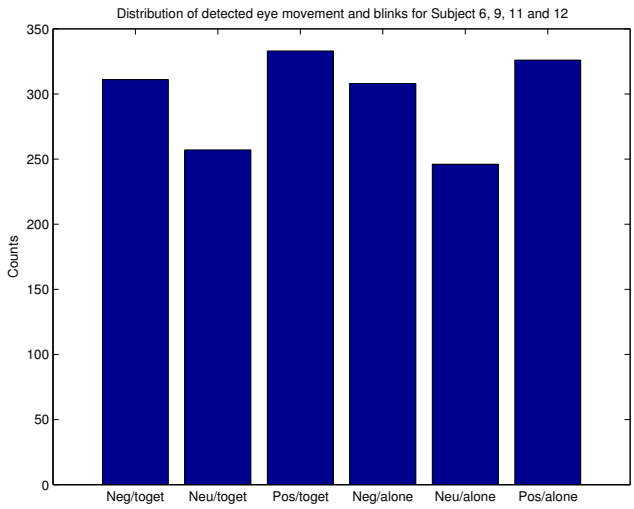

Figure B.2: The figure shows the distribution of detected eye movements and blinks for subject 6, 9, 11 and 12. The figure shows an equal distribution between the two social conditions, Together and Alone, but less detected eye movements and blinks for neutral pictures compared to positive and negative ones.

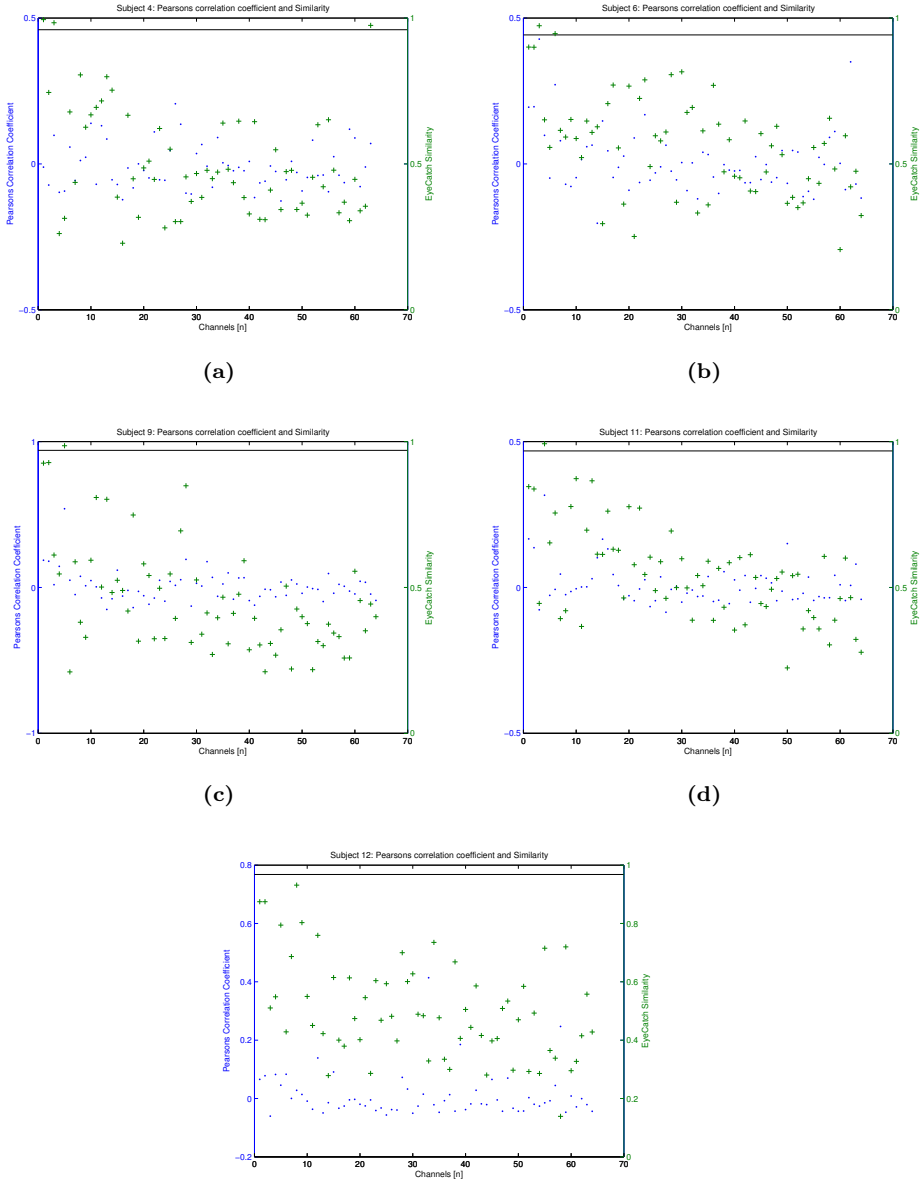

Figure B.3: The figures show the correlation between the eye-tracking data and all 64 ICA components for a) subject 4, b) subject 6, c) subject 9, d) subject 11 and e) subject 12. The correlation is symbolized with blue dots and the blue y-axis to the left. The figure also presents the similarity score given by EyeCatch for all 64 ICA components. These are marked green by + and the corresponding green y-axis to the right. ICA components above the threshold indicated by the vertical line are suggested removed by EyeCatch.

B.3 Cluster-Based Permutation Test

Figure B.4 shows the structure used to define which channels that are neighbors in the cluster-based permutation test. The black dots corresponds to channels, where the red lines symbolize the connection between two channels.

Figure B.5 visualizes the difference between the geodesic and euclidean distance.

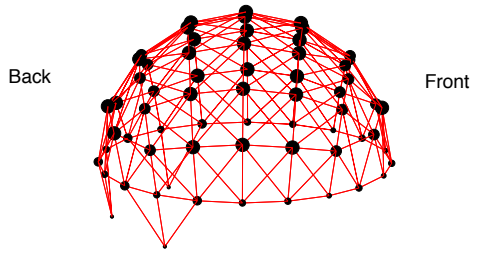

Figure B.4: The figure shows the structure for 64 channels, which is used in the cluster-based permutation test to define the structure of the neighbors. The black dots corresponds to channels, where the red lines symbolize the connection between two channels.

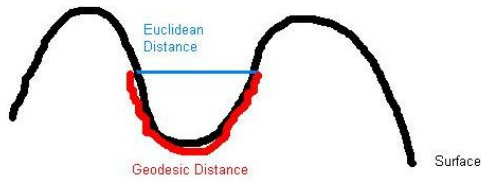

Figure B.5: The figure shows the difference between the geodesic and euclidean distance. The image is obtained from [6].

B.4 Source Reconstruction

Table B.1 shows the λ values for each subject and the MSE when performing source reconstruction, which is obtained on the validation set.

Subject	λ	MSE
3	5.8e-6	0.53
4	1.1e-6	0.23
5	9.4e-6	0.38
6	7.3e-6	0.26
7	3.7e-6	0.25
8	1.5e-6	0.21
9	5.3e-6	0.22
10	1.6e-5	0.48
11	3.4e-6	0.13
12	7.3e-6	0.15

Table B.1: λ values in the MNE and MSE of the validation set for each subject.

Figure B.6 compares the true recorded EEG signal with an estimated version of the signal after performing source reconstruction.

Figure B.7 shows the 116 regions in the AAL atlas with each region corresponding to a color. Below are all the regions written in the order of how they are presented in the x-axis in Figure 7.7, C.8, C.13 and C.18b.

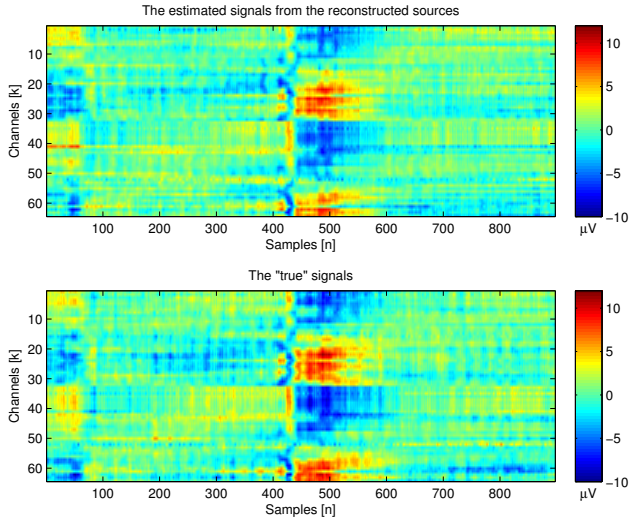

Figure B.6: The figure shows the true (bottom figure) and the estimated (top figure) signal from the source reconstruction. It is obtained for all 64 channels (y-axis) and all 897 samples (x-axis) for one trial. The estimated signal is computed from Equation 3.24.

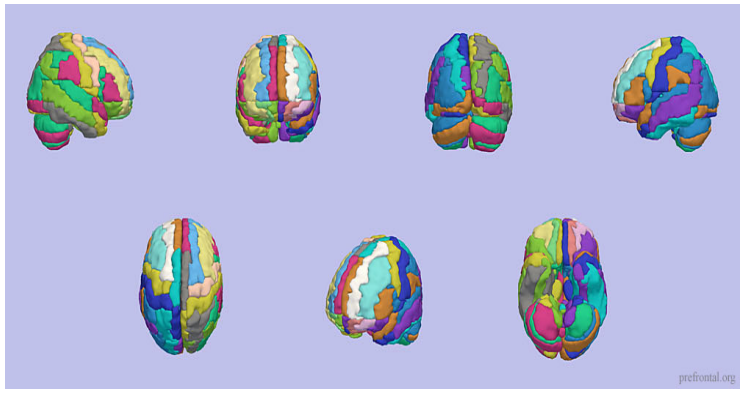

Figure B.7: The figure shows the 116 brain regions from the AAL atlas, where each color corresponds to a region [4].

AAL Regions:

1. Precentral-L
2. Precentral-R
3. Frontal-Sup-L
4. Frontal-Sup-R
5. Frontal-Sup-Orb-L
6. Frontal-Sup-Orb-R
7. Frontal-Mid-L
8. Frontal-Mid-R
9. Frontal-Mid-Orb-L
10. Frontal-Mid-Orb-R
11. Frontal-Inf-Oper-L
12. Frontal-Inf-Oper-R
13. Frontal-Inf-Tri-L
14. Frontal-Inf-Tri-R
15. Frontal-Inf-Orb-L
16. Frontal-Inf-Orb-R
17. Rolandic-Oper-L
18. Rolandic-Oper-R
19. Supp-Motor-Area-L
20. Supp-Motor-Area-R
21. Olfactory-L
22. Olfactory-R
23. Frontal-Sup-Medial-L
24. Frontal-Sup-Medial-R
25. Frontal-Med-Orb-L

26. Frontal-Med-Orb-R
27. Rectus-L
28. Rectus-R
29. Insula-L
30. Insula-R
31. Cingulum-Ant-L
32. Cingulum-Ant-R
33. Cingulum-Mid-L
34. Cingulum-Mid-R
35. Cingulum-Post-L
36. Cingulum-Post-R
37. Hippocampus-L
38. Hippocampus-R
39. ParaHippocampal-L
40. ParaHippocampal-R
41. Amygdala-L
42. Amygdala-R
43. Calcarine-L
44. Calcarine-R
45. Cuneus-L
46. Cuneus-R
47. Lingual-L
48. Lingual-R
49. Occipital-Sup-L
50. Occipital-Sup-R
51. Occipital-Mid-L
52. Occipital-Mid-R

53. Occipital-Inf-L
54. Occipital-Inf-R
55. Fusiform-L
56. Fusiform-R
57. Postcentral-L
58. Postcentral-R
59. Parietal-Sup-L
60. Parietal-Sup-R
61. Parietal-Inf-L
62. Parietal-Inf-R
63. SupraMarginal-L
64. SupraMarginal-R
65. Angular-L
66. Angular-R
67. Precuneus-L
68. Precuneus-R
69. Paracentral-Lobule-L
70. Paracentral-Lobule-R
71. Caudate-L
72. Caudate-R
73. Putamen-L
74. Putamen-R
75. Pallidum-L
76. Pallidum-R
77. Thalamus-L
78. Thalamus-R
79. Heschl-L

80. Heschl-R
81. Temporal-Sup-L
82. Temporal-Sup-R
83. Temporal-Pole-Sup-L
84. Temporal-Pole-Sup-R
85. Temporal-Mid-L
86. Temporal-Mid-R
87. Temporal-Pole-Mid-L
88. Temporal-Pole-Mid-R
89. Temporal-Inf-L
90. Temporal-Inf-R
91. Cerebelum-Crus1-L
92. Cerebelum-Crus1-R
93. Cerebelum-Crus2-L
94. Cerebelum-Crus2-R
95. Cerebelum-3-L
96. Cerebelum-3-R
97. Cerebelum-4-5-L
98. Cerebelum-4-5-R
99. Cerebelum-6-L
100. Cerebelum-6-R
101. Cerebelum-7b-L
102. Cerebelum-7b-R
103. Cerebelum-8-L
104. Cerebelum-8-R
105. Cerebelum-9-L
106. Cerebelum-9-R

107. Cerebelum-10-L
108. Cerebelum-10-R
109. Vermis-1-2
110. Vermis-3
111. Vermis-4-5
112. Vermis-6
113. Vermis-7
114. Vermis-8
115. Vermis-9
116. Vermis-10

Appendix C

Results

The following appendix presents results omitted from Chapter 7. It follows the same structure as the Chapter 7 with three sections concerning the baseline, the emotionally content of pictures and the social context.

C.1 Baseline

Figure C.1 shows the baseline differences between the first and second half of the experiment for all channels, where it is seen that the difference is present in almost all channels.

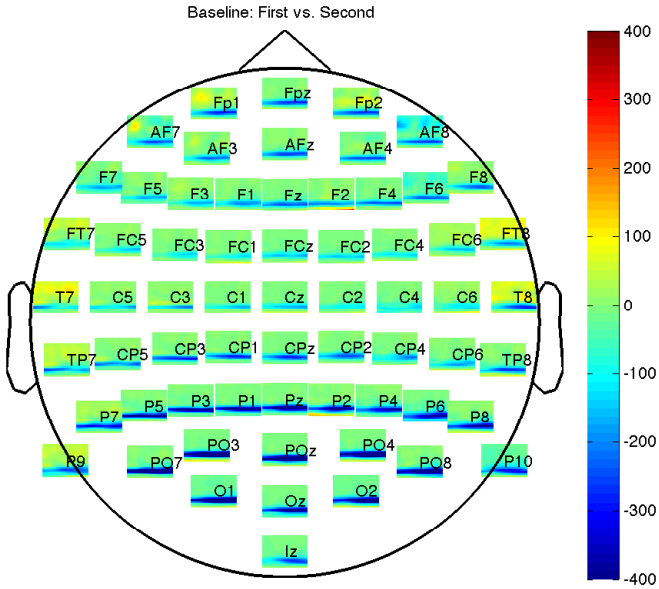

Figure C.1: The figure shows a difference between the first and second half of the EEG recordings. The time axis is from -0.5 to 0 seconds prior to image onset, and the frequency axis is from 4 to 30 Hz. The blue color indicates higher alpha power during the second half of the experiment. The differences are strongest in the parietal/occipital-parietal brain regions, but also clear at the frontal sites.

C.2 Main Factor - Emotional Content of the Pictures

The following section concern the results of testing the emotional content of the pictures.

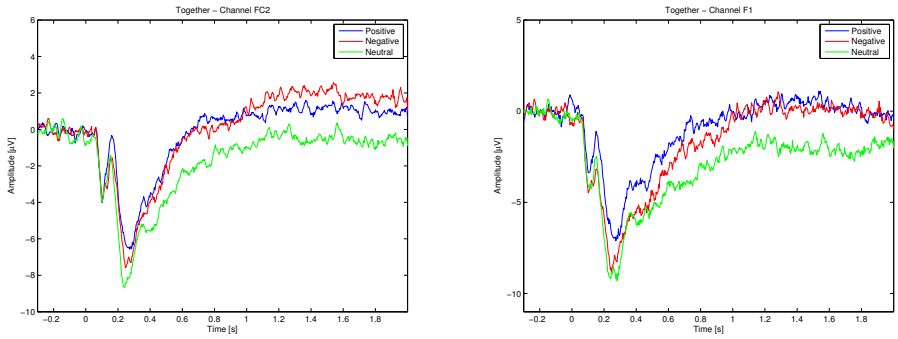

(a) **(b)**

Figure C.2: The figures show ERPs at channel FC2 a) and F1 b) for positive (blue), negative (red) and neutral (green) pictures.

C.2.1 ERP Analysis

Figure C.2 shows the ERPs at channel FC2 and F1 for positive (blue), negative (red) and neutral (green) pictures.

Figure C.3 shows the intersubject variability for the ERPs at channel O2 and CPz divided into positive (top figures), negative (middle figures) and neutral (bottom figures) pictures. Figure C.4 shows the ERPs for all 240 trials within subject 3 at channel O2. It is seen that the variability here is smaller than between subjects.

Figure C.5 and C.6 show the results of the cluster-based permutation test when using a) the early time window and b) the late time window respectively. Compared to using the large time window, more significant clusters are found.

In Figure C.7, the result for the contrast Negative/Positive in the early time window are shown. Two negative significant clusters (p=0.03, and p=0.03) are seen, one ranging from 120 to 180 ms in the centro-frontal area and the second from 200 to 270 ms in the frontal area. The result reflects a difference in the early visual processing between the negative and positive pictures.

Figure C.8 shows AAL regions activated contrasting negative and neutral pictures from 400 to 600 ms. It is seen that several frontal and temporal areas are activated including the left and right Frontal Midline and Inferior Gyrus, and left and right Temporal Midline, Inferior and superior Gyrus.

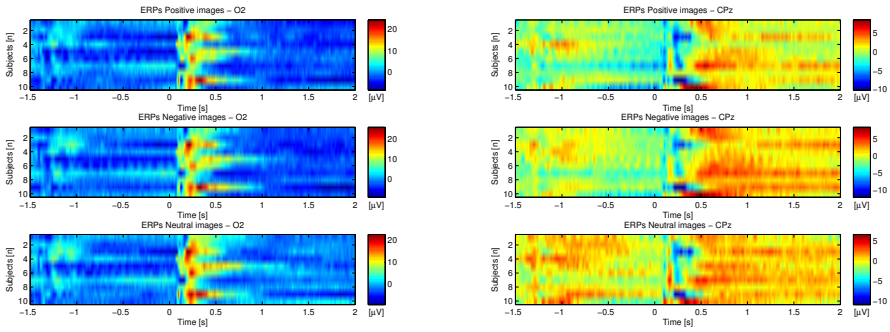

(a) **(b)**

Figure C.3: The figures show the intersubject variability in the ERPs across all ten subjects, for a) channel O2 and b) channel CPz. They are divided into positive (top figures), negative (middle figures) and neutral (bottom figures) pictures. It is seen that the variation between the subjects are larger than between the conditions.

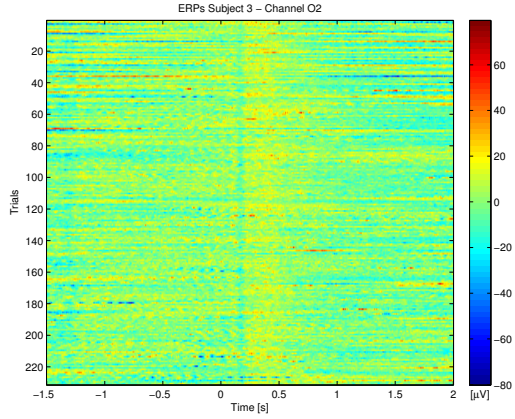

Figure C.4: The figure shows the ERPs for all 240 trials for subject 3 at channel O2.

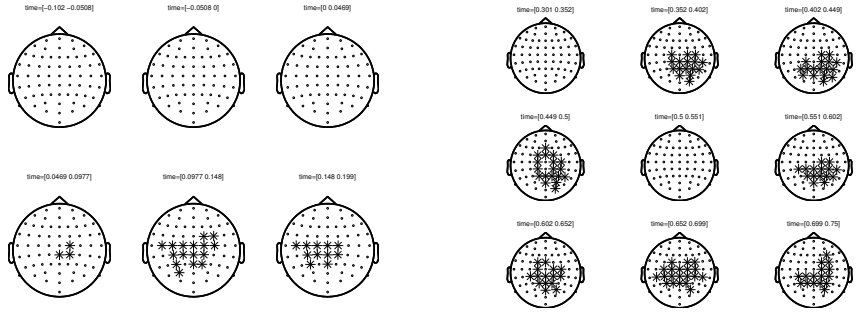

(a) **(b)**

Figure C.5: The figures show the results of the cluster-based permutation test when using the a) early time window and b) the late time window for the contrast Negative/Neutral. Figure a) shows a significant negative cluster (p=0.002) from 90 to 140 ms relative to image onset. Figure b) shows two significant clusters. The first cluster (p=0.04) from 350 to 500 ms, and the second positive cluster (p=0.004) from 550 to 750 ms, both relative to image onset.

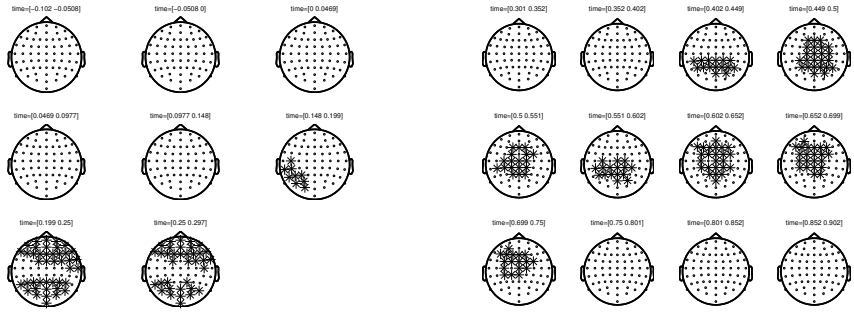

(a) **(b)**

Figure C.6: Figure a) visualizes the contrast Positive/Neutral in the early window. Two clusters are seen, where the first is positive (p=0.006) and is located in the occipital and parietal sites from 230 to 270 ms. The second cluster is negative (p=0.02) and is located at the frontal sites from 170 to 270 ms. Figure b) shows the same contrast in the late window. One positive significant clusters (p=0.002) are found, one from 420 to 720 ms.

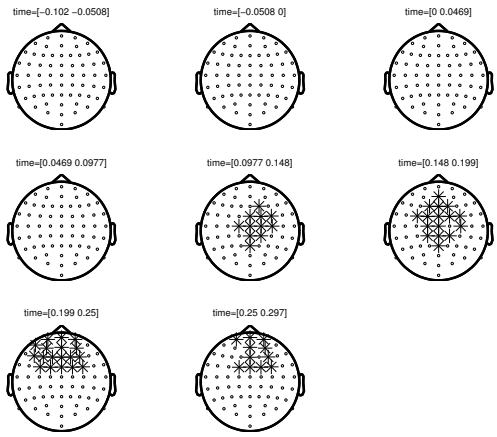

Figure C.7: The figure shows two different significant clusters for the contrast negative versus positive pictures in the early time window. The first negative cluster (p=0.03) are in the time range of 100 to 200 ms located at the centro-frontal area, where the second negative cluster (p=0.03) is found from 200 to 300 ms in the prefrontal and frontal area. A negative cluster reflects a higher response for positive pictures. Recall that the time steps of 50 ms do not reflect the temporal resolution used in the cluster-based permutation test.

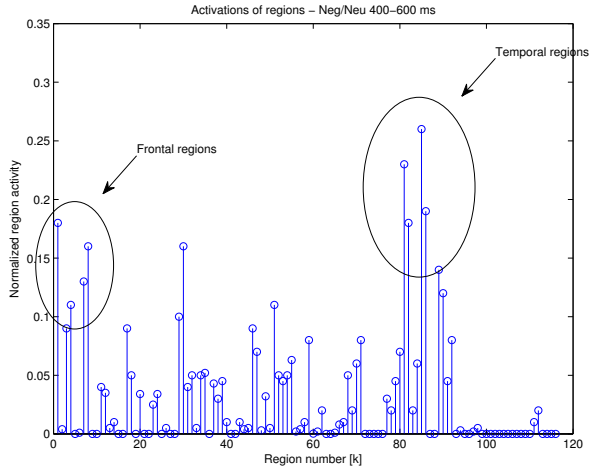

Figure C.8: The figure shows the activated AAL regions for the contrast Negative/Neutral from 400 to 600 ms relative to image onset. It is seen that several frontal and temporal areas are activated including the left and right Frontal Midline and Inferior Gyrus, and left and right Temporal Midline, Inferior and superior Gyrus.

C.2.2 Time-Frequency

Figure C.9 and C.10 show the averaged spectograms across all ten subjects for positive, negative and neutral pictures for channel FCz and O2. The bottom figures show the normalized difference between Positive/Neutral and Negative/Neutral.

In the beta band, the significant cluster (p=0.002) is very wide spread including almost all channels and ranges from 15 to 30 Hz in the frequency band, but most prominent around 20 Hz. The cluster is found in the late window ranging from 600 ms to 1 s after image onset.

Figure C.12 shows found a positive significant cluster in the theta (p=0.002) band and a negative cluster in the alpha (p=0.004) band for the contrast Negative/Neutral. Both clusters are located at the frontal sites, where the theta differences are in the low theta band (4-6 Hz) and alpha is in the upper alpha band (10-12 Hz). The clusters reflect a higher theta power and a lower alpha power for negative pictures compared to neutral ones.

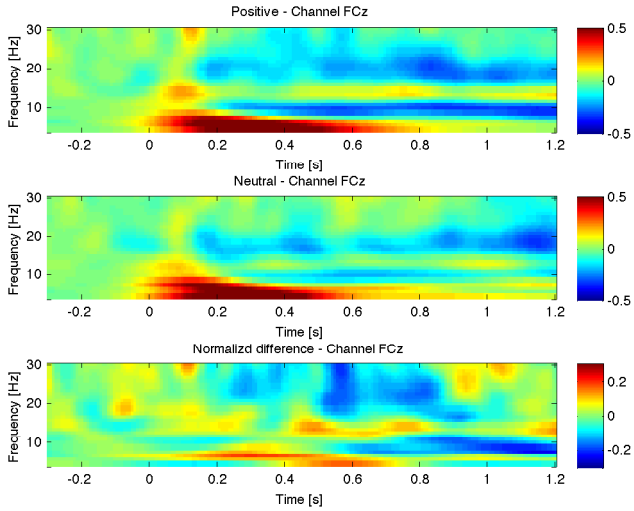

(a)

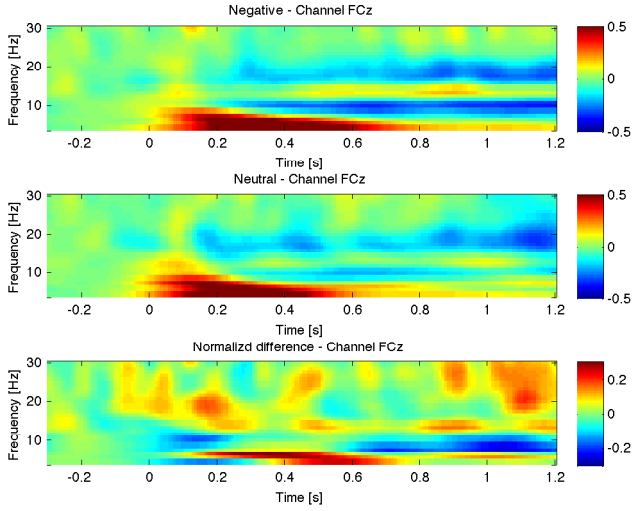

(b)

Figure C.9: The top and middle figures show, for channel FCz, the averaged spectograms across all ten subjects for a) positive and neutral picutres, and b) for negative and neutral pictures. The power is the relative change to the baseline defined from -0.4 to -0.1 prior to image onset. The bottom figures show the normalized difference between Positive/Neutral and Negative/Neutral respectively. It is seen that both positive and negative pictures have higher theta power and lower alpha power compared to neutral ones.

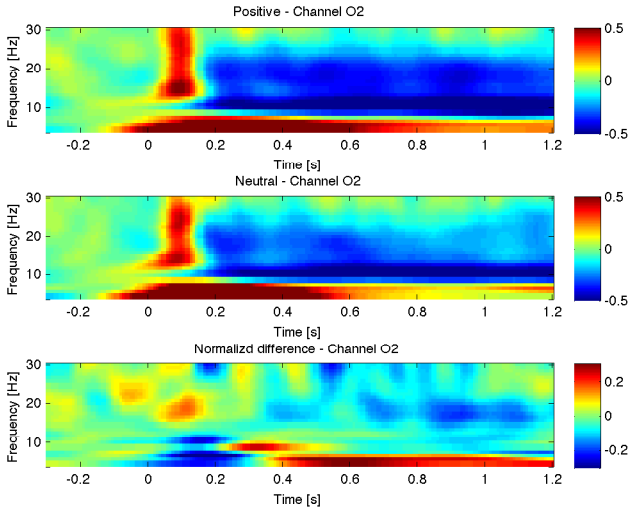

(a)

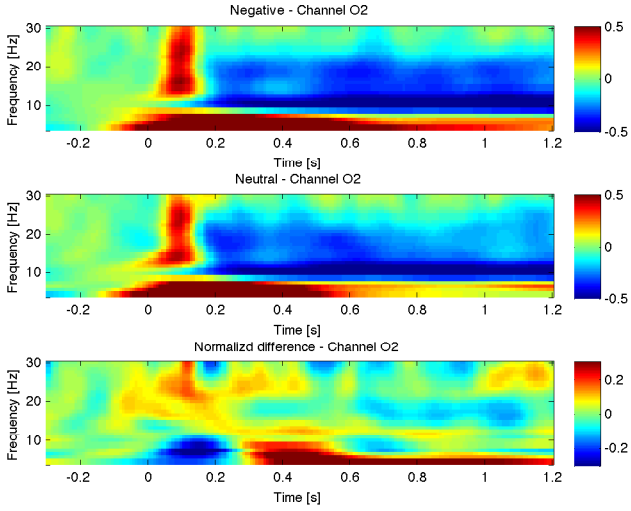

(b)

Figure C.10: The top and middle figures show, for channel O2, the averaged spectograms across all ten subjects for a) positive and neutral picutres, and b) for negative and neutral pictures. The power is the relative change to the baseline defined from -0.4 to -0.1 prior to image onset. The bottom figures show the normalized difference between Positive/Neutral and Negative/Neutral respectively.

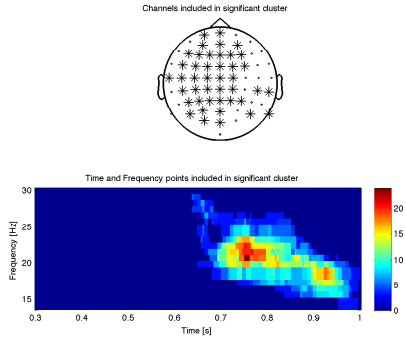

Figure C.11: The figure shows a difference in the beta band. The significant cluster (p=0.002) is very wide spread including almost all channels and ranges from 15 to 30 Hz in the frequency band. The cluster is found in the late window ranging from 600 ms to 1 s after image onset.

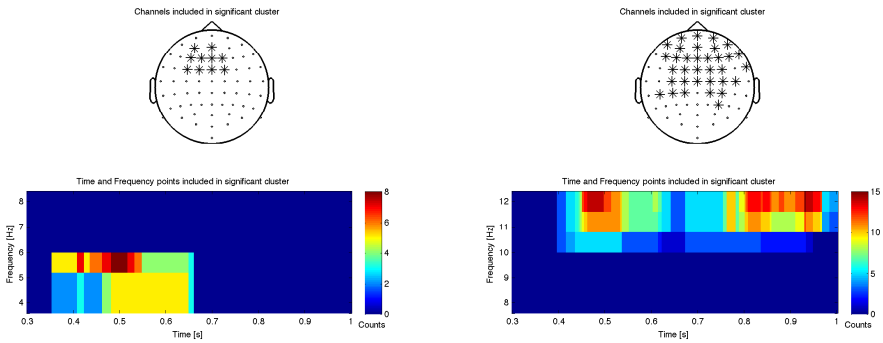

(a) **(b)**

Figure C.12: The figures show results from the cluster-based permutation test for the contrast Negative/Neutral. Figure a) shows a positive significant cluster in the theta (p=0.002) band located at the centro-frontal area. The cluster reflects a higher theta power for negative pictures. Figure b) shows a negative significant cluster in the alpha (p=0.004) band at the central and frontal channel sites. The cluster reflects a higher alpha power for neutral pictures.

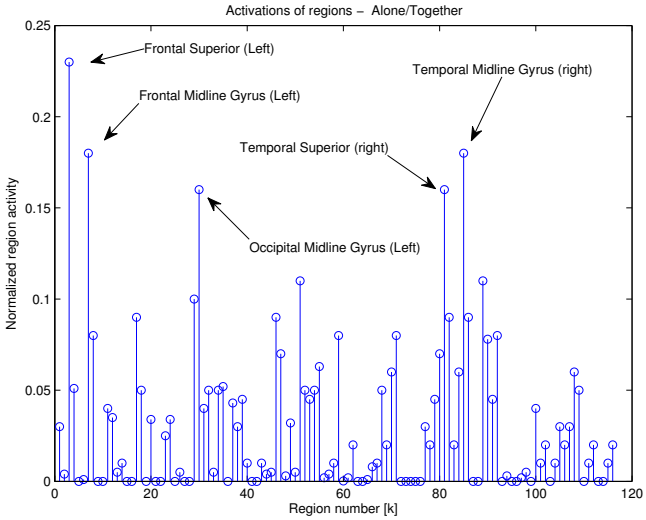

Figure C.13: The figure shows activated AAL regions for the contrast, Alone/Together. It is calculated from 0.7 to 1.2 seconds relative to image onset. The four most activated regions are: left frontal superior, left frontal midline gyrus, left occipital midline gyrus, right temporal midline gyrus and right temporal superior.

C.3 Main Factor - Social Context

The following results concern the tests between the two social conditions.

C.3.1 ERP Context

Figure C.13 shows the activated AAL regions for the contrast Alone/Together from 0.7 to 1.2 seconds relative to image onset. The four most activated regions are: left frontal superior, left frontal midline gyrus, left occipital midline gyrus and right temporal midline gyrus.

Figure C.14 shows the 807 out of the 2015 sources that were included in the found cluster (p=0.09) between Alone/Together when using the cluster-based permutation test on source level.

Figure C.15 shows an almost significant negative cluster (p=0.06) between Alone

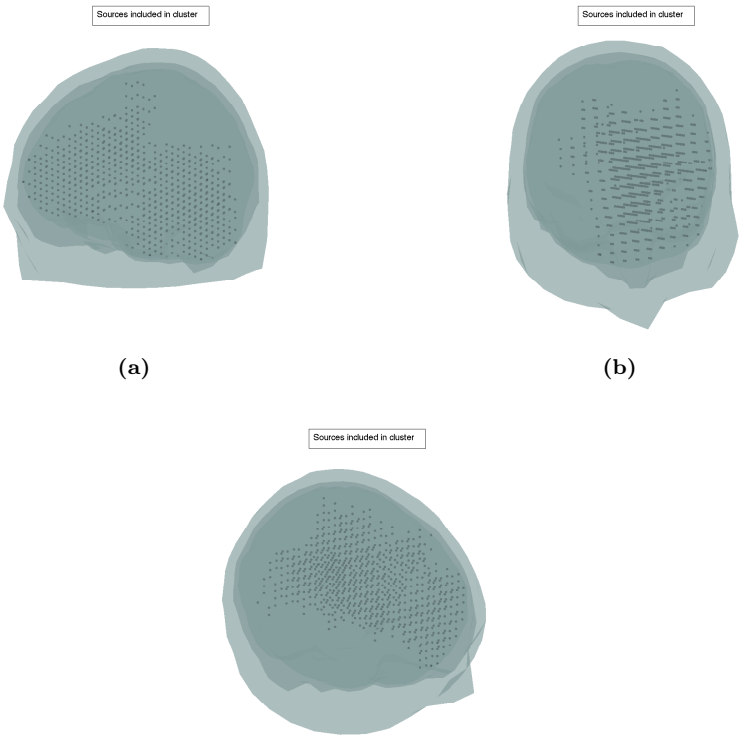

(a) **(b)**

(c)

Figure C.14: The figure shows the cluster, which was found when testing the contrast Alone/Together on source level. The time of the cluster is from 0.700 to 0.950 seconds relative to imagae onset. 807 out of the 2015 sources were included in the cluster.

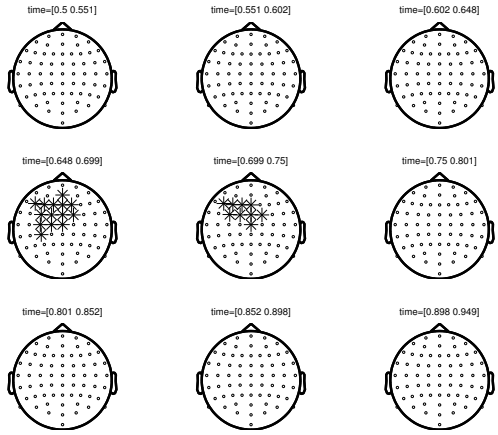

Figure C.15: The figure shows a negative cluster (p=0.06) in the left prefrontal area from 0.650 to 0.750 seconds. The cluster is close to the significance level of 0.05.

and Together for positive pictures. It is located at the left prefrontal area from 650 to 750 ms relative to image onset.

Figure C.16 shows the results testing the contrast Alone/Together on subject level instead of group level.

C.3.2 Time-Frequency

Figure C.17 shows the spectograms for the Together (top figures) and Alone (middle figures) conditions for negative pictures. The bottom figures show the normalized difference between the two conditions. Figure C.18 shows the results from the source reconstruction and which AAL regions that are active. As seen the difference is very widespread including many areas.

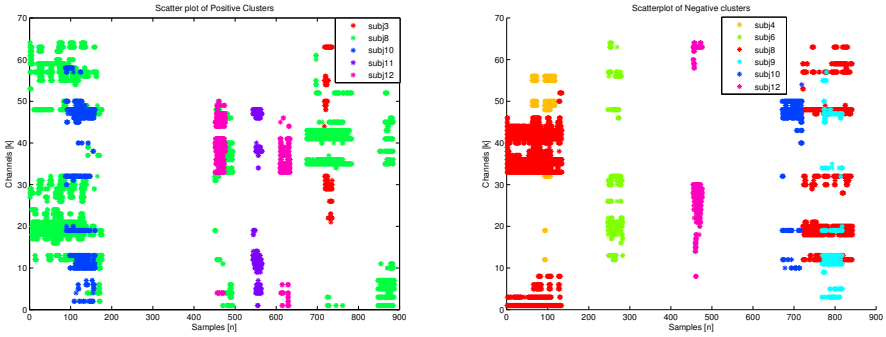

(a) **(b)**

Figure C.16: The figure shows the scatterplot of positive and negative clusters. In a) positive clusters are seen. Figure a) shows that only subject 3, 8, 10, 11 and 12 had positive clusters. Each subject is assigned to a specific color. One subject can have more than one cluster, e.g. subject 12 has four positive clusters. Figure b) shows that only subject 4, 6, 8, 9, 10, 12 had negative clusters.

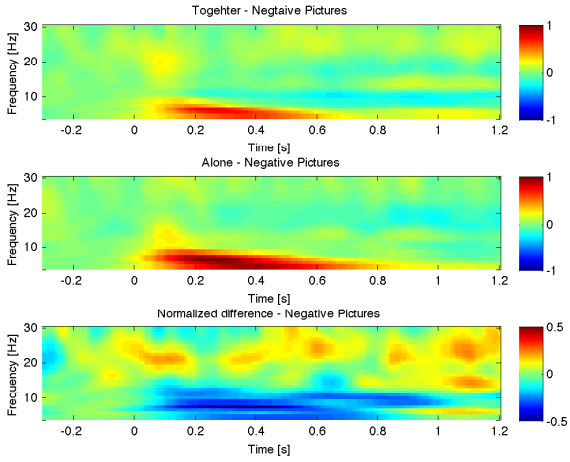

(a)

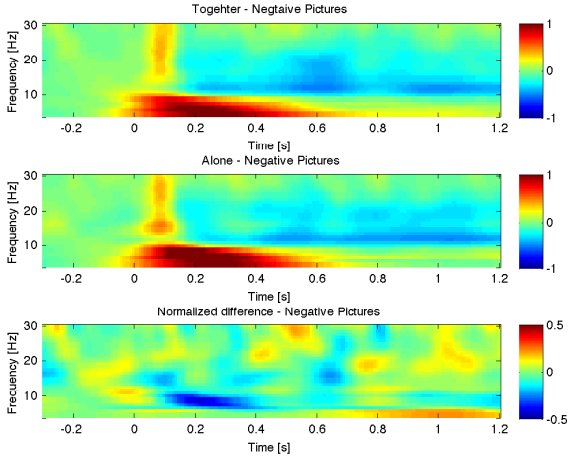

(b)

Figure C.17: The figures show spectograms for two channels a) FCz and b) PO4. The top figures are the average spectograms across all ten subjects for negative pictures in the Together condition, where the middle figures are the spectograms for the Alone condition. The color changes indicate the relative changes with respect to the baseline. The blue color indicates power suppression, where red indicates increased power. The bottom figures show the normalized differences for the contrast Together versus Alone. E.g a blue color means decreased power when viewing the pictures Together.

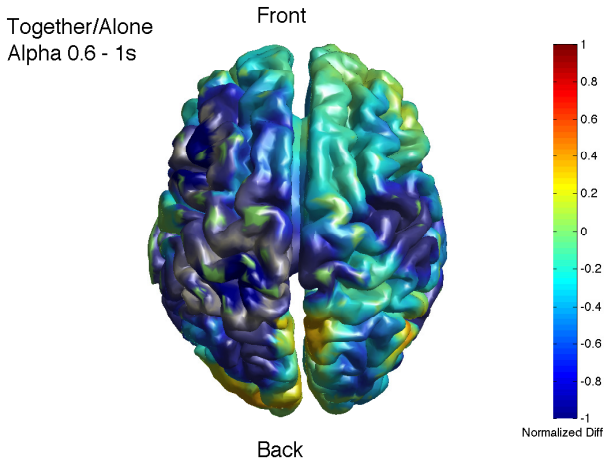

(a)

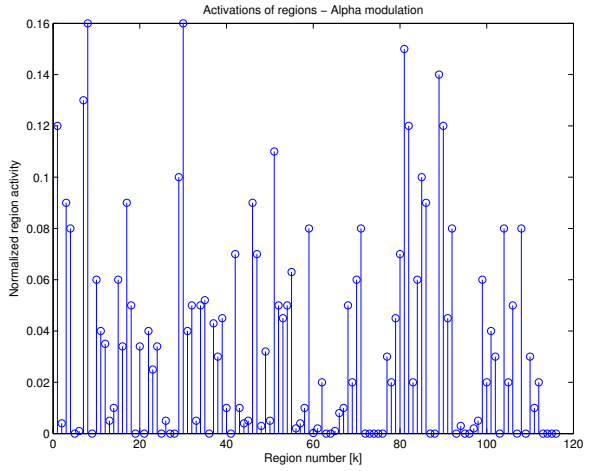

(b)

Figure C.18: The figures show a) the result of the MNE source reconstruction and b) the active AAL regions from 0.6 o 1 second relative to image onset. As both figures indicate, many areas are included and reflect the found differences in the alpha band between Together and Alone. The blue color indicates higher alpha power in the Alone condition.

Bibliography

[1] Biosemi. http://www.biosemi.com/headcap.htm, 2013. [Online; accessed -Marts-2013].

[2] Brain activation cd. http://www.brainactivationcd.com/brain_anatomy.htm, 2013. [Online; accessed -Marts-2013].

[3] Eeglab. http://sccn.ucsd.edu/wiki/Chapter_09:_Decomposing_Data_Using_ICA, 2013. [Online; accessed -4. June-2013].

[4] Prefrontal. http://prefrontal.org/blog/2008/05/brain-art-aal-patchwork/, 2013. [Online; accessed -2. July-2013].

[5] Sr-research. http://www.sr-research.com/EL_1000.html, 2013. [Online; accessed -12. April-2013].

[6] Van essen lab. http://brainvis.wustl.edu/wiki/index.php/Caret:Documentation:MetricSmoothing, 2013. [Online; accessed -7. June-2013].

[7] David J Acunzo, Graham MacKenzie, and Mark CW van Rossum. Systematic biases in early erp and erf components as a result of high-pass filtering. *Journal of neuroscience methods*, 211(2):309, 2012.

[8] Ralph Adolphs. Social cognition and the human brain. *Trends in cognitive sciences*, 3(12):469–479, 1999.

[9] Ralph Adolphs. Cognitive neuroscience of human social behaviour. *Nature Reviews Neuroscience*, 4(3):165–178, 2003.

[10] L.I Aftanas, A.A Varlamov, S.V Pavlov, V.P Makhnev, and N.V Reva. Affective picture processing: event-related synchronization within individually defined human theta band is modulated by valence dimension. *Neuroscience Letters*, 303(2):115–118, 2001.

[11] Faten M Aldhafeeri, Ian Mackenzie, Tony Kay, Jamaan Alghamdi, and Vanessa Sluming. Regional brain responses to pleasant and unpleasant iaps pictures: different networks. *Neuroscience letters*, 512(2):94–98, 2012.

[12] Shun-Ichi Amari. Natural gradient works efficiently in learning. *Neural computation*, 10(2):251–276, 1998.

[13] Laura Astolfi, F Cincotti, D Mattia, C Babiloni, F Carducci, A Basilisco, PM Rossini, S Salinari, Lei Ding, Ying Ni, et al. Assessing cortical functional connectivity by linear inverse estimation and directed transfer function: simulations and application to real data. *Clinical Neurophysiology*, 116(4):920–932, 2005.

[14] Laura Astolfi, F Cincotti, D Mattia, F De Vico Fallani, S Salinari, G Vecchiato, J Toppi, C Wilke, A Doud, H Yuan, et al. Imaging the social brain: multi-subjects eeg recordings during the "chicken's game". In *Engineering in Medicine and Biology Society (EMBC), 2010 Annual International Conference of the IEEE*, pages 1734–1737. IEEE, 2010.

[15] Laura Astolfi, Febo Cincotti, Donatella Mattia, M Grazia Marciani, Luiz A Baccala, Fabrizio de Vico Fallani, Serenella Salinari, Mauro Ursino, Melissa Zavaglia, Lei Ding, et al. Comparison of different cortical connectivity estimators for high-resolution eeg recordings. *Human brain mapping*, 28(2):143–157, 2006.

[16] Laura Astolfi, Jlenia Toppi, Fabrizio De Vico Fallani, Giovanni Vecchiato, Serenella Salinari, Donatella Mattia, Febo Cincotti, and Fabio Babiloni. Neuroelectrical hyperscanning measures simultaneous brain activity in humans. *Brain topography*, 23(3):243–256, 2010.

[17] Kassem A Awada, David R Jackson, Jeffery T Williams, Donald R Wilton, Stephen B Baumann, and Andrew C Papanicolaou. Computational aspects of finite element modeling in eeg source localization. *Biomedical Engineering, IEEE Transactions on*, 44(8):736–752, 1997.

[18] Fabio Babiloni and Laura Astolfi. Social neuroscience and hyperscanning techniques: Past, present and future. *Neuroscience & Biobehavioral Reviews*, 2012.

[19] Fabio Babiloni, Laura Astolfi, Febo Cincotti, Donatella Mattia, Andrea Tocci, A Tarantino, MG Marciani, S Salinari, S Gao, A Colosimo, et al. Cortical activity and connectivity of human brain during the prisoner's

dilemma: an eeg hyperscanning study. In *Engineering in Medicine and Biology Society, 2007. EMBS 2007. 29th Annual International Conference of the IEEE*, pages 4953–4956. IEEE, 2007.

[20] Fabio Babiloni, F Cincotti, D Mattia, F De Vico Fallani, A Tocci, L Bianchi, S Salinari, MG Marciani, A Colosimo, and L Astolfi. High resolution eeg hyperscanning during a card game. In *Engineering in Medicine and Biology Society, 2007. EMBS 2007. 29th Annual International Conference of the IEEE*, pages 4957–4960. IEEE, 2007.

[21] Luiz A Baccala and Koichi Sameshima. Partial directed coherence: a new concept in neural structure determination. *Biological cybernetics*, 84(6):463–474, 2001.

[22] Sylvain Baillet, John C Mosher, and Richard M Leahy. Electromagnetic brain mapping. *Signal Processing Magazine, IEEE*, 18(6):14–30, 2001.

[23] Anthony J Bell and Terrence J Sejnowski. An information-maximization approach to blind separation and blind deconvolution. *Neural computation*, 7(6):1129–1159, 1995.

[24] Olivier Bertrand, Jorge Bohorquez, and Jacques Pernier. Time-frequency digital filtering based on an invertible wavelet transform: an application to evoked potentials. *Biomedical Engineering, IEEE Transactions on*, 41(1):77–88, 1994.

[25] Nima Bigdely-Shamlo, Ken Kreutz-Delgado, Christian Kothe, and Scott Makeig. Eyecatch: Data-mining over half a million eeg independent components to construct a fully-automated eye-component detector. *IEEE Engineering in Biology and Medicine Conference, Osaka, Japan 2013*.

[26] Christopher M Bishop et al. *Pattern recognition and machine learning*, volume 1. springer New York, 2006.

[27] Margaret M Bradley, Maurizio Codispoti, Dean Sabatinelli, Peter J Lang, et al. Emotion and motivation ii: Sex differences in picture processing. *Emotion*, 1(3):300–319, 2001.

[28] Margaret M Bradley, Steven Hamby, Andreas Löw, and Peter J Lang. Brain potentials in perception: picture complexity and emotional arousal. *Psychophysiology*, 44(3):364–373, 2007.

[29] Nicholas Christenfeld, Williams Gerin, Wolfgang Linden, Mara Sanders, Jennifer Mathur, James D Deich, and Thomas G Pickering. Social support effects on cardiovascular reactivity: Is a stranger as effective as a friend? *Psychosomatic Medicine*, 59(4):388–398, 1997.

[30] Maurizio Codispoti, Vera Ferrari, and Margaret M Bradley. Repetition and event-related potentials: distinguishing early and late processes in affective picture perception. *Journal of Cognitive Neuroscience*, 19(4):577–586, 2007.

[31] D. Louis Collins, Alex P Zijdenbos, Vasken Kollokian, John G Sled, Noor J Kabani, Colin J Holmes, and Alan C Evans. Design and construction of a realistic digital brain phantom. *Medical Imaging, IEEE Transactions on*, 17(3):463–468, 1998.

[32] Bruce N Cuthbert, Harald T Schupp, Margaret M Bradley, Niels Birbaumer, Peter J Lang, et al. Brain potentials in affective picture processing: covariation with autonomic arousal and affective report. *Biological psychology*, 52(2):95–111, 2000.

[33] Richard J Davidson and William Irwin. The functional neuroanatomy of emotion and affective style. *Trends in cognitive sciences*, 3(1):11–21, 1999.

[34] Andrea De Cesarei and Maurizio Codispoti. When does size not matter? effects of stimulus size on affective modulation. *Psychophysiology*, 43(2):207–215, 2006.

[35] Andrea De Cesarei and Maurizio Codispoti. Affective modulation of the lpp and α-erd during picture viewing. *Psychophysiology*, 48(10):1397–1404, 2011.

[36] Arnaud Delorme and Scott Makeig. Eeglab: an open source toolbox for analysis of single-trial eeg dynamics including independent component analysis. *Journal of neuroscience methods*, 134(1):9–21, 2004.

[37] Guy Demoment. Image reconstruction and restoration: Overview of common estimation structures and problems. *Acoustics, Speech and Signal Processing, IEEE Transactions on*, 37(12):2024–2036, 1989.

[38] Florin Dolcos and Roberto Cabeza. Event-related potentials of emotional memory: encoding pleasant, unpleasant, and neutral pictures. *Cognitive, Affective, & Behavioral Neuroscience*, 2(3):252–263, 2002.

[39] Guillaume Dumas, Jacqueline Nadel, Robert Soussignan, Jacques Martinerie, and Line Garnero. Inter-brain synchronization during social interaction. *PLoS One*, 5(8):e12166, 2010.

[40] Michael D Ernst. Permutation methods: A basis for exact inference. *Statistical Science*, 19(4):676–685, 2004.

[41] Matthias Ertl, Maria Hildebrandt, Kristina Ourina, Gregor Leicht, and Christoph Mulert. Emotion regulation by cognitive reappraisal–the role of frontal theta oscillations. *NeuroImage*, 81:412–421, 2013.

[42] Fabrizio De Vico Fallani, Vincenzo Nicosia, Roberta Sinatra, Laura Astolfi, Febo Cincotti, Donatella Mattia, Christopher Wilke, Alex Doud, Vito Latora, Bin He, et al. Defecting or not defecting: how to "read" human behavior during cooperative games by eeg measurements. *PloS one*, 5(12):e14187, 2010.

[43] J. Randall Flanagan and Roland S Johansson. Action plans used in action observation. *Nature*, 424(6950):769–771, 2003.

[44] Christos A Frantzidis, Charalampos Bratsas, Christos L Papadelis, Evdokimos Konstantinidis, Costas Pappas, and Panagiotis D Bamidis. Toward emotion aware computing: an integrated approach using multichannel neurophysiological recordings and affective visual stimuli. *Information Technology in Biomedicine, IEEE Transactions on*, 14(3):589–597, 2010.

[45] John Freund. *Miller and Freund's probability and statistics for engineers*. Pearson Education International, 2005.

[46] Pascal Fries, René Scheeringa, and Robert Oostenveld. Finding gamma. *Neuron*, 58(3):303–305, 2008.

[47] Chris D Frith. The social brain? *Philosophical Transactions of the Royal Society B: Biological Sciences*, 362(1480):671–678, 2007.

[48] Helen L Gallagher and Christopher D Frith. Functional imaging of 'theory of mind'. *Trends in cognitive sciences*, 7(2):77–83, 2003.

[49] Julie Grèzes, CD Frith, and Richard E Passingham. Inferring false beliefs from the actions of oneself and others: an fmri study. *Neuroimage*, 21(2):744–750, 2004.

[50] Nynke A Groenewold, Esther M Opmeer, Peter de Jonge, André Aleman, and Sergi G Costafreda. Emotional valence modulates brain functional abnormalities in depression: Evidence from a meta-analysis of fmri studies. *Neuroscience & Biobehavioral Reviews*, 37:152–163, 2012.

[51] Bahar Güntekin, Erol Başar, et al. Event-related beta oscillations are affected by emotional eliciting stimuli. *Neuroscience letters*, 483(3):173–178, 2010.

[52] Matti S Hämäläinen and RJ Ilmoniemi. Interpreting magnetic fields of the brain: minimum norm estimates. *Medical & biological engineering & computing*, 32(1):35–42, 1994.

[53] Riitta Hari and Miiamaaria V Kujala. Brain basis of human social interaction: from concepts to brain imaging. *Physiological reviews*, 89(2):453–479, 2009.

[54] Satoru Hayasaka and Thomas E Nichols. Combining voxel intensity and cluster extent with permutation test framework. *Neuroimage*, 23(1):54–63, 2004.

[55] Christoph S Herrmann, Axel Mecklinger, and Erdmut Pfeifer. Gamma responses and erps in a visual classification task. *Clinical Neurophysiology*, 110(4):636–642, 1999.

[56] Sture Holm. A simple sequentially rejective multiple test procedure. *Scandinavian journal of statistics*, pages 65–70, 1979.

[57] Ivo Hostens, Jan Seghers, Arthur Spaepen, and Herman Ramon. Validation of the wavelet spectral estimation technique in biceps brachii and brachioradialis fatigue assessment during prolonged low-level static and dynamic contractions. *Journal of Electromyography and kinesiology*, 14(2):205–215, 2004.

[58] Tzyy-Ping Jung, Colin Humphries, Te-Won Lee, Scott Makeig, Martin J McKeown, Vicente Iragui, and Terrence J Sejnowski. Extended ica removes artifacts from electroencephalographic recordings. *Advances in neural information processing systems*, pages 894–900, 1998.

[59] Valer Jurcak, Daisuke Tsuzuki, and Ippeita Dan. 10/20, 10/10, and 10/5 systems revisited: their validity as relative head-surface-based positioning systems. *Neuroimage*, 34(4):1600–1611, 2007.

[60] Andreas Keil, Margaret M Bradley, Olaf Hauk, Brigitte Rockstroh, Thomas Elbert, and Peter J Lang. Large-scale neural correlates of affective picture processing. *Psychophysiology*, 39(5):641–649, 2002.

[61] Andreas Keil, Matthias M Müller, Thomas Gruber, Christian Wienbruch, Margarita Stolarova, and Thomas Elbert. Effects of emotional arousal in the cerebral hemispheres: a study of oscillatory brain activity and event-related potentials. *Clinical Neurophysiology*, 112(11):2057–2068, 2001.

[62] Patrick H Khader, Kerstin Jost, Charan Ranganath, and Frank Rösler. Theta and alpha oscillations during working-memory maintenance predict successful long-term memory encoding. *Neuroscience letters*, 468(3):339–343, 2010.

[63] Wolfgang Klimesch. Eeg alpha and theta oscillations reflect cognitive and memory performance: a review and analysis. *Brain research reviews*, 29(2):169–195, 1999.

[64] Wolfgang Klimesch. Alpha-band oscillations, attention, and controlled access to stored information. *Trends in cognitive sciences*, 16(12):606–617, 2012.

[65] Wolfgang Klimesch, M Doppelmayr, Th Pachinger, and B Ripper. Brain oscillations and human memory: Eeg correlates in the upper alpha and theta band. *Neuroscience letters*, 238(1):9–12, 1997.

[66] Wolfgang Klimesch, M Doppelmayr, H Russegger, and Th Pachinger. Theta band power in the human scalp eeg and the encoding of new information. *Neuroreport*, 7(7):1235–1240, 1996.

[67] Wolfgang Klimesch, Paul Sauseng, and Simon Hanslmayr. Eeg alpha oscillations: the inhibition–timing hypothesis. *Brain research reviews*, 53(1):63–88, 2007.

[68] Gennady G Knyazev. Motivation, emotion, and their inhibitory control mirrored in brain oscillations. *Neuroscience & Biobehavioral Reviews*, 31(3):377–395, 2007.

[69] Hedy Kober, Lisa Feldman Barrett, Josh Joseph, Eliza Bliss-Moreau, Kristen Lindquist, and Tor D Wager. Functional grouping and cortical–subcortical interactions in emotion: A meta-analysis of neuroimaging studies. *Neuroimage*, 42(2):998, 2008.

[70] Peter König, Michael Plöchl, and Jose Pablo Ossandón. Combining eeg and eye tracking: Identification, characterization and correction of eye movement artifacts in electroencephalographic data. *Frontiers in human neuroscience*, 6, 2012.

[71] Ivana Konvalinka, Markus Bauer, Carsten Stahlhut, Lars Kai Hansen, Andreas Roepstorff, and Chris D. Frith. Frontal alpha oscillations distinguish leaders from followers: Multivariate decoding of mutually interacting brains. *In Proceeding*.

[72] Ivana Konvalinka and Andreas Roepstorff. The two-brain approach: how can mutually interacting brains teach us something about social interaction? *Frontiers in Human Neuroscience*, 6, 2012.

[73] Fanny Lachat, Laurent Hugueville, Jean-Didier Lemaréchal, Laurence Conty, and Nathalie George. Oscillatory brain correlates of live joint attention: a dual-eeg study. *Frontiers in Human Neuroscience*, 6, 2012.

[74] Peter J Lang, Margaret M Bradley, and Bruce N Cuthbert. International affective picture system (iaps): Technical manual and affective ratings, 1999.

[75] Bhagwandas Pannalal Lathi. *Signal processing and linear systems*, volume 1. Berkeley Cambridge Press, 1998.

[76] Te-Won Lee, Mark Girolami, and Terrence J Sejnowski. Independent component analysis using an extended infomax algorithm for mixed subgaussian and supergaussian sources. *Neural computation*, 11(2):417–441, 1999.

[77] Fa-Hsuan Lin, Thomas Witzel, Matti S Hämäläinen, Anders M Dale, John W Belliveau, and Steven M Stufflebeam. Spectral spatiotemporal imaging of cortical oscillations and interactions in the human brain. *Neuroimage*, 23(2):582–595, 2004.

[78] Yuelu Liu, Haiqing Huang, Menton McGinnis-Deweese, Andreas Keil, and Mingzhou Ding. Neural substrate of the late positive potential in emotional processing. *The Journal of Neuroscience*, 32(42):14563–14572, 2012.

[79] Steven J Luck. *An introduction to the event-related potential technique (cognitive neuroscience)*. The MIT Press, 2005.

[80] Steven J Luck and Emily S Kappenman. *The Oxford Handbook of Event-Related Potential Components*. OUP USA, 2012.

[81] David J.C. MacKay. Maximum likelihood and covariant algorithms for independent component analysis. Technical report, University of Cambridge, 1996.

[82] Eric Maris and Robert Oostenveld. Nonparametric statistical testing of eeg-and meg-data. *Journal of neuroscience methods*, 164(1):177–190, 2007.

[83] Kyle E Mathewson, Gabriele Gratton, Monica Fabiani, Diane M Beck, and Tony Ro. To see or not to see: prestimulus α phase predicts visual awareness. *The Journal of neuroscience*, 29(9):2725–2732, 2009.

[84] MATLAB. *version 7.13.0.564 (R2011b)*. The MathWorks Inc., Natick, Massachusetts, 2011.

[85] Brenton W McMenamin, Alexander J Shackman, Lawrence L Greischar, and Richard J Davidson. Electromyogenic artifacts and electroencephalographic inferences revisited. *Neuroimage*, 54(1):4–9, 2011.

[86] Andrea Mognon, Jorge Jovicich, Lorenzo Bruzzone, and Marco Buiatti. Adjust: An automatic eeg artifact detector based on the joint use of spatial and temporal features. *Psychophysiology*, 48(2):229–240, 2011.

[87] Douglas C Montgomery. *Design and analysis of experiments*. Wiley New York, 2001.

[88] Morten Mørup, Lars Kai Hansen, and Sidse M Arnfred. Erpwavelab: A toolbox for multi-channel analysis of time–frequency transformed event related potentials. *Journal of neuroscience methods*, 161(2):361–368, 2007.

[89] Matthias M Müller, Andreas Keil, Thomas Gruber, and Thomas Elbert. Processing of affective pictures modulates right-hemispheric gamma band eeg activity. *Clinical Neurophysiology*, 110(11):1913–1920, 1999.

[90] Muhammad Naeem, Girijesh Prasad, David R Watson, and JA Kelso. Electrophysiological signatures of intentional social coordination in the 10–12hz range. *Neuroimage*, 59(2):1795–1803, 2012.

[91] Borna Noureddin, Peter D Lawrence, and Gary E Birch. Time-frequency analysis of eye blinks and saccades in eog for eeg artifact removal. In *Neural Engineering, 2007. CNE'07. 3rd International IEEE/EMBS Conference on*, pages 564–567. IEEE, 2007.

[92] Paul L Nunez and Ramesh Srinivasan. *Electric fields of the brain: the neurophysics of EEG*. Oxford University Press, USA, 2006.

[93] Jonas K Olofsson, Steven Nordin, Henrique Sequeira, and John Polich. Affective picture processing: an integrative review of erp findings. *Biological psychology*, 77(3):247, 2008.

[94] Jonas K Olofsson and John Polich. Affective visual event-related potentials: Arousal, repetition, and time-on-task. *Biological psychology*, 75(1):101, 2007.

[95] Robert Oostenveld, Pascal Fries, Eric Maris, and Jan-Mathijs Schoffelen. Fieldtrip: open source software for advanced analysis of meg, eeg, and invasive electrophysiological data. *Computational intelligence and neuroscience*, 2011:1, 2011.

[96] Robert Oostenveld, Dick F Stegeman, Peter Praamstra, and Adriaan van Oosterom. Brain symmetry and topographic analysis of lateralized event-related potentials. *Clinical neurophysiology*, 114(7):1194–1202, 2003.

[97] M. Carmen Pastor, Margaret M Bradley, Andreas Löw, Francesco Versace, Javier Moltó, and Peter J Lang. Affective picture perception: Emotion, context, and the late positive potential. *Brain research*, 1189:145, 2008.

[98] Luiz Pessoa and Ralph Adolphs. Emotion processing and the amygdala: from a'low road'to'many roads' of evaluating biological significance. *Nature Reviews Neuroscience*, 11(11):773–783, 2010.

[99] Kaare Brandt Petersen and Michael Syskind Pedersen. The matrix cookbook, 2006.

[100] Michael Kai Petersen, Carsten Stahlhut, Arkadiusz Stopczynski, Jakob Eg Larsen, and Lars Kai Hansen. Smartphones get emotional: mind reading images and reconstructing the neural sources. In *Affective Computing and Intelligent Interaction*, pages 578–587. Springer, 2011.

[101] John G. Proakis and Dimitris G. Manolakis. Digital signal processing: principles, algorithms, and application. 2007.

[102] Dale Purves, George J Augustine, David Fitzpatrick, Lawrence C Katz, Anthony-Samuel LaMantia, James O McNamara, S Mark Williams, et al. *Summation of Synaptic Potentials*. Sinauer Associates, 2001.

[103] William J Ray and Harry W Cole. Eeg alpha activity reflects attentional demands, and beta activity reflects emotional and cognitive processes. *Science*, 228(4700):750–752, 1985.

[104] Daniel C Richardson, Merrit A Hoover, and Arezou Ghane. Joint perception: gaze and the presence of others. In *Proceedings of the 30th Annual Conference of the Cognitive Science Society*, pages 309–314, 2008.

[105] Daniel C Richardson, Chris NH Street, Joanne YM Tan, Natasha Z Kirkham, Merrit A Hoover, and Arezou Ghane Cavanaugh. Joint perception: gaze and social context. *Frontiers in Human Neuroscience*, 6, 2012.

[106] Guillaume A Rousselet. Does filtering preclude us from studying erp timecourses? *Frontiers in Psychology*, 3, 2012.

[107] Bella Rozenkrants, Jonas K Olofsson, and John Polich. Affective visual event-related potentials: Arousal, valence, and repetition effects for normal and distorted pictures. *International journal of psychophysiology: official journal of the International Organization of Psychophysiology*, 67(2):114, 2008.

[108] Dean Sabatinelli, Peter J Lang, Andreas Keil, and Margaret M Bradley. Emotional perception: correlation of functional mri and event-related potentials. *Cerebral Cortex*, 17(5):1085–1091, 2007.

[109] Leonhard Schilbach, Bert Timmermans, Vasudevi Reddy, Alan Costall, Gary Bente, Tobias Schlicht, and Kai Vogeley. Toward a second-person neuroscience. *Behav. Brain Sci*, 2012.

[110] Leonhard Schilbach, Marcus Wilms, Simon B Eickhoff, Sandro Romanzetti, Ralf Tepest, Gary Bente, N Jon Shah, Gereon R Fink, and Kai Vogeley. Minds made for sharing: initiating joint attention recruits reward-related neurocircuitry. *Journal of Cognitive Neuroscience*, 22(12):2702–2715, 2010.

[111] Harald T Schupp, Bruce N Cuthbert, Margaret M Bradley, John T Cacioppo, Tiffany Ito, and Peter J Lang. Affective picture processing: The late positive potential is modulated by motivational relevance. *Psychophysiology*, 37(2):257–261, 2000.

[112] Natalie Sebanz, Harold Bekkering, and Günther Knoblich. Joint action: bodies and minds moving together. *Trends in cognitive sciences*, 10(2):70–76, 2006.

[113] Stephens Seeley and Tate. *Anatomy and Physiology*. McGraw-Hill, 2008.

[114] Anil K Seth. Measuring autonomy and emergence via granger causality. *Artificial life*, 16(2):179–196, 2010.

[115] Carsten Stahlhut. Eeg source localization using a hierarchical bayesian approach. Master's thesis, The Technical University of Denmark, 2008.

[116] Catherine Tallon-Baudry and Olivier Bertrand. Oscillatory gamma activity in humans and its role in object representation. *Trends in cognitive sciences*, 3(4):151–162, 1999.

[117] Emmanuelle Tognoli, Julien Lagarde, Gonzalo C DeGuzman, and JA Kelso. The phi complex as a neuromarker of human social coordination. *Proceedings of the National Academy of Sciences*, 104(19):8190–8195, 2007.

[118] Shanbao Tong and Nitish Vyomesh Thakor. *Quantitative EEG analysis methods and clinical applications*. Artech House Publishers, 2009.

[119] N. Tzourio-Mazoyer, B Landeau, D Papathanassiou, F Crivello, O Etard, N Delcroix, Bernard Mazoyer, and M Joliot. Automated anatomical labeling of activations in spm using a macroscopic anatomical parcellation of the mni mri single-subject brain. *Neuroimage*, 15(1):273–289, 2002.

[120] Hanneke Van Dijk, Jan-Mathijs Schoffelen, Robert Oostenveld, and Ole Jensen. Prestimulus oscillatory activity in the alpha band predicts visual discrimination ability. *The Journal of Neuroscience*, 28(8):1816–1823, 2008.

[121] Frank Van Overwalle and Kris Baetens. Understanding others' actions and goals by mirror and mentalizing systems: a meta-analysis. *Neuroimage*, 48(3):564–584, 2009.

[122] Rufin VanRullen, R Vanrullen, et al. Four common conceptual fallacies in mapping the time course of recognition. *Frontiers in psychology*, 2:365, 2011.

[123] Filipa Campos Viola, Jeremy Thorne, Barrie Edmonds, Till Schneider, Tom Eichele, Stefan Debener, et al. Semi-automatic identification of independent components representing eeg artifact. *Clin. Neurophysiol*, 120(5):868–877, 2009.

[124] Kai Vogeley, P Bussfeld, Albert Newen, S Herrmann, F Happe, P Falkai, W Maier, NJ Shah, GR Fink, and K Zilles. Mind reading: neural mechanisms of theory of mind and self-perspective. *Neuroimage*, 14(1):170–181, 2001.